

1. REPORT NO. CR-167996	2. GOVERNMENT AGENCY	3. RECIPIENT'S CATALOG NO.	
4. TITLE AND SUBTITLE Energy Efficient Engine - Turbine Transition Duct Model Technology Report		5. REPORT DATE August 1982	6. PERFORMING ORG. CODE
7. AUTHOR(S) K. Leach and R. Thulin	8. PERFORMING ORG. REPT. NO. PWA-5594-215		10. WORK UNIT NO.
9. PERFORMING ORG. NAME AND ADDRESS UNITED TECHNOLOGIES CORPORATION Pratt & Whitney Aircraft Group Commercial Products Division		11. CONTRACT OR GRANT NO. NAS3-20646	
12. SPONSORING AGENCY NAME AND ADDRESS National Aeronautics and Space Administration Lewis Research Center 21000 Brookpark Road, Cleveland, Ohio 44135		13. TYPE REPT./PERIOD COVERED Contractor Report	
15. SUPPLEMENTARY NOTES Prepared in cooperation with NASA Project Engineer, Mr. M. Vanco, NASA Lewis Research Center, Cleveland, OH		14. SPONSORING AGENCY CODE	
16. ABSTRACT The Low-Pressure Turbine Transition Duct Model Technology Program was directed toward substantiating the aerodynamic definition of a turbine transition duct for the Energy Efficient Engine. This effort was successful in demonstrating an aerodynamically viable compact duct geometry and the performance benefits associated with a low camber low-pressure turbine inlet guide vane. The program consisted of two phases. Phase 1, which focused on testing the transition duct design for the flight propulsion system, verified the pressure loss goal of 0.7 percent. Also, strut fairing pressure distributions, as well as wall pressure coefficients, were in close agreement with analytical predictions. In Phase 2, duct modifications for the integrated core/low spool were evaluated. The total pressure loss was 1.59 percent. Although the increase in exit area in this design produced higher wall loadings, reflecting a more aggressive aerodynamic design, pressure profiles showed no evidence of flow separation. Overall, the results acquired from this program have provided pertinent design and diagnostic information for the design of a turbine transition duct for both the flight propulsion system and the integrated core/low spool.			
17. KEY WORDS (SUGGESTED BY AUTHOR(S)) Low Loss Transition Duct Strut Fairing Low Camber Turbine First Vane Turbine Transition Duct Energy Efficient Engine Low-Pressure Turbine		18. DISTRIBUTION STATEMENT Unclassified - Unlimited	
19. SECURITY CLASS THIS (REPT) Unclassified	20. SECURITY CLASS THIS (PAGE) Unclassified	21. NO. PGS	22. PRICE *

FOREWORD

The Energy Efficient Engine Component Development and Integration Program is being conducted under parallel National Aeronautics and Space Administration contracts to the Pratt & Whitney Aircraft Group, Commercial Products Division and the General Electric Company. The overall project is under the direction of Mr. Carl C. Ciepluch. Mr. John W. Schaefer is the NASA Assistant Project Manager for the Pratt & Whitney Aircraft effort under Contract NAS3-20646, and Mr. M. Vanco is the NASA Project Engineer responsible for the portion of the program described in this report. Mr. William B. Gardner is the Pratt & Whitney Aircraft Program Manager for the Energy Efficient Engine Program. This report was prepared by Mr. K. Leach and Mr. R. Thulin of Pratt & Whitney Aircraft.

TABLE OF CONTENTS

	Page
SECTION 1.0 SUMMARY	1
SECTION 2.0 INTRODUCTION	3
SECTION 3.0 LOW-PRESSURE TURBINE TRANSITION DUCT RIG DESIGN	5
3.1 Introduction	5
3.2 Transition Duct Test Rig	6
3.2.1 Rig Design Approach	6
3.2.2 Build 1 Transition Duct Rig Design	7
3.2.3 Build 2 Transition Duct Rig Design	13
3.2.4 Transition Duct Rig Description	18
3.3 Rig Fabrication and Assembly	23
3.3.1 Fabrication	23
3.3.2 Assembly	23
SECTION 4.0 TEST PROGRAM AND PROCEDURES	25
4.1 Test Plan	25
4.2 Instrumentation	28
4.2.1 Surface Static Pressure Taps	32
4.2.2 Total Pressure Rakes	32
4.2.3 Wedge Probes	32
4.2.4 Claw Probes	32
4.3 Test Facility	32
4.4 Data Recording and Reduction	34
4.4.1 Data Recording	34
4.4.2 Data Reduction	35
4.4.3 Data Acquisition System Accuracy	35
SECTION 5.0 RESULTS AND ANALYSIS	37
5.1 Introduction	37
5.2 Aerodynamic Characterization	37
5.2.1 Strut Fairing Inlet Aerodynamics	37
5.2.2 Strut Fairing Exit Aerodynamics	39
5.2.3 Rig Duct Exit Aerodynamics	47
5.3 Airfoil/Duct Pressure Distribution	54
5.3.1 Duct Wall Loadings (Duct Wall Diffusion)	54
5.3.2 Strut Fairing Aerodynamics	59
5.3.3 Low-Pressure Turbine Inlet Guide Vane Aerodynamics	72
5.4 Summary of Results	72
SECTION 6.0 CONCLUDING REMARKS	75
APPENDIX A BUILD 1 AIRFOIL COORDINATES	77
APPENDIX B BUILD 2 AIRFOIL COORDINATES	85
LIST OF SYMBOLS	95
REFERENCES	97

LIST OF ILLUSTRATIONS

<u>Number</u>	<u>Title</u>	<u>Page</u>
2-1	Low-Pressure Turbine Transition Duct Test Program Logic Diagram	3
3-1	Cross-Sectional View of the Energy Efficient Engine Turbine Section Showing the High-Pressure Turbine Rotor, Transition Duct, Low-Pressure Turbine and Exit Guide Vane	5
3-2	Build 1 Transition Duct Flowpath Definition	7
3-3	Strut Fairing Blockage Profile Based On Streamline Analysis	8
3-4	Build 1 Transition Duct Separation Criterion	8
3-5	Build 1 Transition Duct Predicted Inner and Outer Wall Pressure Coefficients	9
3-6	Strut Fairing Mean Section Pressure Profile	11
3-7	Build 1 Strut Fairing Root, Mean, and Tip Stacking Arrangement	11
3-8	Build 1 Inlet Guide Vane Design Pressure Distribution	12
3-9	Build 1 Inlet Guide Vane Stacking Arrangement	12
3-10	Build 2 Transition Duct Flowpath Definition	14
3-11	Build 2 Transition Duct Effective Flow Area Based on Streamline Analysis	15
3-12	Integrated Core/Low Spool Transition Duct Predicted Inner and Outer Wall Pressure Coefficients	15
3-13	Typical Strut Fairing Section Pressure Profile	17
3-14	Build 2 Strut Fairing Stacking Arrangement (Reference Figure 3-10)	18
3-15	Inlet Guide Vane Mean Section Pressure Profile Mean Airfoil Section	19
3-16	Build 2 Inlet Guide Vane Stacking Arrangement	20

LIST OF ILLUSTRATIONS (Continued)

<u>Number</u>	<u>Title</u>	<u>Page</u>
3-17	Energy Efficient Engine Transition Duct Rig	21
3-18	Transition Duct Inlet Screen Design Characteristics	22
3-19	Transition Duct Preswirl Vane Design Characteristics	22
3-20	Assembled Test Rig	24
4-1	Instrumentation Map - Build 2 Inner Diameter	31
4-2	Instrumentation Map - Build 2 Outer Diameter	31
4-3	Total Pressure Rakes Used at the Strut Fairing Inlet and Inlet Guide Vane Exit Planes	33
4-4	Wedge Probes Used at the Strut Fairing Inlet Plane to Measure Total Pressure, Static Pressure, and Air Angle	33
4-5	Wedge Probe Calibration Results	34
5-1	Build 1 Strut Fairing Inlet Air Angle Average Spanwise Profile	38
5-2	Build 2 Strut Fairing Inlet Air Angle Average Spanwise Profile	38
5-3	Build 1 Average Strut Fairing Inlet Spanwise Mach Number Profiles	40
5-4	Build 2 Average Strut Fairing Inlet Spanwise Mach Number Profiles	40
5-5	Build 1 Transition Duct Pressure Loss	41
5-6	Build 2 Transition Duct Pressure Loss	41
5-7	Strut Fairing Loss Contour Profile for Build 2 At Design Conditions	43
5-8	Strut Fairing Loss Contour Profile for Build 2 At Off-Design Conditions	44
5-9	Strut Fairing Spanwise Exit Angle for Build 1 Configuration	45

LIST OF ILLUSTRATIONS (Continued)

<u>Number</u>	<u>Title</u>	<u>Page</u>
5-10	Strut Fairing Spanwise Exit Air Angle for Build 2 Configuration	45
5-11	Build 1 Transition Duct Strut Fairing Average Spanwise Exit Mach Number Profile	46
5-12	Build 2 Transition Duct Strut Fairing Average Spanwise Exit Mach Number Profile	47
5-13	Build 1 Transition Duct and Inlet Guide Vane Pressure Loss	48
5-14	Build 2 Transition Duct and Inlet Guide Vane Pressure Loss	48
5-15	Build 2 Loss Contour Plot At Design Conditions Showing the Wakes from Low-Pressure Turbine Inlet Guide Vanes	49
5-16	Build 2 Loss Contour Plot At Off-Design Conditions Showing the Wakes from Low-Pressure Turbine Inlet Guide Vanes	50
5-17	Build 1 Inlet Guide Vane Exit Air Angle Data	52
5-18	Build 2 Inlet Guide Vane Exit Air Angle Data	52
5-19	Inlet Guide Vane Exit Mach Number Trends for Build 1	53
5-20	Inlet Guide Vane Exit Mach Number Trends for Build 2	53
5-21	Build 1 Transition Duct Wall Loadings At Design and Off-Design Conditions	55
5-22	Build 1 Transition Duct Wall Loadings At Design and Off-Design Conditions	56
5-23	Build 2 Transition Duct Wall Loadings At Design and Off-Design Conditions	57
5-24	Build 2 Transition Duct Wall Loadings At Design and Off-Design Conditions	58
5-25	Build 1 Strut Fairing Design Point Static Pressure Distributions at 10 Percent Span	60

LIST OF ILLUSTRATIONS (Continued)

<u>Number</u>	<u>Title</u>	<u>Page</u>
5-26	Build 1 Strut Fairing Design Point Static Pressure Distributions at 50 Percent Span	60
5-27	Build 1 Strut Fairing Design Point Static Pressure Distributions at 90 Percent Span	61
5-28	Build 1 Strut Fairing Off-Design Static Pressure Distributions at 10 Percent Span	61
5-29	Build 1 Strut Fairing Off-Design Static Pressure Distributions at 50 Percent Span	62
5-30	Build 1 Strut Fairing Off-Design Static Pressure Distributions at 90 Percent Span	62
5-31	Build 2 Strut Fairing Design Point Static Pressure Distributions at 15 Percent Span	64
5-32	Build 2 Strut Fairing Design Point Static Pressure Distributions at 53 Percent Span	64
5-33	Build 2 Strut Fairing Design Point Static Pressure Distributions at 90 Percent Span	65
5-34	Build 2 Strut Fairing Off-Design Static Pressure Distributions at 15 Percent Span	65
5-35	Build 2 Strut Fairing Off-Design Static Pressure Distributions at 53 Percent Span	66
5-36	Build 2 Strut Fairing Off-Design Static Pressure Distributions at 90 Percent Span	66
5-37	Build 2 Strut Fairing Mean Section Pressure Distribution Data	67
5-38	Build 2 Strut Fairing Mean Section Pressure Distribution Data	67
5-39	Build 2 Strut Fairing Mean Section Pressure Distribution Data	68
5-40	Build 2 Strut Fairing Mean Section Pressure Distribution Data	68

LIST OF ILLUSTRATIONS (Continued)

<u>Number</u>	<u>Title</u>	<u>Page</u>
5-41	Build 2 Strut Fairing Mean Section Pressure Distribution Data	69
5-42	Build 2 Strut Fairing Mean Section Pressure Distribution Data	69
5-43	Build 2 Strut Fairing Mean Section Pressure Distribution Data	70
5-44	Build 2 Strut Fairing Mean Section Pressure Distribution Data, Off-Design	70
5-45	Build 2 Strut Fairing Mean Section Pressure Distribution Data, Off-Design	71
5-46	Build 2 Strut Fairing Mean Section Pressure Distribution Data, Off-Design	71
5-47	Build 1 Inlet Guide Vane Design Measured Pressure Distribution Data	73
5-48	Build 1 Inlet Guide Vane Measured Off-Design Pressure Distribution Data	73
5-49	Build 2 Inlet Guide Vane Design Measured Pressure Distribution Data	74
5-50	Build 2 Inlet Guide Vane Off-Design Measured Pressure Distribution Data	74

LIST OF TABLES

<u>Table</u>	<u>Title</u>	<u>Page</u>
3-I	Transition Duct General Aerodynamics	6
3-II	Build 1 Transition Duct Rig Design Aerodynamics	9
3-III	Transition Duct Strut Fairing Summary - Airfoil Planar Sections	10
3-IV	Build 1 Low-Pressure Turbine Inlet Guide Vane General Aerodynamics	13
3-V	Build 2 Transition Duct Rig Design Aerodynamics	16
3-VI	Transition Duct Strut Fairing Summary - Airfoil Planar Sections	17
3-VII	Build 2 Low-Pressure Turbine Inlet Guide Vane General Aerodynamics	19
4-I	Data Acquisition Sequence - Build 1	26
4-II	Data Acquisition Sequence - Build 2	27
4-III	Transition Duct Rig Instrumentation - Build 1	28
4-IV	Transition Duct Rig Instrumentation - Build 2	30
5-I	Summary of Strut Fairing Inlet Conditions	39
5-II	Energy Efficient Engine Transition Duct Performance	54

SECTION 1.0

SUMMARY

The Low-Pressure Turbine Transition Duct Model Technology Program was directed toward substantiating the aerodynamic definition of the turbine transition duct for the Energy Efficient Engine. This effort was successful in demonstrating an aerodynamically viable compact duct geometry and the performance benefits associated with a low camber low-pressure turbine inlet guide vane.

The program consisted of two phases. In the first phase, the performance of the transition duct designed for a flight propulsion system was evaluated. The second phase focused on demonstrating design changes required for the integrated core/low spool. All testing was conducted with a scale model of the transition duct configuration, which incorporated sufficient instrumentation for an accurate characterization of component pressure distribution, exit profiles and flow properties.

Phase I results verified the duct pressure loss goal of 0.7 percent at design point conditions. Also, strut fairing pressure distributions, as well as wall pressure coefficients, were in close agreement with analytical predictions. Duct inlet flow perturbations, simulating off-design operating conditions, showed no aerodynamic instabilities. On the basis of these results, a duct design with an area ratio of 1.5, length-to-height ratio of 3.0, and a non-working strut fairing was confirmed for the flight propulsion system.

The duct modifications evaluated during Phase 2, which included a 5 percent increase in the exit annulus area along with geometry changes to the fairing for aerodynamic compatibility for the low-pressure turbine in the integrated core/low spool, increased the total pressure loss to 1.59 percent. Although the increase in exit area produced higher wall loadings, reflecting a more aggressive aerodynamic design, pressure profiles showed no evidence of flow separation. In addition, inlet and exit pressure profiles of the low camber turbine inlet guide vane showed the desired low loss performance.

Overall, the results from these tests indicate that the transition duct designs for both the flight propulsion system and integrated core/low spool are aerodynamically stable and provide the low-pressure turbine rotor inlet with a flowfield that is insensitive to high-pressure turbine exit conditions. Since model results are scaleable to the full size component, these results provide a firm basis to proceed with the design of a full scale transition duct for the integrated core/low spool. These results have also contributed substantially towards extending the data base for designing low loss transition ducts for the next generation of gas turbine engines.

PRECEDING PAGE BLANK NOT FILMED

SECTION 2.0

INTRODUCTION

The National Aeronautics and Space Administration sponsored Pratt & Whitney Aircraft Energy Efficient Engine Component Development and Integration Program is directed toward the development of technology to achieve greater fuel efficiency for future commercial gas turbine engines. The overall goals outlined for the program include a reduction in fuel consumption of at least 12 percent and a reduction in direct operating cost of at least 5 percent relative to the Pratt & Whitney Aircraft JT9D-7A reference engine. To demonstrate the technology to achieve these goals, the program is presently divided into three tasks:

- Task 1 Propulsion System Analysis, Design and Integration
- Task 2 Component Analysis, Design and Development
- Task 4 Integrated Core/Low Spool Design, Fabrication and Test

As part of the Task 2 effort, a turbine transition duct was designed for both the integrated core/low spool and the flight propulsion system. The component design is based on aggressive aerodynamics to achieve a compact, low loss duct configuration. The purpose of the Low-Pressure Turbine Transition Duct Model Technology Program was to verify the aerodynamic definitions of each design and to provide technical guidance during the design process. This program was scheduled to ensure timely interaction with the low-pressure turbine component effort, as shown in Figure 2-1.

This report presents the results of the Low-Pressure Turbine Transition Duct Model Technology Program. Section 3 provides a discussion of the transition duct rig designs. Section 4 describes the test program, and section 5 presents the results of the test program. Concluding remarks are presented in section 6.

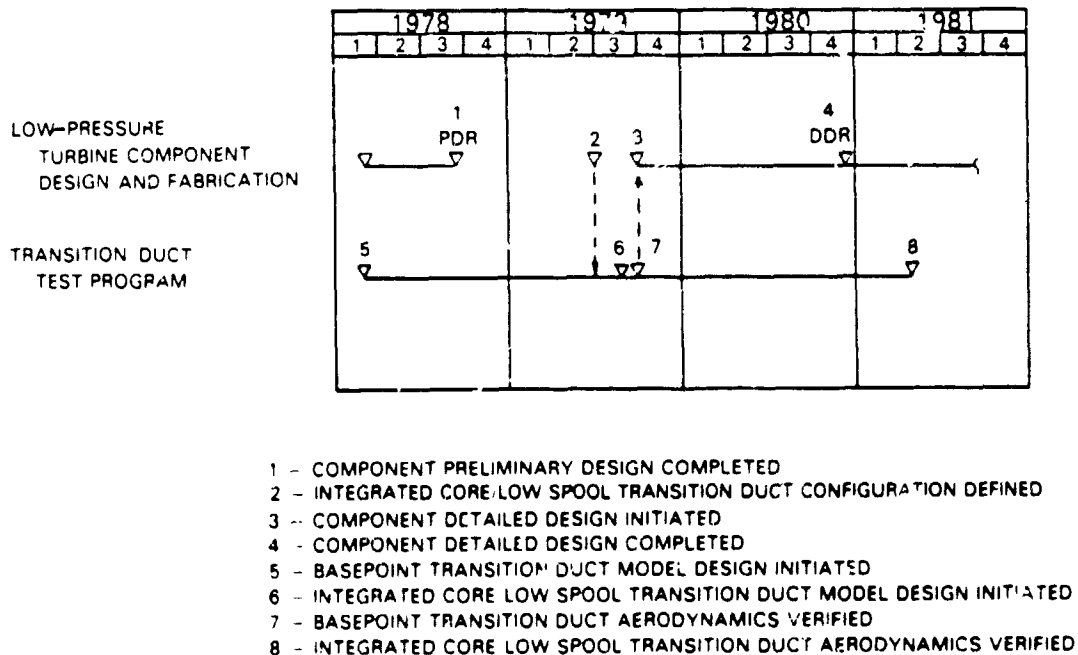


Figure 2-1 Low-Pressure Turbine Transition Duct Test Program Logic Diagram

SECTION 3.0

LOW-PRESSURE TURBINE TRANSITION DUCT RIG DESIGN

3.1 INTRODUCTION

In the Energy Efficient Engine turbine system, the turbine transition duct provides the gas path transition between the high-pressure turbine exit and the low-pressure turbine inlet to establish the desired flow conditions for the low-pressure turbine inlet. In terms of its mechanical arrangement, the transition duct provides a frame for the rear high and low-pressure rotor support and the rear engine mount. This arrangement permits a straddle mounted or simply-supported high-pressure rotor system for improved clearance control. In addition, centralizing the rotor mass between and near the support structure provides improved control of case and rotor deflections caused by normally encountered flight loads.

A cross-sectional view of the transition duct, low-pressure turbine system, and exit guide vane, as integrated in the turbine section of the Energy Efficient Engine, is shown in Figure 3-1. The transition duct performance goal, in terms of percent total pressure loss, is 0.7 percent for both the integrated core/low spool and the flight propulsion system.

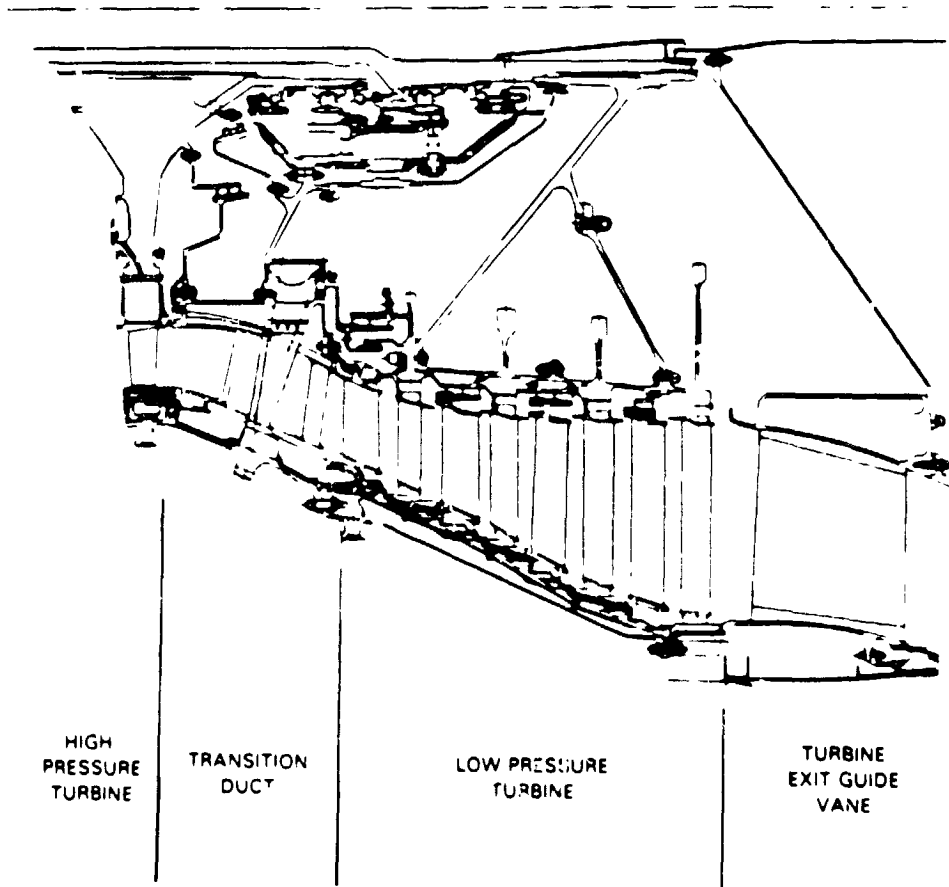


Figure 3-1 Cross-Sectional View of the Energy Efficient Engine Turbine Section Showing the High-Pressure Turbine Rotor, Transition Duct, Low-Pressure Turbine and Exit Guide Vane

The transition duct aerodynamic definition introduces certain technology challenges. These include the following: (1) proper spanwise air angle and Mach number distribution into the low-pressure turbine rotor, (2) no flow separation through the duct, (3) low loss strut fairing, (4) aerodynamic tolerance to high-pressure turbine off-design exit conditions, and (5) aerodynamic compatibility between the strut fairing and the unique low camber first vane in the low-pressure turbine. These challenges were addressed in the rig design and test effort.

3.2 TRANSITION DUCT TEST RIG

3.2.1 Rig Design Approach

Two builds of the transition duct rig were designed and fabricated for use in this technology program. The first (build 1) was designed to assess the aerodynamic characteristics of the transition duct for the flight propulsion system and was scaled to 0.6961 of the flight propulsion system size to match the engine Reynolds number. The second (build 2) was designed to verify the performance characteristics of the transition duct for the integrated core/low spool and was scaled to 0.7434 of the integrated core/low spool size to maximize the use of existing rig hardware from build 1.

The aerodynamic definition for each build of the transition duct rig was based on a series of analyses to establish the flowpath, airfoil contours and flow characteristics. These are discussed for each of the two builds of the transition duct in the following sections. The general parameters governing the transition duct aerodynamic design for both the flight propulsion system and the integrated core/low spool are presented in Table 3-I.

TABLE 3-I
TRANSITION DUCT GENERAL AERODYNAMICS
(At Aerodynamic Design Point)

	<u>FLIGHT PROPULSION SYSTEM</u>	<u>INTEGRATED CORE/LOW SPOOL</u>
Annulus Area Ratio	1.50	1.57
Effective Area Ratio	1.26	1.42
Effective Turning, deg*	0	5
$\Delta P_T/P_T$ (%) Goal	0.7	0.7

* α_2 gas - α_2 free vortex

3.2.2 Build 1 Transition Duct Rig Design

Flowpath

The flowpath of the flight propulsion system transition duct configuration was established during the preliminary design phase of the program for an engine thrust size of 182,376 N (41,000 lbf). The flight propulsion system duct length was 21.0 cm (8.26 in). Its annulus area ratio was 1.50 and its length-to-height ratio was 3.0. The flowpath definition is shown in Figure 3-2 and it identifies the axial and radial positions of the strut fairing and turbine inlet guide vane.

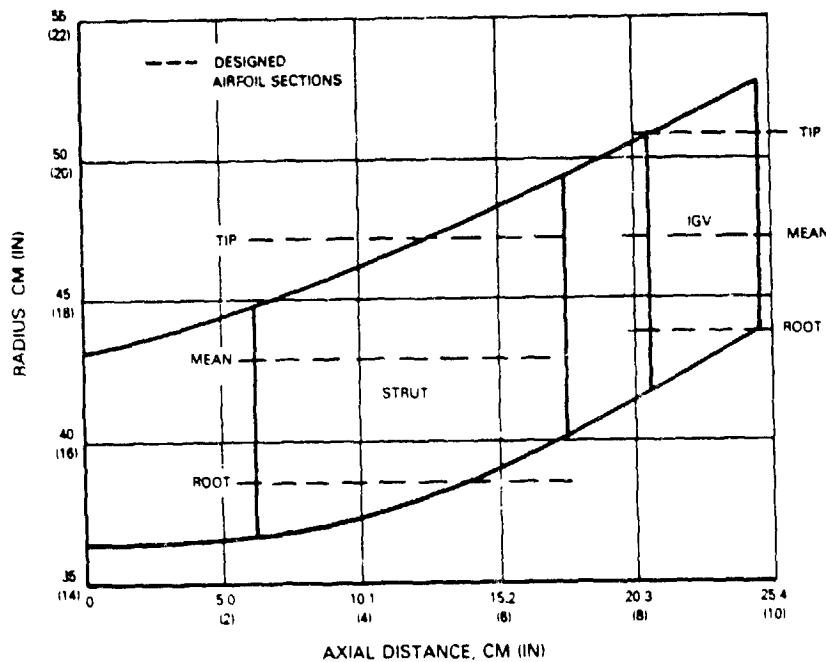


Figure 3-2 Build 1 Transition Duct Flowpath Definition

A streamline analysis, utilizing an inviscid, two-dimensional, axisymmetric model, was used in designing the transition duct flowpath. The desired duct contour geometry was assumed to be smooth and was input together with a radial blockage profile used to simulate the transition duct strut fairing. The resulting axial area variation used in this analysis is shown in Figure 3-3. Inlet temperature, pressure, and angle profiles were set by the high-pressure turbine rotor exit conditions. An analysis of the transition duct flowpath was conducted to determine if flow separation occurred. Results of this analysis are shown in Figure 3-4. Levels of wall friction at the strut trailing edge for the inner and outer walls indicate that the duct should be free of separation. These results are also indicated in Figure 3-5 where the predicted inner and outer wall pressure coefficients are shown. The design aerodynamics from the streamline analysis for the build 1 rig are summarized in Table 3-II.

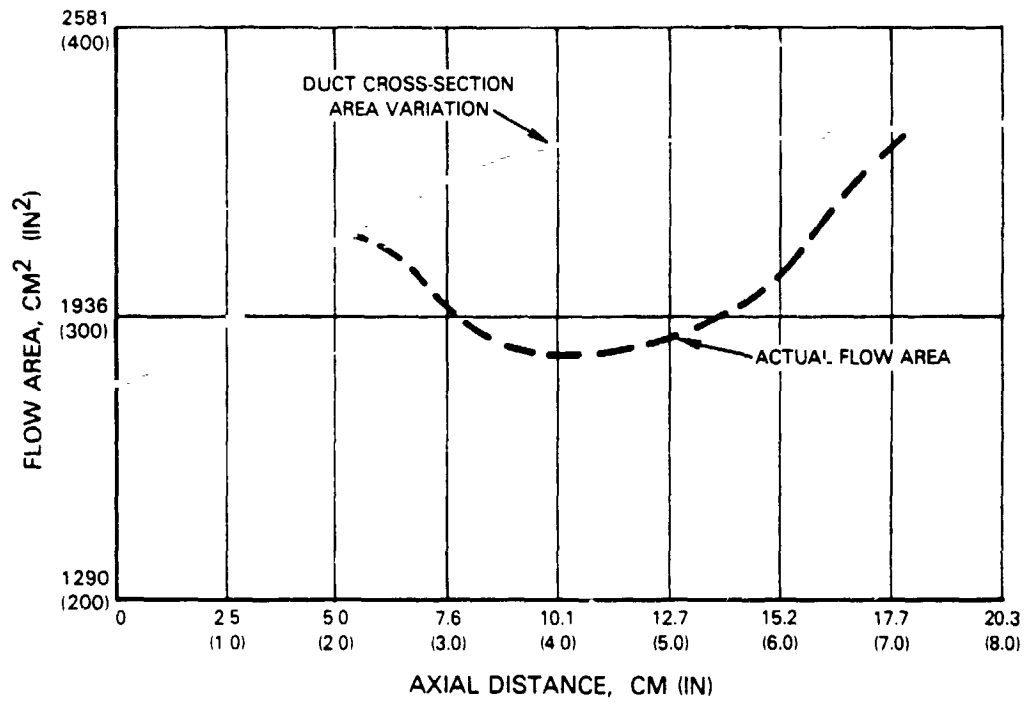


Figure 3-3 Strut Fairing Blockage Profile Based On Streamline Analysis

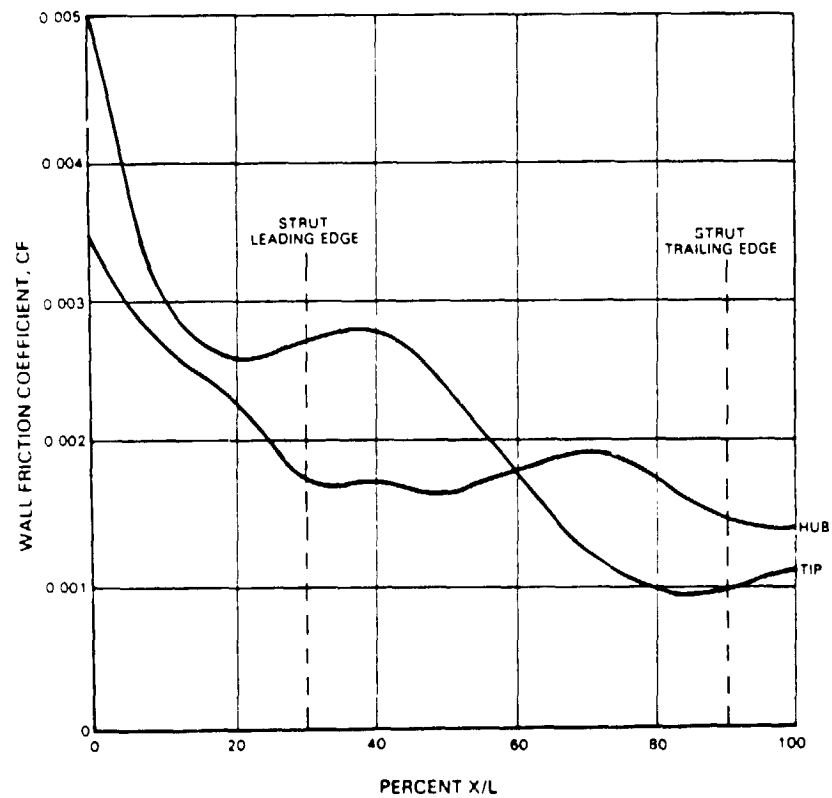


Figure 3-4 Build 1 Transition Duct Separation Criterion

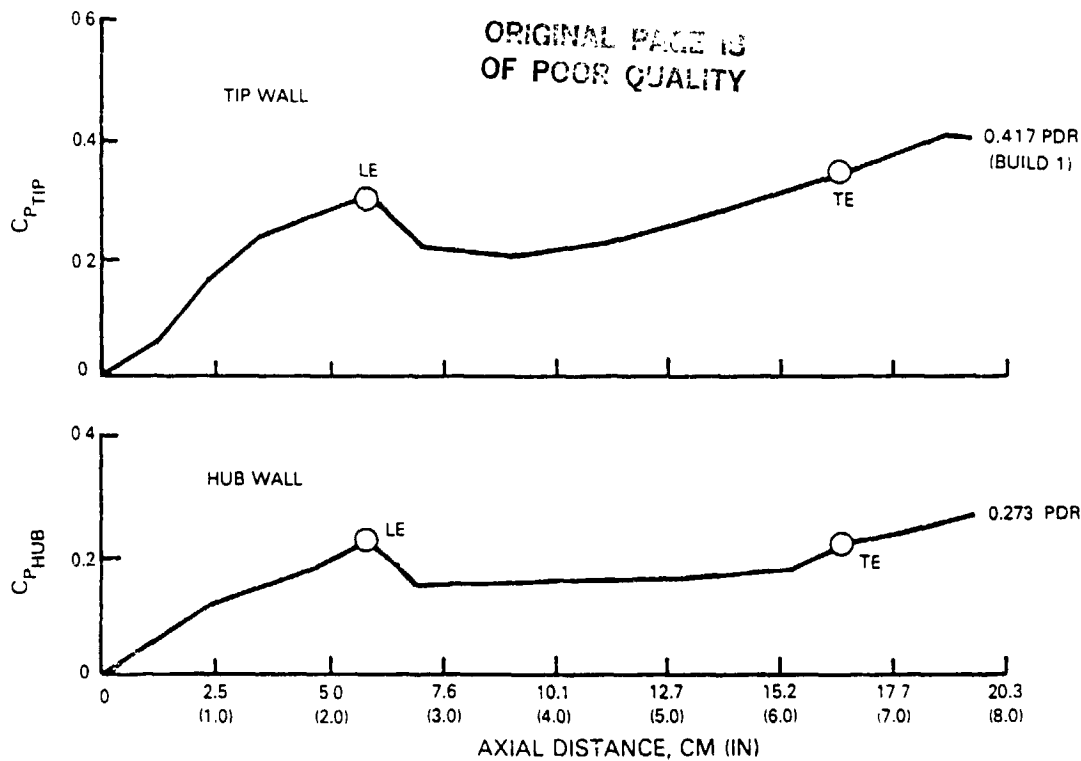


Figure 3-5 Build 1 Transition Duct Predicted Inner and Outer Wall Pressure Coefficients

TABLE 3-11

BUILD 1 TRANSITION DUCT RIG DESIGN AERODYNAMICS
(Flight Propulsion System)

	Root	Mean	Tip
<u>HPT Exit</u>			
Mach No.	0.527	0.500	0.546
Air Angle, deg	41.31	45.03	53.02
<u>Strut Fairing Leading Edge</u>			
Mach No.	0.463	0.445	0.455
Air Angle, deg	148.01	141.07	135.01
Metal Angle, deg	148.01	141.07	135.01
Incidence, deg	0.0	0.0	0.0
<u>Strut Exit</u>			
Mach No.	0.437	0.405	0.413
Air Angle, deg	32.32	36.58	43.47
Metal Angle, deg	31.0	35.2	44.2
Gas Turning, deg	-0.33	+2.35	+1.52
Effective Turning, deg	0.0	0.0	0.0
<u>IGV Inlet</u>			
Mach No.	0.422	0.395	0.390
Air Angle, deg	147.80	142.92	137.95
Metal Angle, deg	142.80	137.92	130.95
Incidence, deg	-5.0	-5.0	-7.0
<u>IGV Exit</u>			
Mach No.	0.709	0.650	0.627
Air Angle, deg	24.30	24.30	24.30
Metal Angle, deg	24.30	24.30	24.30
Air Turning, deg	7.90	12.78	17.75

For this design and test, all angles were referenced from tangential. The airfoil design inlet angles were measured clockwise from tangential, and the exit angles and all test measured angles were measured counter clockwise from tangential.

Strut Fairing

The transition duct has a series of struts to provide structural support of the number 4 and 5 bearing compartment. To minimize blockage and pressure loss, the struts are encased by aerodynamically-shaped fairings.

There are 14 strut fairings in the build 1 configuration. The main criteria governing the fairing aerodynamic design were thickness and the air conditions shown in Table 3-II. The fairing thickness was established at 2.54 cm (1 in) to accommodate the structural strut. The fairing is a 65 series circular arc nonworking foil that provides low loss and the proper flow conditions to the low-pressure turbine inlet. A summary of the turbine strut fairing design characteristics is presented in Table 3-III. Airfoil computer-aided design programs were used for determining the strut fairing pressure distribution. An acceptable pressure distribution for the mean section is shown in Figure 3-6. Figure 3-7 shows the stacking arrangement of the root, mean and tip sections of the airfoil.

TABLE 3-III

TRANSITION DUCT STRUT FAIRING SUMMARY
AIRFOIL PLANAR SECTIONS
(Flight Propulsion System Build 1 Design)

	<u>Root</u>	<u>Mean</u>	<u>Tip</u>
Radius at Stacking Point, cm (in)	39.1 (15.40)	43.5 (17.14)	47.9 (18.87)
Axial Chord, cm (in)	11.4 (4.5)	11.4 (4.5)	11.4 (4.5)
Actual Chord, cm (in)	20.3 (8.0)	18.7 (7.4)	16.2 (6.4)
Maximum Thickness, cm (in)	2.54 (1.0)	2.54 (1.0)	2.54 (1.0)
Gap/Chord Ratio	0.864	1.04	1.32
Inlet Metal Angle	144.50	138.00	132.10
Inlet Air Angle	144.50	138.00	132.10
Inlet Mach Number	0.451	0.446	0.466
Exit Metal Angle	31.1	31.2	39.8
Exit Air Angle	35.83	39.65	46.38
Exit Mach Number	0.456	0.417	0.401

Inlet Guide Vane

In the Energy Efficient Engine, the high and low pressure spools are counter-rotating. This results in the requirement for a unique low camber inlet guide vane in the low-pressure turbine for improved performance. The build 1 inlet guide vane aerodynamic parameters are presented in Table 3-IV. An acceptable pressure distribution for the mean section of the inlet guide vane is presented in Figure 3-8. Figure 3-9 shows the stacking arrangement of the vane.

ORIGINAL FACE IS
OF POOR QUALITY

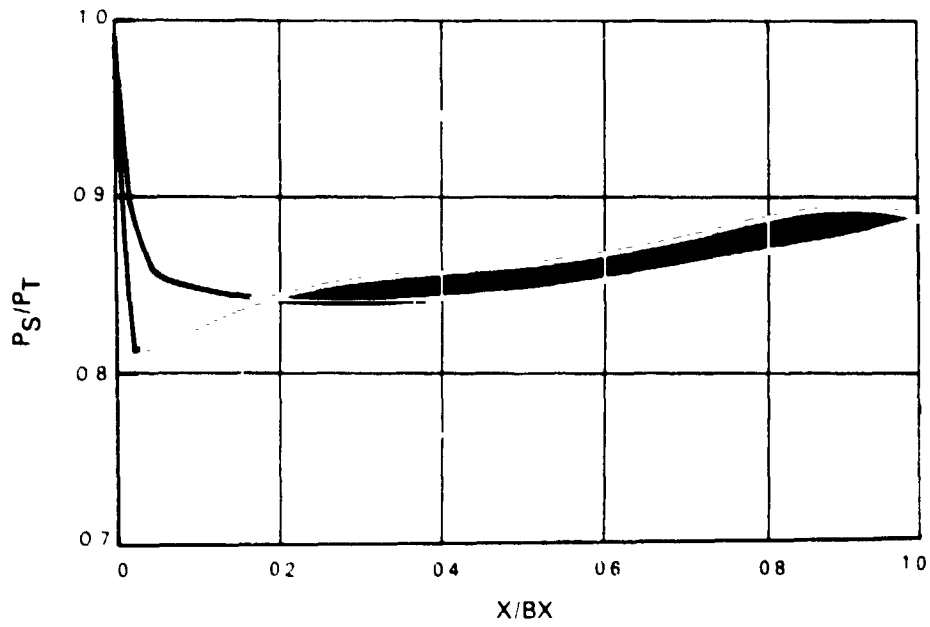


Figure 3-6 Strut Fairing Mean Section Pressure Profile

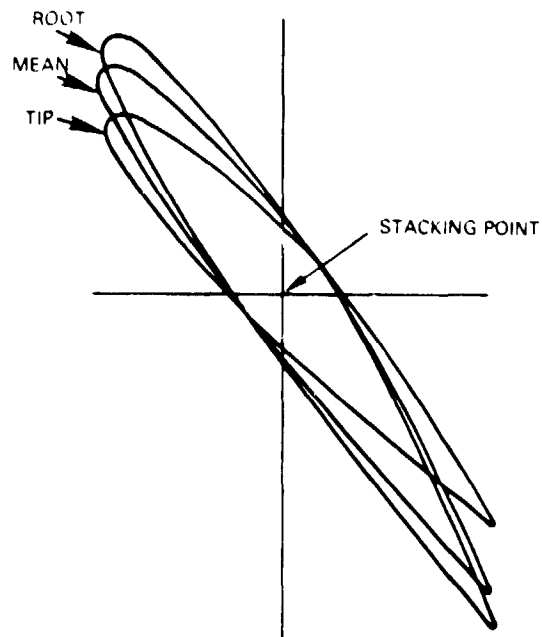


Figure 3-7 Build 1 Strut Fairing Root, Mean, and Tip Stacking Arrangement

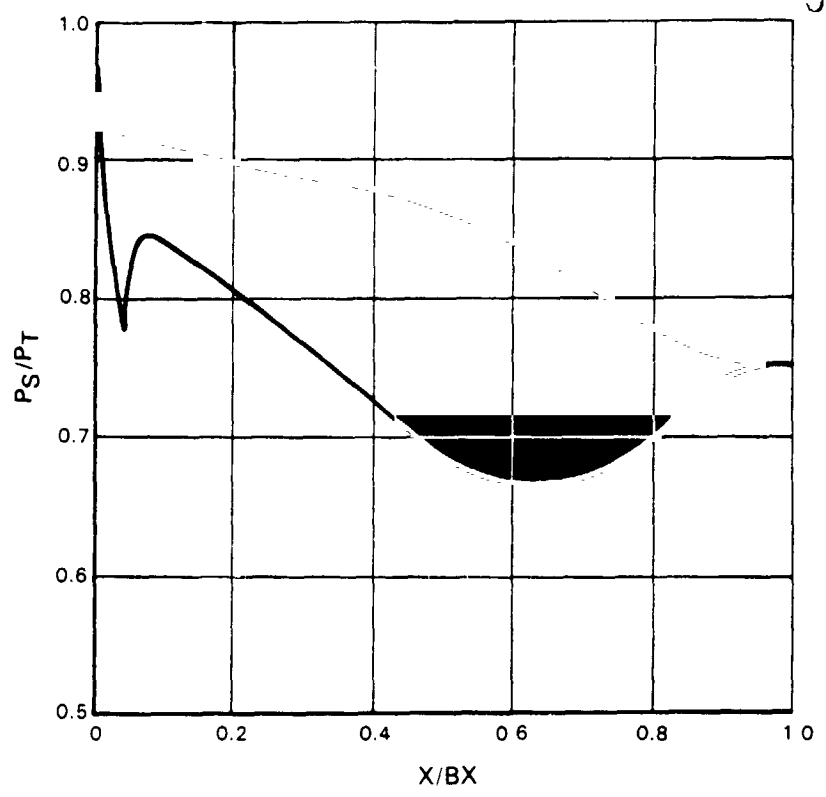


Figure 3-8 Build 1 Inlet Guide Vane Design Pressure Distribution

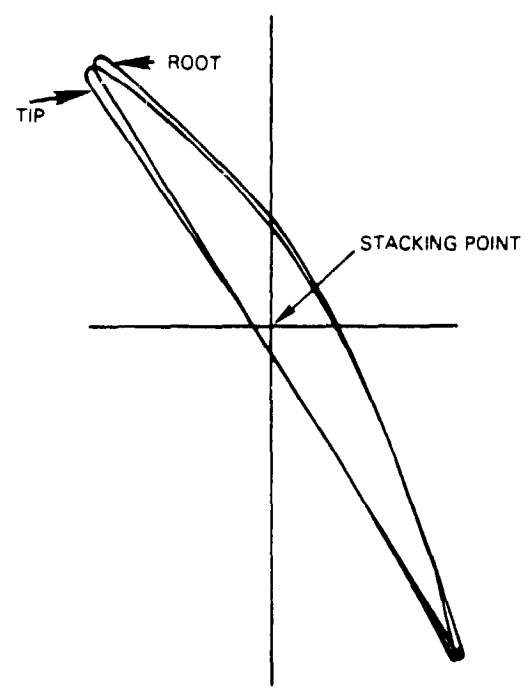


Figure 3-9 Build 1 Inlet Guide Vane Stacking Arrangement

TABLE 3-IV

LOW-PRESSURE TURBINE INLET GUIDE VANE GENERAL AERODYNAMICS
(Build 1 Design)

	Root Trailing Edge	Mean Trailing Edge	Tip Trailing Edge
Radius, cm (in)	44.50 (17.52)	47.98 (18.89)	51.48 (20.27)
Actual Chord, cm (in)	7.72 (3.04)	7.69 (3.03)	7.56 (2.98)
Axial Chord, cm (in)	4.19 (1.65)	4.19 (1.65)	4.19 (1.65)
No. of Foils	54	54	54
Gap/Chord Ratio	1.24	1.33	1.43
Leading Edge Diameter cm (in)	0.203 (0.080)	0.177 (0.070)	0.177 (0.070)
Inlet Metal Angle, deg	139.6	137.4	131.0
Inlet Air Angle, deg	144.6	142.4	138.0
Inlet Mach No.	0.410	0.387	0.367
Exit Metal Angle, deg	24.3	24.3	24.3
Exit Air Angle, deg	24.3	24.3	24.3
Exit Mach No.	0.705	0.654	0.617
Incidence, deg	-5	-5	-7

3.2.3 Build 2 Transition Duct Rig Design

In the second phase of the transition duct test program, modifications were made to the transition duct test rig to reflect the definition of the transition duct that evolved for the integrated core/low spool.

The rig hardware in build 2 is similar to that of build 1 with the exception of the flowpath and airfoils. The major differences relative to the build 1 duct are as follows:

- o Five percent increase in area ratio (1.50 to 1.57)
- o A reduction in the number of strut fairings from 14 to 11
- o Canting the strut fairing
- o An increase in strut fairing effective turning from 0 to 5 degrees
- o Modifications to the inlet guide vane

Flowpath

Certain modifications were made to the flowpath in the build 2 transition duct configuration to reflect the revisions required for the integrated core/low spool. The changes are apparent in Figure 3-10, which presents a comparison of the flight propulsion system transition duct scaled to the duct in the integrated core/low spool. As indicated, the outer wall curvature and radial height for the duct in the integrated core/low spool were changed to accommodate a 5 percent increase in the exit annulus area ratio (1.57 compared to 1.50). In addition, the overall axial length has been increased slightly. These modifications, however, did not affect the length-to-height ratio, which remained at 3.0 for each duct configuration.

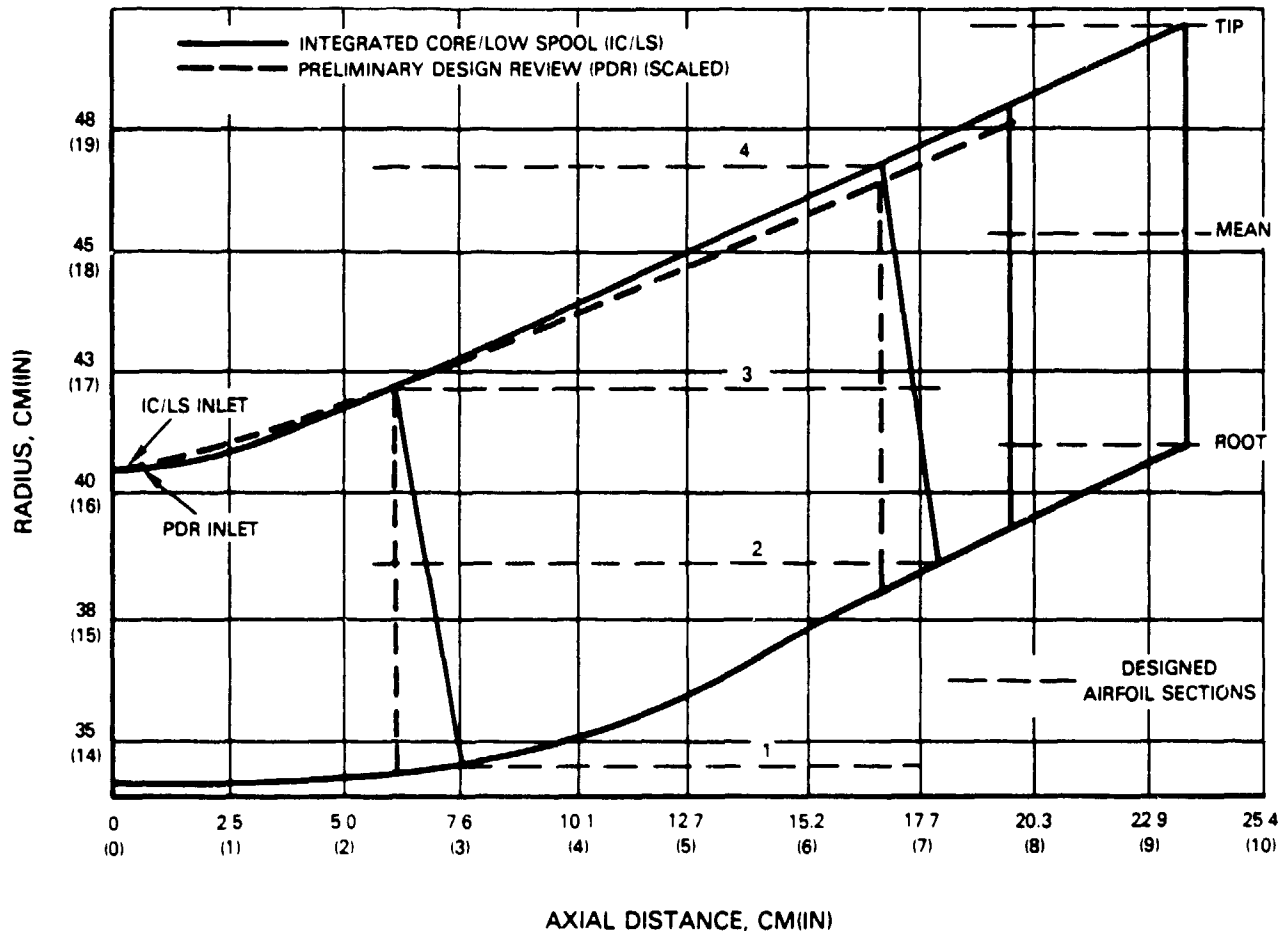


Figure 3-10 Build 2 Transition Duct Flowpath Definition

The same streamline analysis techniques used in the build 1 analysis were employed in build 2. The transition duct effective flow area, as used in the streamline analysis, is shown in Figure 3-11. Loss profile data acquired during build 1 were also used for a more accurate representation.

The results of an analysis of the integrated core/low spool transition duct, showing the predicted inner and outer wall pressure coefficients, are presented in Figure 3-12. In comparison to the Build 1 design, the transition duct flowpath for the integrated core/low spool is a more aggressive design, as indicated by the high level of diffusion. Analysis indicated that the flow will not separate from the outer wall, although the levels of pressure coefficient are near levels for the onset of separation. Table 3-V presents a summary of the design aerodynamics from the streamline analysis for build 2.

ORIGINAL PAGE IS
OF POOR QUALITY

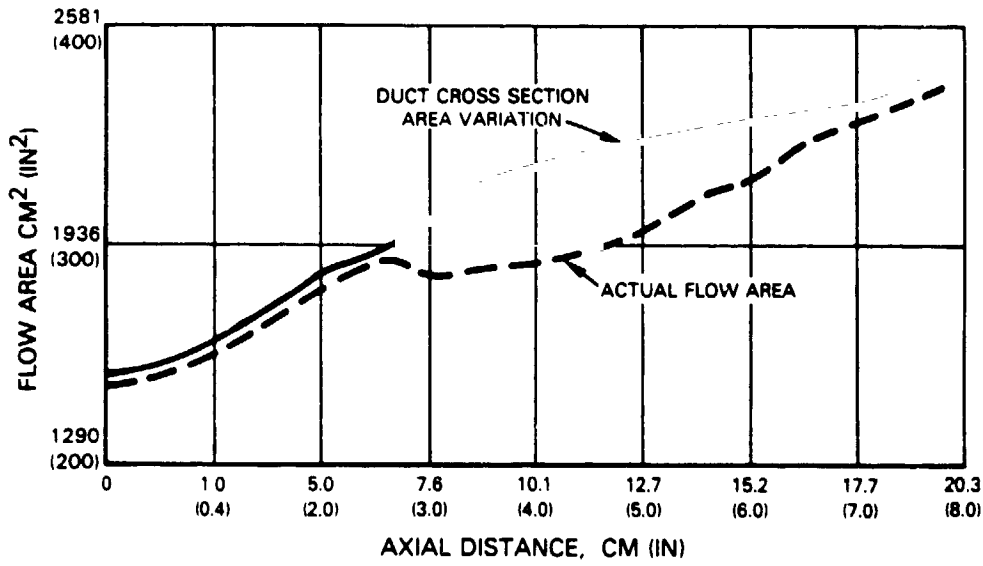


Figure 3-11 Build 2 Transition Duct Effective Flow Area Based on Streamline Analysis

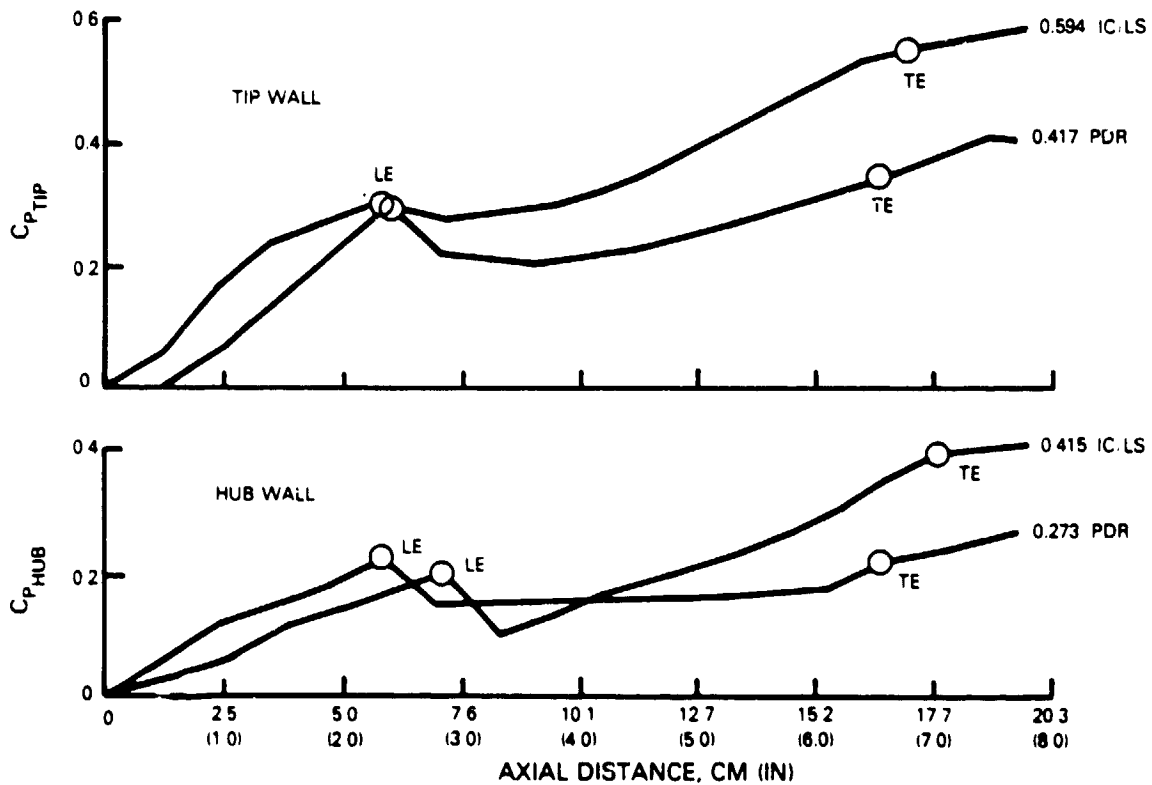


Figure 3-12 Integrated Core/Low Spool Build 2 Transition Duct Predicted Inner and Outer Wall Pressure Coefficients

TABLE 3-V

BUILD 2 TRANSITION DUCT RIG DESIGN AERODYNAMICS
(Integrated Core/Low Spool)

	<u>Root</u>	<u>Mean</u>	<u>Tip</u>
<u>Inlet</u>			
Mach No.	0.594	0.560	0.573
Air Angle, deg	38.04	43.36	48.45
<u>Strut Fairing Leading Edge</u>			
Mach No.	0.526	0.498	0.480
Air Angle, deg	151.23	143.75	141.36
Metal Angle, deg	153.0	146.5	140.0
Incidence, deg	-1.77	-2.75	1.36
<u>Strut Exit</u>			
Mach No.	0.398	0.403	0.324
Air Angle, deg	35.00	38.50	42.00
Metal Angle, deg	43.0	51.3	54.8
Air Turning, deg	-6.23	-2.25	-3.36
Effective Turning, deg	5	5	5
<u>IGV Inlet</u>			
Mach No.	0.396	0.395	0.304
Air Angle, deg	144.43	141.28	139.63
Metal Angle, deg	141.43	138.28	136.63
Incidence Angle, deg	-3	-3	-3
<u>IGV Exit</u>			
Mach No.	0.652	0.654	0.541
Air Angle, deg	26.72	24.22	21.72
Metal Angle, deg	26.72	24.22	21.72
Air Turning, deg	+10.81	+14.30	+17.67

Strut Fairing

Several modifications were made to the strut fairing design to accommodate the flowpath changes. First, the strut fairing was changed from a nonworking to a working foil, turning the airflow 5 degrees to provide the proper inlet flow-field to the low-pressure turbine. Second, the posture was changed by canting the airfoil tangentially approximately 11 degrees and shifting the root section axially rearward. Third, the number of strut fairings was reduced from 14 to 11 to preclude a possible vibratory excitation induced by a high-pressure turbine blade passing frequency. Finally, the airfoil series was revised from a 65 circular arc to a 400 series to improve incidence range. Computer-aided design programs were used to determine the strut fairing pressure distribution. An acceptable pressure distribution of a typical section is shown in Figure 3-13.

ORIGINAL PAGE IS
OF POOR QUALITY

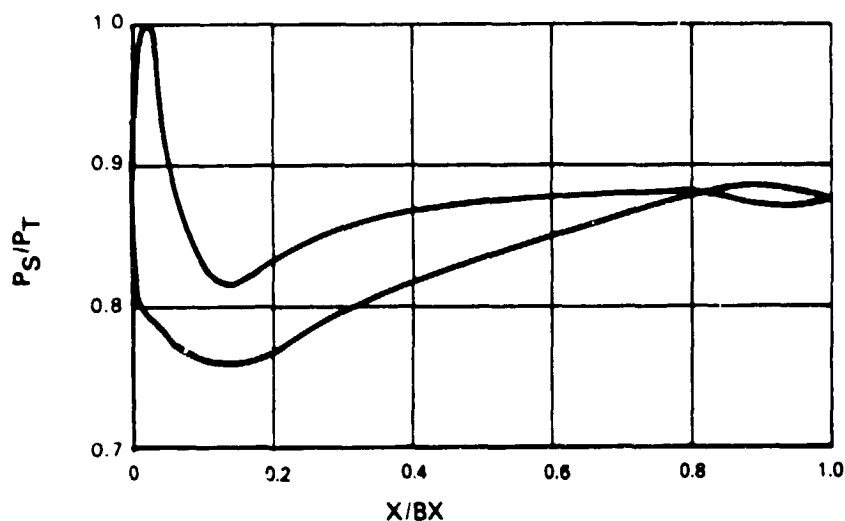


Figure 3-13 Typical Strut Fairing Section Pressure Profile

A summary of the transition duct strut fairing airfoil design characteristics at several spanwise stacking point locations, as shown in Figure 3-10, is presented in Table 3-VI. The stacking arrangement of the strut fairing is shown in Figure 3-14.

TABLE 3-VI

TRANSITION DUCT STRUT FAIRING SUMMARY
AIRFOIL PLANAR SECTIONS
(Integrated Core/Low Spool Build 2 Design)

Spanwise Section	1	2	3	4
Radius*, cm (in)	35.00 (13.78)	39.19 (15.43)	42.74 (16.83)	47.44 (18.68)
Axial Chord, cm (in)	10.9 (4.32)	11.2 (4.43)	11.5 (4.53)	11.7 (4.64)
Actual Chord, cm (in)	20.4 (8.03)	17.3 (6.81)	15.6 (6.14)	14.9 (5.88)
Maximum Thickness, cm (in)	2.54 (1.0)	2.54 (1.0)	2.54 (1.0)	2.54 (1.0)
Gap/Chord Ratio	0.98	1.29	1.59	1.82
Inlet Metal Angle, deg	150.2	144.5	138.7	131.6
Inlet Air Angle, deg	148.5	142.5	141.8	148.1
Inlet Mach No.	0.51	0.50	0.48	0.43
Exit Metal Angle, deg	33.4	44.1	51.0	54.9
Exit Air Angle, deg	31.9	35.3	38.4	42.4
Exit Mach No.	0.37	0.40	0.40	0.31

*At Stacking Point

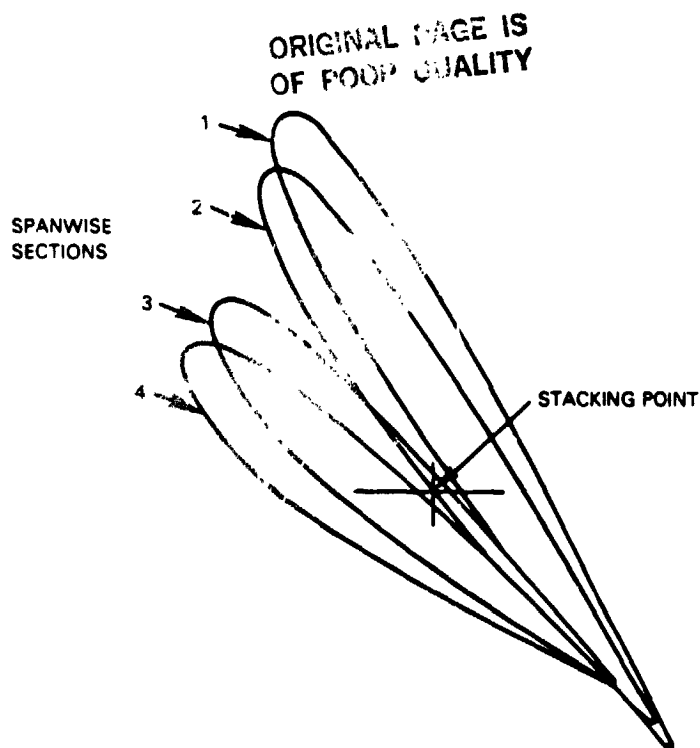


Figure 3-14 Build 2 Strut Fairing Stacking Arrangement (Reference Figure 3-10)

Inlet Guide Vane

Modifications to the inlet guide vane were based primarily on the results acquired from the related Energy Efficient Engine Subsonic Cascade Test Program (see Reference 1). These tests indicated that improved negative incidence capability could be obtained if the design incidence was adjusted from a build 1 value of -5 degrees to -3 degrees. This information was incorporated into the design of the build 2 low camber first vane. Furthermore, the vane leading edge was changed from a circular to an elliptical geometry for improved performance. Based on these results, the acceptable pressure distribution for the mean section of the inlet guide vane is shown in Figure 3-15.

The aerodynamic parameters of the build 2 inlet guide vane are presented in Table 3-VII. The airfoil stacking arrangement is shown in Figure 3-19.

3.2.4 Transition Duct Rig Description

The turbine transition duct rig is designed to simulate the full scale component in the Energy Efficient Engine in order to provide a comprehensive assessment of component aerodynamics. A cross-sectional view of the rig is presented in Figure 3-17. Basically, the rig has three major sections. The first is the rig inlet, which contains an inlet screen to regulate the inlet turbulence level and preswirl vanes to regulate air angle to the strut fairing. The second section is the transition duct itself, scaled to approximately 70 percent of the full size geometry. It also contains the strut fairings. The rig exit is the third section, which simulates the low-pressure turbine inlet and contains the low camber inlet guide vane.

ORIGINAL PAGE IS
OF POOR QUALITY

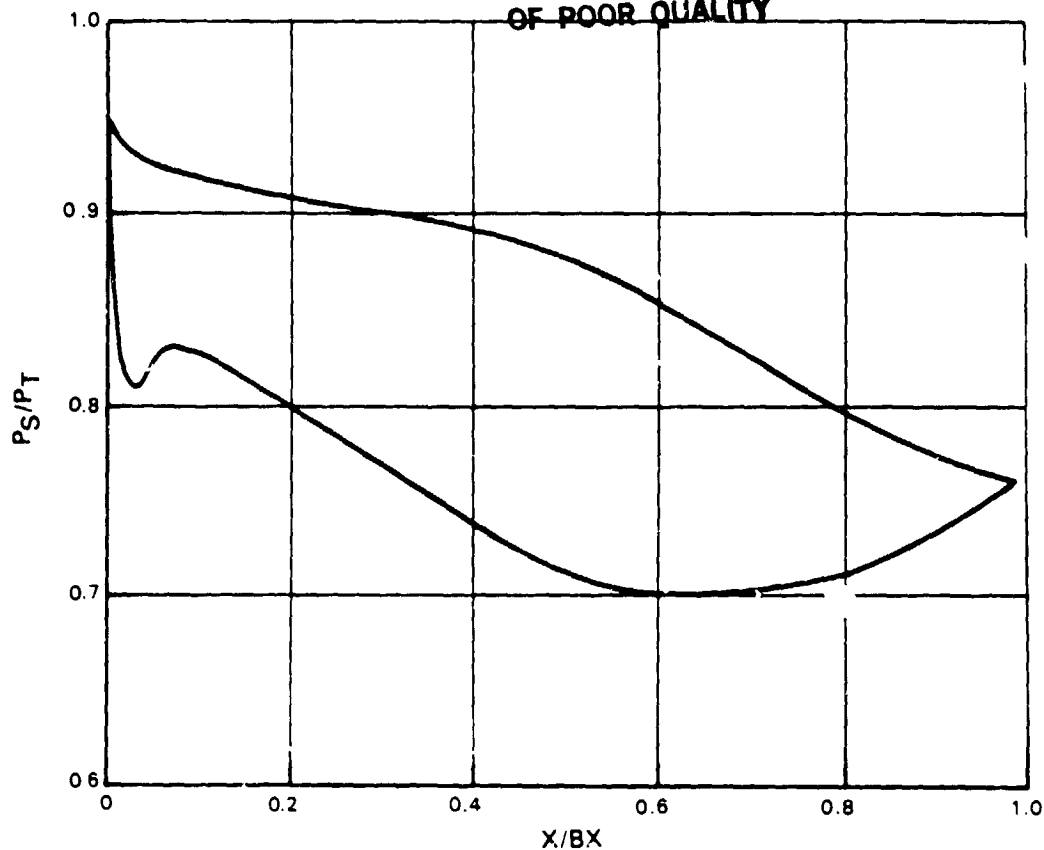


Figure 3-15 Inlet Guide Vane Mean Section Pressure Profile Mean Airfoil Section

TABLE 3-VII

LOW-PRESSURE TURBINE INLET GUIDE VANE GENERAL AERODYNAMICS
(Build 2)

	<u>Trailing Edge Root</u>	<u>Trailing Edge Mean</u>	<u>Trailing Edge Tip</u>
Radius, cm (in)	41.63 (16.39)	46.02 (18.12)	50.39 (19.84)
Actual Chord, cm (in)	6.98 (2.75)	7.13 (2.81)	7.59 (2.99)
Axial Chord, cm (in)	3.98 (1.55)	3.98 (1.57)	3.96 (1.56)
No. of Foils	54	54	54
Gap/Chord Ratio	1.21	1.35	1.48
Leading Edge Ellipse Ratio	4:1	4:1	4:1
Leading Edge Minor Axis, cm (in)	0.088 (0.035)	0.088 (0.035)	0.088 (0.035)
Inlet Metal Angle, deg	139.8	137.4	136.0
Inlet Air Angle, deg	142.8	140.4	139.0
Inlet Mach No.	0.403	0.377	0.267
Exit Metal Angle, deg	26.7	24.2	21.7
Exit Air Angle, deg	26.7	24.2	21.7
Exit Mach No.	0.652	0.654	0.541
Incidence Angle, deg	-3	-3	-3

ORIGINAL PAGE IS
OF POOR QUALITY

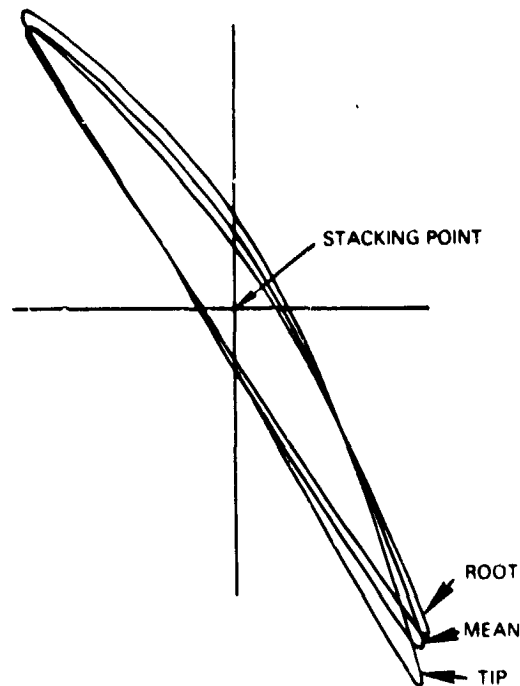


Figure 3-16 Build 2 Inlet Guide Vane Stacking Arrangement

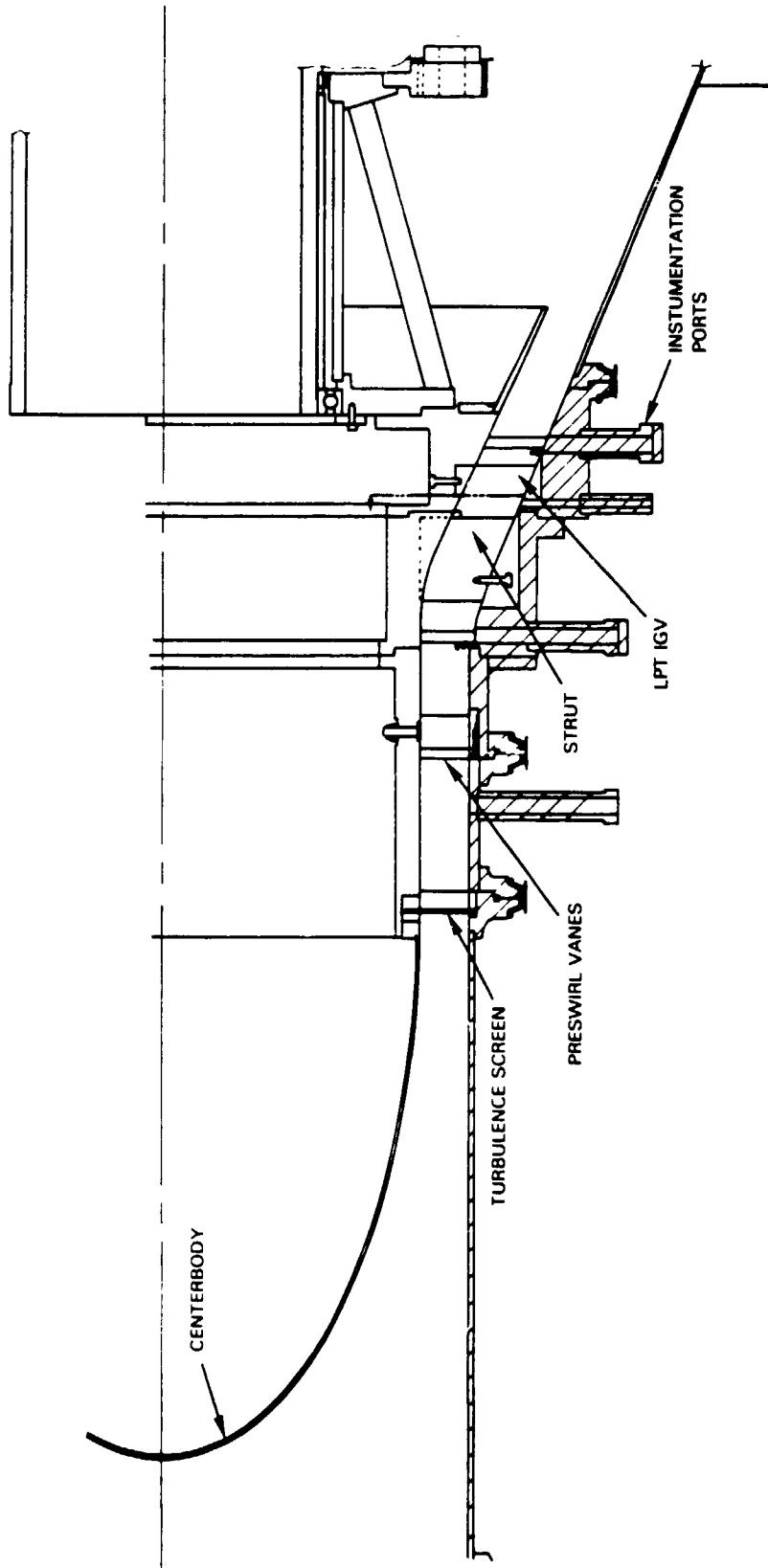
The rig was designed so that the inner body had a rotational capability of 55 degrees. This enabled precise indexing of the struts in relation to the instrumentation probes, which penetrated the flowpath from the outer wall at the strut fairing inlet, strut fairing exit, and low-pressure turbine inlet guide vane exit planes, as indicated in Figure 3-17.

The inner body of the rig was cantilevered off a bearing support and rotated from its downstream end by means of a positioning electric motor and reduction gearing. A potentiometer was connected to the gearing to determine the relative angular position of the rotating section. Control and instrumentation cables crossed through the exit plenum and exited through a side port.

The inlet screen was designed to reduce distortion from the inlet ducting and to produce a turbulence level of 4 percent at the inlet to the pre-swirl vanes for a more realistic representation of actual engine conditions. This screen was designed to produce a pressure loss of not more than one velocity head. The screen drag and turbulence design curves are shown in Figure 3-18.

Eighty pre-swirl vanes were used to match the exit air angle distribution of the high-pressure turbine component. These vanes were designed as double circular arc airfoils. The design section pressure distributions for this type of airfoil are represented in Figure 3-19. These airfoils were mounted on a stem to allow restaggering for off-design testing.

ORIGINAL PAGE IS
OF POOR QUALITY



CROSS HATCHED PARTS-NON ROTATING

Figure 3-17 Energy Efficient Engine Transition Duct Rig

ORIGINAL DESIGN
OF POOR QUALITY

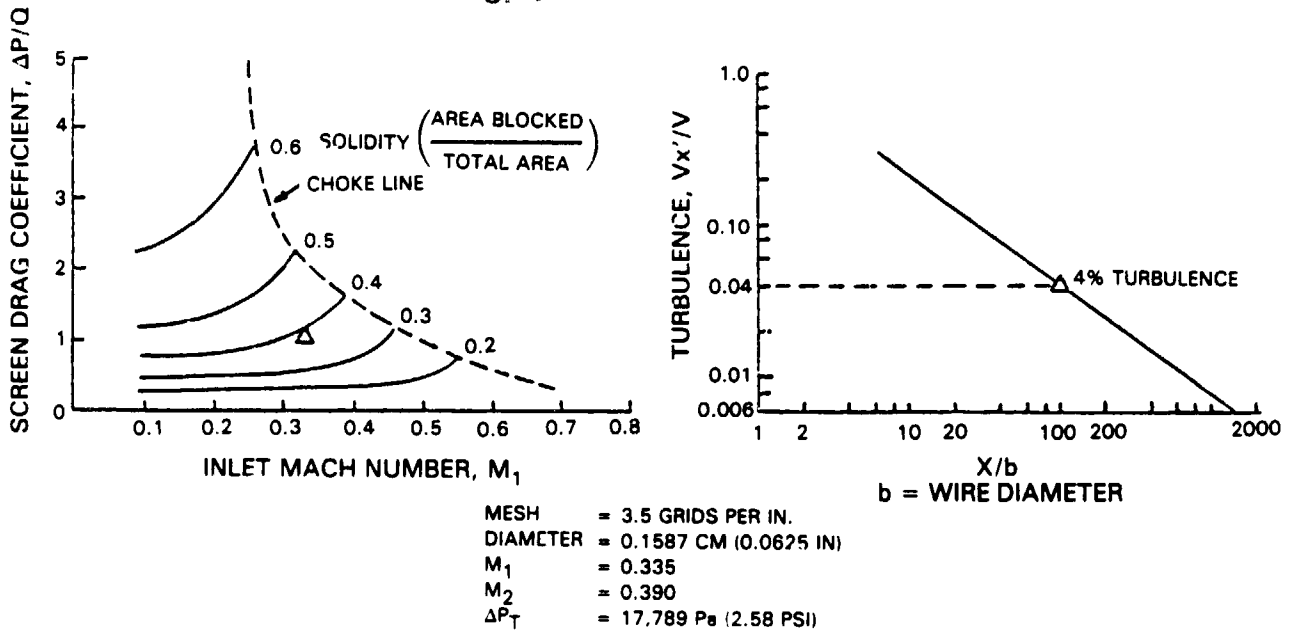


Figure 3-18 Transition Duct Inlet Screen Design Characteristics

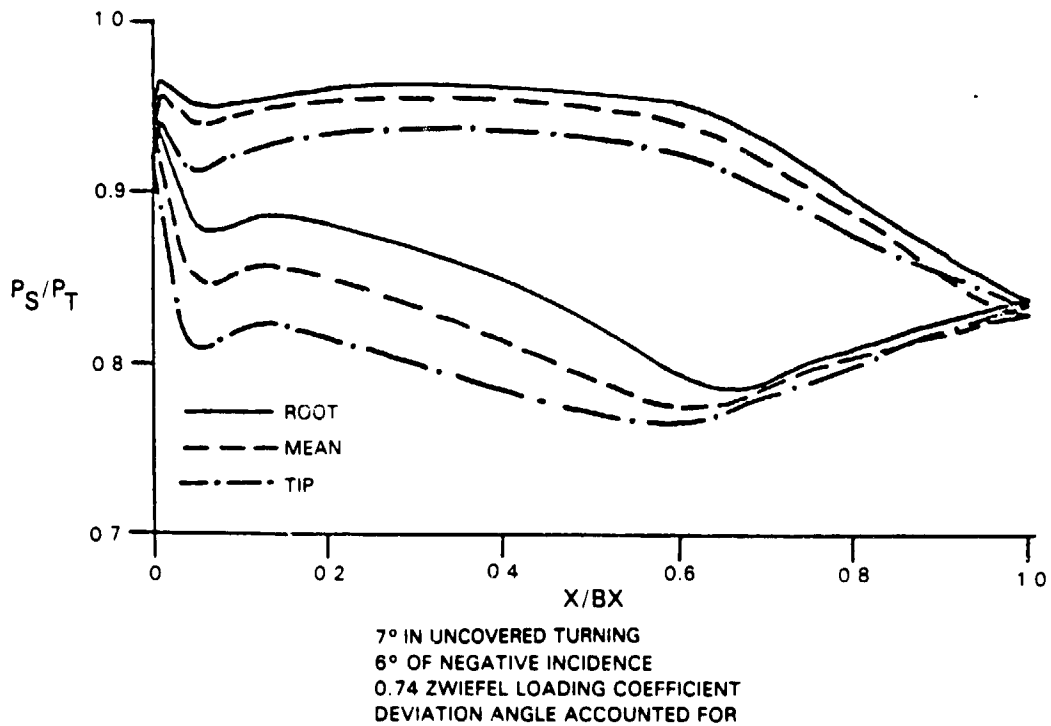


Figure 3-19 Transition Duct Preswirl Vane Design Characteristics

The struts, low-pressure turbine inlet guide vanes, and turbulence screen were bolted to and rotate with the aluminum inner body. The contoured outer wall shroud sections were also made of aluminum. These shroud sections were bolted to the struts and vanes, permitting simultaneous rotation of both the vanes and shroud sections. The shrouds were sealed against the outer body with Teflon 'O' rings to prevent flow leaks. The spun aluminum centerbody seated onto the inner rig section to complete the duct test section.

The rig featured quick-disconnect band clamps and 14 instrument probe ports. The quick-disconnect band clamps permitted rapid disassembly of the rig, which facilitated pre-swirl vane adjustments. The 14 instrument probe ports permitted quick probe changes and facilitated probe lead connection checks.

3.3 RIG FABRICATION AND ASSEMBLY

3.3.1 Fabrication

Transition duct components and adapting facility hardware were fabricated from conventional materials using standard machining operations. The flowpath was fabricated from aluminum, and pre-swirl vanes were fabricated from 316 stainless steel sheet metal.

In build 1, twenty turbine transition duct strut fairings were machined to the design contour from 6061-T-6 aluminum. Three sections of four of these fairings were arc-traced and showed a maximum deviation of 0.050 cm (0.020 in) at the leading edge. All were within specification at mid-chord.

Eleven turbine transition duct structural strut fairing were machined to the build 2 design contour from 6061-T-6 aluminum. Three sections on all eleven struts were arc-traced. The maximum deviation was 0.040 cm (0.016 in) at the leading edge of the fairing. All were within specification at mid-chord.

Sixty inlet guide vanes were machined to the build 1 design contour from 6061-T-6 aluminum. Three sections on four of the airfoils were arc-traced and were within ± 0.010 cm (0.004 in) of design intent.

Sixty inlet guide vanes were also machined to the build 2 design contour from 6061-T-6 aluminum. Three sections on four of these airfoils were arc-traced, and fifty-four of these airfoils were selected on the basis of chord length and surface finish inspections.

3.3.2 Assembly

Following fabrication, the pre-swirl vanes were installed into the inlet ring, and each vane chord angle was individually set to an average angle of 121.3 degrees with a standard deviation of 0.34 percent for build 1 and an average angle of 119.7 degrees with a standard deviation of 0.08 percent for build 2. These airfoils were restaggered for the off-design test to 111.3 degrees with a standard deviation of 0.1 percent for build 1 and to 112.8 degrees with a standard deviation of 0.1 percent for build 2.

The fairing was bolted into slots in the inner flowpath. The strut tips were then machined to match the flowpath, and the outer shroud was bolted into place. The gap resulting from the intersection of the strut and flowpath was filled with epoxy to match the engine fillet radius. The location of the strut in build 1 was shifted forward 0.25 cm (0.10 in). In build 2 it was within print tolerance. The stagger angles for both builds were within 0.1 degree.

The inlet guide vanes were bolted into slots in the inner flowpath. The vane tips were machined to match the flowpath, and the outer shroud was bolted into place. The gap resulting from the intersection of the vane and flowpath was filled with epoxy to match the engine fillet radius. For both builds, the location of the vanes was within 0.012 cm (0.005 in) of axial location and within 0.1 degree of stagger.

The flowpath and airfoils were final assembled at the test stand with the required instrumentation. The final assembled rig is shown in Figure 3-20.



Figure 3-20 Assembled Test Rig

SECTION 4.0

TEST PROGRAM AND PROCEDURES

4.1 TEST PLAN

The test program comprised two phases. In the first phase (build 1), the transition duct for the flight propulsion system was evaluated, while the second phase (build 2) focused on substantiating design changes for the transition duct in the integrated core/low spool. However, before the rig test program was initiated, a series of functional test system checks was conducted. Verification of the operation of data acquisition systems and test instrumentation and rig and facility plumbing hookups was made. The rig test program was initiated after satisfactory operation of these systems was demonstrated.

The test matrices for builds 1 and 2 are presented in Tables 4-I and 4-II, respectively. As shown, each phase of testing consists of two main tests. The first test was structured to assess transition duct rig aerodynamic performance at design conditions. For the second test, the rig inlet air angle was varied to evaluate the aerodynamic tolerance of the transition duct rig to high-pressure turbine off-design exit conditions. For each test series, the rig inlet temperature was 65°C (150°F). The inlet pressure was varied between 117,211 to 124,106 Pa (17 to 18 psia), until the desired strut inlet Mach numbers, shown in Table 4-I, were attained. This enabled the rig to match the Reynolds number at the engine conditions.

Testing at both design and off-design conditions involved a series of three individual data acquisition points, as shown in the test matrices. The format outlined in the following paragraphs was employed for each of the two tests in each build.

Testing at the first point was conducted to obtain the axial static pressure distribution on the outer wall in order to ascertain if the flow was separation free. Also, a spanwise and gapwise traverse of the strut fairing inlet and exit planes was made with total pressure and air angle probes to evaluate the high-pressure turbine exit conditions, the transition duct and strut fairing pressure loss characteristics and the inlet conditions to the low-pressure turbine inlet guide vane. After the required data were accumulated, the rig was shut down so that the traversing instrumentation at the strut fairing exit plane could be moved to the inlet guide vane exit for the next acquisition point.

In the second data acquisition, a spanwise and gapwise traverse of the strut fairing inlet and the low-pressure turbine guide vane exit was performed to determine the pressure loss from the transition duct inlet to the exit of the exit guide vane, and the low-pressure turbine first rotor inlet conditions.

The final acquisition was conducted to obtain axial static pressure distributions of the inner wall to determine if the flow was separation free. Strut fairing surface static pressures were measured at 10, 50, and 90 percent span to determine if the desired aerodynamics were achieved. The surface static pressure at 50 percent span of the turbine inlet guide vane was also measured to determine whether the guide vane was separation free and achieved the desired aerodynamics.

TABLE 4-1
DATA ACQUISITION SEQUENCE BUILD 1

(Test 1 - Design Conditions)

<u>Acquisition Point</u>	<u>Instrumentation</u>	<u>Inlet Conditions</u>		
		<u>Mach No</u>	<u>Air Angle</u>	<u>Reynolds No</u>
1	Outer Wall Statics Inlet Probes Strut Fairing Exit Probes	0.510	46.0 deg	4.6x10 ⁵
2	Inlet Probes Inlet Guide Vane Exit Probes	↓	↓	↓
3	Strut Fairing Contour Static Pressure Taps Inlet Guide Vane Contour Static Pressure Taps Inner Wall Statics			

(Test 2 - Off-Design Conditions)

1	Outer Wall Statics Inlet Probes Strut Fairing Exit Probes	0.460	51.0 deg	4.3x10 ⁵
2	Inlet Probes Inlet Guide Vane Exit Probes	↓	↓	↓
3	Strut Fairing Contour Static Pressure Taps Inlet Guide Vane Contour Static Pressure Taps Inner Wall Statics			

TABLE 4-II

DATA ACQUISITION SEQUENCE BUILD 2

(Test 1 - Design Conditions)

<u>Acquisition Point</u>	<u>Instrumentation</u>	<u>Inlet Conditions</u>		
		<u>Mach No</u>	<u>Air Angle</u>	<u>Reynolds No</u>
1	Outer Wall Statics Inlet Probes Strut Fairing Exit Probes	0.567	43.6 deg	5.0×10^5
2	Inlet Probes Inlet Guide Vane Exit Probes	↓	↓	↓
3	Strut Fairing Contour Static Pressure Taps Inlet Guide Vane Contour Static Pressure Taps Inner Wall Statics			

(Test 2 - Off-Design Conditions)

1	Outer Wall Statics Inlet Probes Strut Fairing Exit Probes	0.501	48.6 deg	4.6×10^5
2	Inlet Probes Inlet Guide Vane Exit Probes	↓	↓	↓
3	Strut Fairing Contour Static Pressure Taps Inlet Guide Vane Contour Static Pressure Taps Inner Wall Statics			

4.2 INSTRUMENTATION

The test rig incorporated a sufficient number of sensors to determine total pressure loss, wall pressure coefficients, airfoil pressure distributions, Mach numbers, and air angles. This instrumentation consisted of surface static pressure taps, total pressure rakes, wedge probes, boundary layer probes, and claw probes. The instrumentation used in the build 1 transition duct rig is listed in Table 4-III, and that used in the build 2 rig is listed in Table 4-IV.

Traversing probes were positioned at the strut fairing inlet, strut fairing exit and inlet guide vane exit planes. Probes at the strut fairing and inlet guide vane exit were circumferentially located 1.5 strut gaps apart. The probes were positioned so that the same strut fairing could be traversed past both probes during a traverse of 2 strut gaps, thereby allowing a direct comparison of 2 probe readings at the same location. They were also positioned so that any wakes resulting from the strut fairing inlet instrumentation did not influence the instrumentation at strut fairing exit or inlet guide vane exit. Figures 4-1 and 4-2 show the relative position of the instrumentation in the build 2 rig (view looking at the inner radius) and the build 2 airfoils (view looking at the outer diameter radius).

TABLE 4-III
TRANSITION DUCT RIG (BUILD 1) INSTRUMENTATION

<u>Type</u>	<u>Quantity</u>	<u>Angle (deg)</u>
<u>Inlet Reference</u>		
Total Pressure and Total Temperature	3	(at 90, 210, and 330 deg)
<u>Strut Fairing Inlet</u>		
Boundary Layer	2	six-element (at 340 deg, OD, and ID)
Wedge Probe	2	(at 174 and 354 deg)
Total Pressure Rake	2	ten-element rakes (at 20 and 200 deg)
<u>Strut Fairing Exit</u>		
Claw Probe	2	(at 10 and 50 deg)
<u>Inlet Guide Vane Exit</u>		
Total Pressure Rake	4	ten-element rakes (at 0, 40, 180, and 220 deg)
Claw Probe	2	(at 30 and 350 deg)

TABLE 4-III (continued)

Static Pressure Taps

<u>Type</u>	<u>Quantity</u>	<u>Angle (deg)</u>
Inner and Outer Duct Wall	54	Starting at Trailing Edge of Pre-Swirl Vanes and Proceeding Every 1.25 cm (0.5 in) Axially to Rig Exit - Following Streamtube
Strut Fairing Inlet Inner Wall	4	Equally Spaced
Strut Fairing Inlet Outer Wall	4	Equally Spaced
One Strut Passage:		
	10	- 10% Span Pressure Side
	10	- 50% Span Pressure Side
	10	- 90% Span Pressure Side
	10	- 10% Span Suction Side
	10	- 50% Span Suction Side
	10	- 90% Span Suction Side
Strut Trailing Edge	1	at 50% Span
Strut Trailing Edge	6	at ID Wall
Strut Fairing Exit Outer Wall	4	Equally Spaced
One LPT First Stage Vane Passage:		
	10	- 50% Span Suction Side
	5	- 50% Span Pressure Side
	1	- 50% Span Trailing Edge
Inlet Guide Vane Exit Inner Wall	4	Equally Spaced
Inlet Guide Vane Exit Outer Wall	4	Equally Spaced

TABLE 4-IV
TRANSITION DUCT RIG (BUILD 2) INSTRUMENTATION

<u>Type</u>	<u>Quantity</u>	<u>Angle (deg)</u>
<u>Inlet Reference</u>		
Total pressure 50% Span	3	4.72 in Upstream of turbulence screen at 90, 210, and 330 deg
Total temperature 50% Span	3	
<u>Strut Fairing Inlet</u>		
Total pressure rake	2*	20, 200
Wedge/Claw probe	2	167.3, 347.3
Boundary layer probe	2	340 (ID and OD)
Inner wall static pressure	4	0, 90, 180, 270
Outer wall static pressure	4	0, 90, 180, 270
<u>Strut Fairing Exit</u>		
Claw probe	2	16.37, 65.46, 130.92, 327.28
Inner wall static pressure	4	0, 90, 180, 270
Outer wall static pressure	4	0, 90, 180, 270
<u>Inlet Guide Vane Exit</u>		
Total pressure rake	4*	0, 49.1, 180, 229.1
Claw probe	2	39.09, 350
Inner wall static pressure	4	30, 120, 210, 300
Outer wall static pressure	4	30, 120, 210, 300
<u>Static Pressure Taps</u>		
Streamwise inner wall static pressure**	27	every 1.25 cm (0.50 in) axially
Streamwise outer wall static pressure**	27	every 1.25 cm (0.50 in) axially
<u>Strut contour static pressure</u>		
10% Span	20	<u>Percent Axial Chord</u> Pressure Surface: 5, 10, 15, 20, 30, 34, 60, 70, 80, 90
50% Span	21	Suction Surface: 5, 10, 15, 20, 30, 45, 60, 70, 80, 90
90% Span	20	In addition to above, 50% span has 1 tap at 100% chord.
<u>Strut pitchwise static pressure</u>		
Inner wall	6	Equally spaced across gap
Outer wall	6	
<u>Inlet Guide Vane Contour static pressure</u>		
50% Span	16	<u>Percent Axial Chord</u> Pressure Surface: 5, 10, 25, 50, 75; Suction Surface: 5, 10, 20, 30, 40, 50, 60, 70, 80, 90; 1 tap at 100% chord

* ten element

** One streamline, from the strut fairing inlet to the rig exit, was instrumented with static pressure taps.

ORIGINAL PAGE IS
OF POOR QUALITY

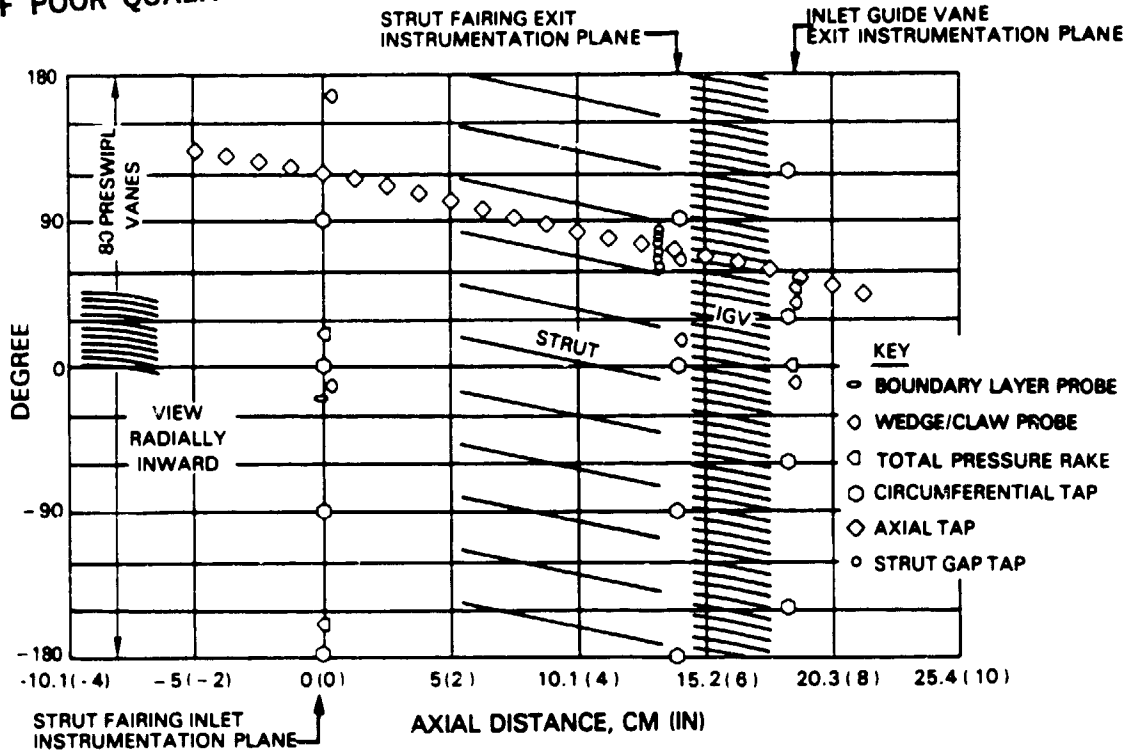


Figure 4-1 Instrumentation Map - Build 2 Inner Diameter

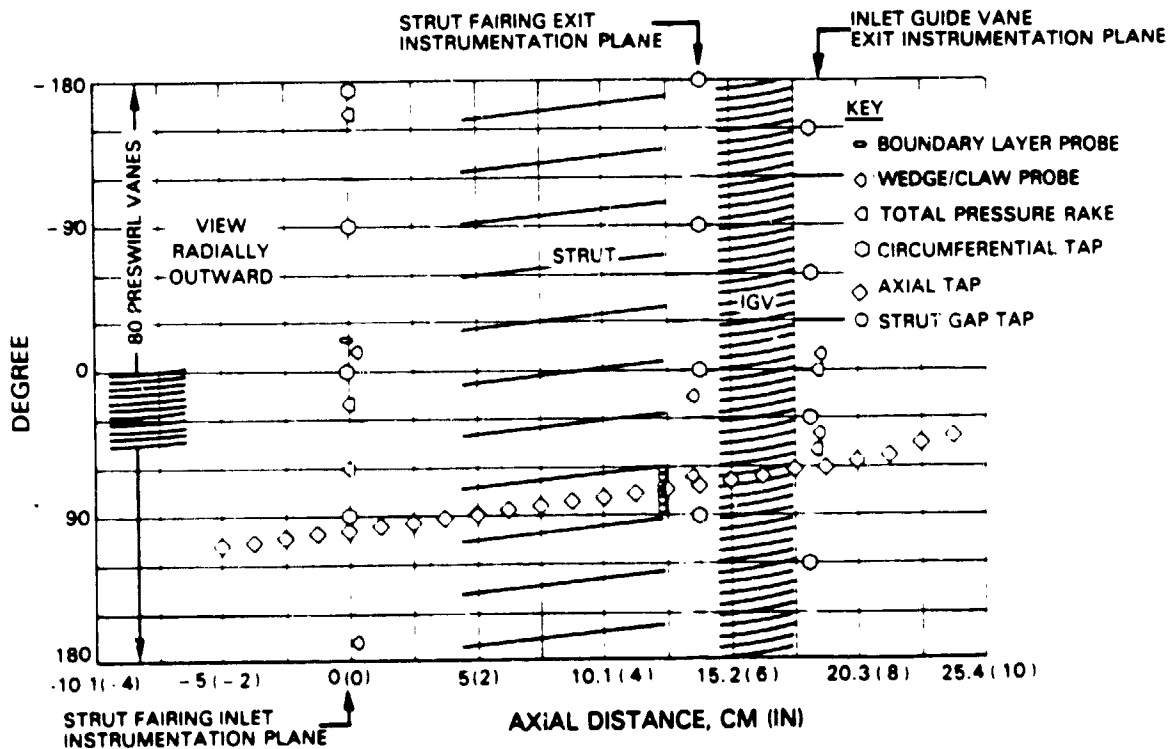


Figure 4-2 Instrumentation Map - Build 2 Outer Diameter

4.2.1 Surface Static Pressure Taps

The surface static pressure taps were located at the inner and outer duct wall, starting at the trailing edge of the pre-swirl vanes and proceeding every 1.25 cm (0.5 in) axially toward the rig exit. Selected strut fairings were instrumented with static pressure taps at 10, 50 and 90 percent span to record airfoil pressure distributions. Also, selected inlet guide vanes were instrumented at 50 percent span for the acquisition of pressure distribution data.

4.2.2 Total Pressure Rakes

The total pressure rake shown in Figure 4-3 was used at the strut fairing inlet and inlet guide vane exit planes to record inlet and exit total pressure. These probes had 10 kiel heads across the span and remained stationary as the airfoils rotated, producing a circumferential traverse. The kiel head probes were calibrated as a function of Mach number and had an error of less than 0.01 percent.

4.2.3 Wedge Probes

Wedge probes were used at the strut fairing inlet plane to measure total pressure, static pressure, and air angle. This probe, as shown in Figure 4-4, featured a leading edge sensor to record total pressure and two static pressure sensors on the side of the probe that were balanced to measure air angle. The wedge probe traversed in a radial direction and remained stationary as the airfoils rotated, producing a circumferential traverse.

With the probe balanced, the leading edge sensor was calibrated for total pressure as a function of Mach number and found to have a error of less than 0.01 percent. The side sensors for the balanced probe were calibrated for static pressure as a function of Mach number, as shown in Figure 4-5.

4.2.4 Claw Probes

Claw probes were used at both the strut fairing exit and inlet guide vane exit because they permitted measurements closer to the wall than the wedge probe. The claw probe functioned similarly to the wedge probe and measured both total pressure and air angle. The claw probe traversed in a radial direction and remained stationary as the airfoils rotated, producing a circumferential traverse. The leading edge sensor was calibrated for total pressure as a function of Mach number and had an error of less than 0.01 percent.

4.3 TEST FACILITY

The transition duct rig was run at the United Technologies Research Center (UTRC) jet burner test stand. This stand is a self-contained cold flow and combustion facility having seven test cells, three control rooms, a compressor room, work area, and fuel pump room. Three of the seven test cells are designed for hot flow or combustion testing. The remaining four are utilized for cold flow testing such as that conducted in this program



Figure 4-3 Total Pressure Rake Used at the Strut Fairing Inlet and Inlet Guide Vane Exit Planes



Figure 4-4 Wedge Probe Used at the Strut Fairing Inlet Plane to Measure Total Pressure, Static Pressure, and Air Angle

ORIGINAL PAGE IS
OF POOR QUALITY

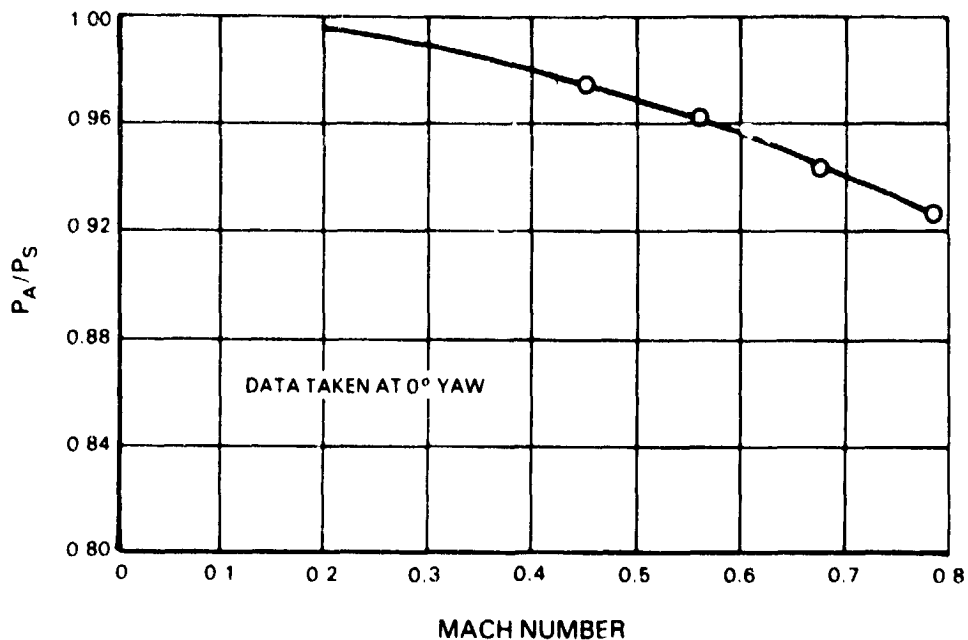


Figure 4-5 Wedge Probe Calibration Results

Low-pressure air is supplied to the cold flow test cells and to one combustion test cell by two multistage Allis-Chalmers compressors nominally rated at an airflow rate of 19 kg/sec (43 lb/sec) at a pressure of 202,707 Pa (29.4 psi) and 7 kg/sec (17 lb/sec) at a maximum pressure of 340,603 Pa (49.4 psi). This air may be heated to 204°C (400°F) with a Todd heat exchanger. Test stand piping and valving permit the compressors to be used as exhausters. A pressure ratio greater than 8:1 may be obtained by using one of the compressors on pressure and the other one as an exhauster.

High-pressure air is also available to all test cells at steady state airflow rates of up to 4 kg/sec (10 lb/sec) at pressures up to 2,068,440 Pa (300 psi). Higher airflow rates of up to 68 kg/sec (150 lb/sec) may be obtained by 'blowing down' three 1524 m³ (5000 ft³) storage tanks, which are part of the system and are pressurized to 2,757,920 Pa (400 psi) by the compressors. At full pressure, the tanks hold 13,970 kg (30,800 lbs) of air. The cold flow, high-pressure air supply can be boosted to 3,998,984 Pa (580 psi) at steady state airflow rates of up to 1.82 kg/sec (4 lb/sec) by a boost compressor.

4.4 DATA RECORDING AND REDUCTION

4.4.1 Data Recording

All rig data were collected through the United Technologies Research Laboratories Low Speed Acquisition and Recording Console (LARC). This system records data onto a section of Univac magnetic tape, and checks the recorded value against the input. All of the pressures, temperatures and air angles were recorded in this manner.

Raw data were available for individual sensor readings during the run. A complete data collection printout was available within 24 hours.

4.4.2 Data Reduction

The data from the Low Speed Acquisition and Recording Console tape were first computer processed to apply the required probe calibrations and to order the data. The data were then plotted and reviewed to permit an identification of any data anomalies. Following the review, the ordered data were processed to average the total pressures, air angles, and static pressures measured during data acquisitions 1 and 2. From these data, Mach numbers at the three instrumentation locations were calculated, along with the pressure losses for the transition duct and the transition duct and the inlet guide vane.

Spanwise profiles of total pressure, air angle and Mach number were plotted at the three instrumentation locations. In addition, spanwise loss profiles were plotted for the transition duct and for the transition duct and inlet guide vane.

4.4.3 Data Acquisition System Accuracy

The data acquisition system for the transition duct test measured and recorded pressures, temperatures, and air angles. The type of data acquired and the degree of accuracy for each type recorded are described in the following paragraphs.

Pressure measurements were made using calibrated probes and static taps. The pressures were measured using transducers, which were calibrated with dead weight testers and traceable to the National Bureau of Standards. The output from the transducers was recorded using the United Technologies Research Laboratories Low Speed Acquisition and Recording Console (LARC) system. The accuracy of this system for pressure measurements was 0.15 percent.

Temperature measurements were made using standard thermocouple wire and an electronic ice junction. The accuracy of this system for temperature measurement was 2.2°C (4°F).

Air angle was measured with a balancing air angle probe mounted in a rotating traverse can. The angular rotation of the probe was measured using a shaft encoder mounted on the traverse can (the shaft encoder reading was calibrated at the test stand to the true position of the probes). The probe was then rotated in the flow stream while the rig was operational. This was done until the side pressure taps of the probes were balanced. The shaft encoder reading of the balanced probe was then recorded on the LARC data recording system. The accuracy of this system for air angle measurements was 3 degrees.

SECTION 5.0

RESULTS AND ANALYSIS

5.1 INTRODUCTION

This section presents the results and analysis of data acquired from builds 1 and 2. For the most part, data for each build are compared to the prediction at design conditions. Direct comparisons between data from builds 1 and 2, however, are not meaningful because of the geometry differences between the two transition duct configurations

The following section, Section 5.2, provides a characterization of system aerodynamics. The discussion of results is presented in terms of strut fairing inlet aerodynamics, strut fairing exit aerodynamics, and rig duct exit aerodynamics. Section 5.3 contains pressure distributions of the duct walls, strut fairing and low-pressure turbine inlet guide vane. Section 5.4 presents a summary of the test results.

5.2 AERODYNAMIC CHARACTERIZATION

5.2.1 Strut Fairing Inlet Aerodynamics

Strut fairing inlet conditions were set to match the high-pressure turbine design exit conditions by adjusting the rig flow and preswirl vane stagger angle. Off-design inlet conditions were set by revising the inlet angle 5 degrees more axial with the preswirl vanes and using the same flow rate.

The measured build 1 inlet air angle average spanwise profile at design and off-design conditions is compared to the design point prediction in Figure 5-1. This figure shows that the spanwise average of the measured inlet angles at design conditions is 0.8 degree more tangential than the design intent and the spanwise measured profile matches the predicted profile to within 2 degrees. Results at off-design conditions show the average inlet angle to be 4.1 degrees more axial than the design point data with a spanwise profile that has approximately the same slope. The 4.1 degree difference is sufficiently large to indicate the effect of off-design operation.

Similar measurements for the build 2 rig are shown in Figure 5-2. This figure shows that at the design conditions the average inlet angle is 1.5 degrees more tangential than the prediction and the spanwise profile has a steeper slope. At the root, the air angle is 5 degrees more tangential than the design intent, which caused the strut fairing incidence to become approximately 3 degrees positive. The off-design data show the average inlet angle to be 7.1 degrees more axial than the design point data with a spanwise profile that has approximately the same slope. With this angle, both design and off-design data bracket the prediction and the difference is sufficiently large to indicate the effects of off-design operation.

ORIGINAL PAGE IS
OF POOR QUALITY

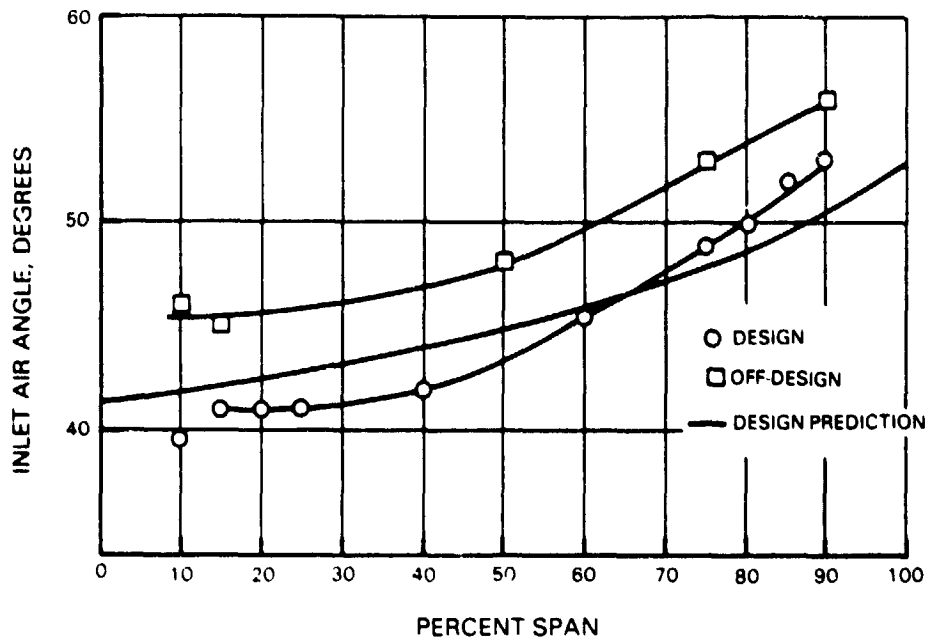


Figure 5-1 Build 1 Strut Fairing Inlet Air Angle Average Spanwise Profile

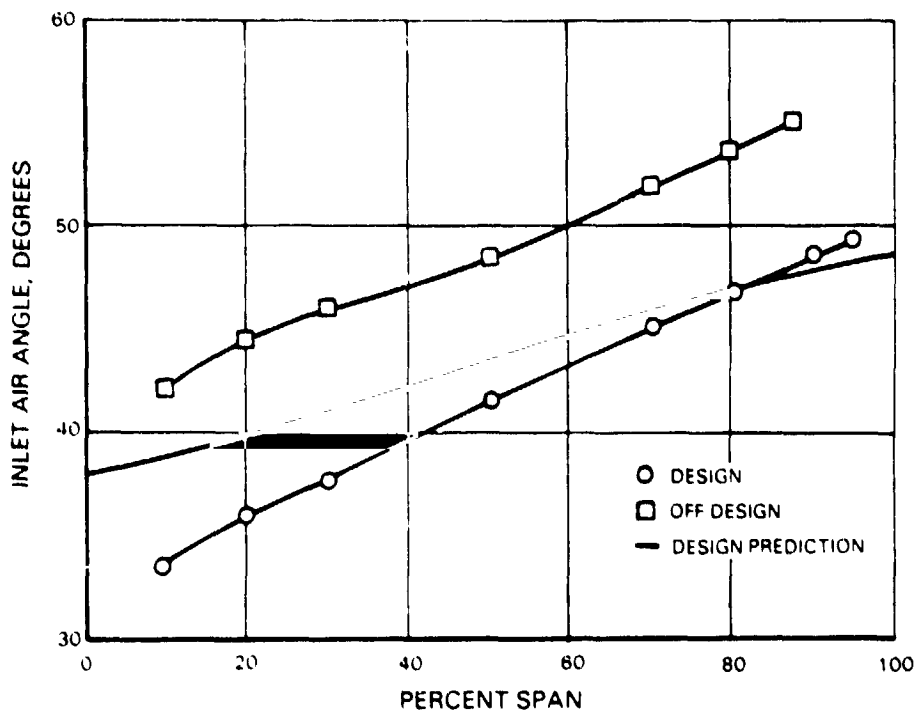


Figure 5-2 Build 2 Strut Fairing Inlet Air Angle Average Spanwise Profile

The inlet Mach number average spanwise profile was calculated using the spanwise total pressure data from the wedge probes and a linear interpolation between the inner and outer wall static pressure taps. The build 1 average spanwise Mach number profiles are presented in Figure 5-3. This figure shows the average design point inlet Mach number is 0.03 below the design intent of 0.51. Off-design data show a decrease in average inlet Mach number to 0.44. This was a result of continuity, i.e. flow level was maintained with a more axial inlet angle which resulted in a lower inlet velocity.

The build 2 average spanwise Mach number profiles are presented in Figure 5-4. This figure shows the average design point inlet Mach number is 0.04 above the design intent level of 0.57. The off-design data show a decrease in average inlet Mach number to 0.50, which is again a result of continuity.

Table 5-I presents a summary of the strut fairing inlet conditions. Overall, the measured inlet angles and Mach numbers are in close agreement to the design intent.

TABLE 5-I
SUMMARY OF STRUT FAIRING INLET CONDITIONS

<u>Build 1</u>	<u>Design Intent</u>	<u>Design Measured</u>	<u>Off-Design Intent</u>	<u>Off-Design Measured</u>
Inlet Angle, deg	46.0	45.2	51.0	49.3
Inlet Mach No.	0.510	0.48	0.46	0.44
<u>Build 2</u>				
Inlet Angle, deg	43.6	42.1	48.6	49.2
Inlet Mach No.	0.567	0.605	0.501	0.504

5.2.2 Strut Fairing Exit Aerodynamics

Pressure Loss Assessment

The total pressure loss across the transition duct was measured by a simultaneous traverse of the strut fairing inlet and exit. The build 1 duct spanwise average total pressure loss at both design and off-design conditions is shown in Figure 5-5. At design point conditions, the trend shows the high loss regions to be within approximately 25 percent span of the inner wall and 15 percent span of the outer wall. When design data are mass averaged with the corresponding spanwise air angle profile, the loss level is 0.7 percent $\Delta P_T/P_T$, which meets the goal for the flight propulsion system transition duct design. Moreover, this level of pressure loss is substantially lower than the design prediction of 1.5 percent.

ORIGINAL PAGE IS
OF POOR QUALITY

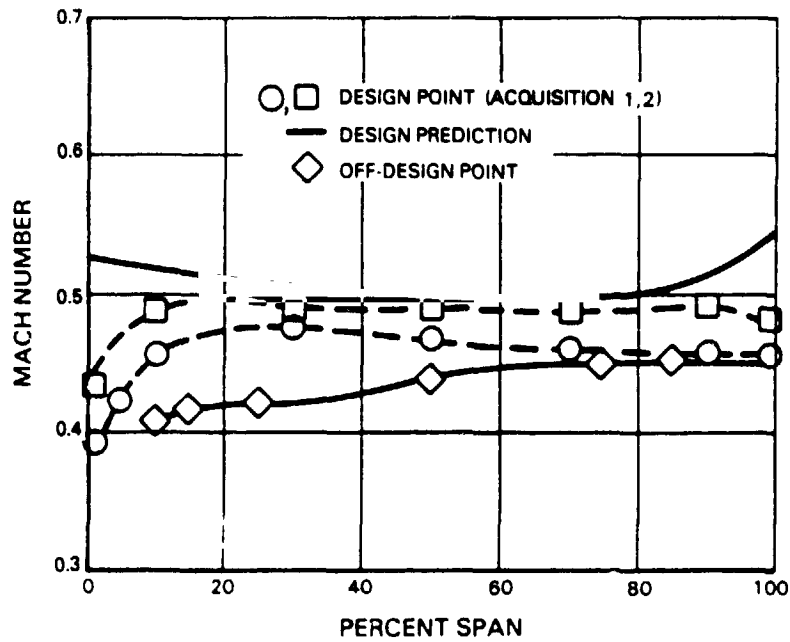


Figure 5-3 Build 1 Average Strut Fairing Inlet Spanwise Mach Number Profiles

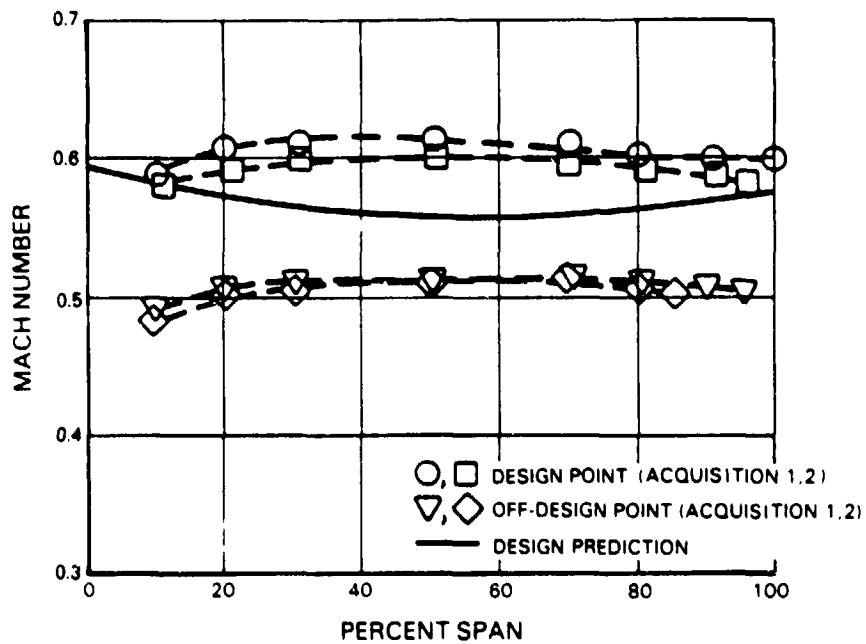


Figure 5-4 Build 2 Average Strut Fairing Inlet Spanwise Mach Number Profiles

ORIGINAL PAGES
OF POOR QUALITY

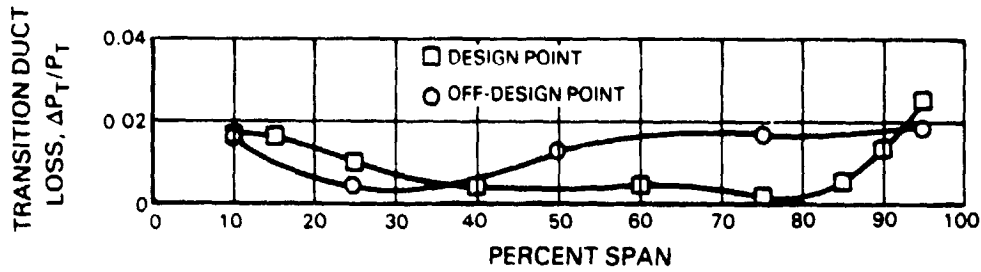


Figure 5-5 Build 1 Transition Duct Pressure Loss

At off-design conditions, the pressure loss is lower in the inner region and higher from approximately 30 percent span towards the tip. The mass averaged loss at off-design is 1.3 percent $\Delta P_T/P_T$. In comparison to the design value, this higher loss is a result of the nonworking strut fairing being required to turn the air.

Figure 5-6 shows the measured duct pressure loss in the build 2 configuration at design and off-design conditions. Data trends at design conditions show that the high loss regions are within approximately 30 percent span of the inner and outer walls. The mass averaged loss was 1.59 percent $\Delta P_T/P_T$, which was lower than the prediction of 1.8 percent. At off-design, the pressure loss is lower in the inner and outer regions but slightly higher in the midspan region. The mass averaged loss for the off-design point was 1.37 percent $\Delta P_T/P_T$. The lower loss at off-design is a result of the lower endwall loss from a more axial inlet angle (reduced turning) and the lower inlet Mach number.

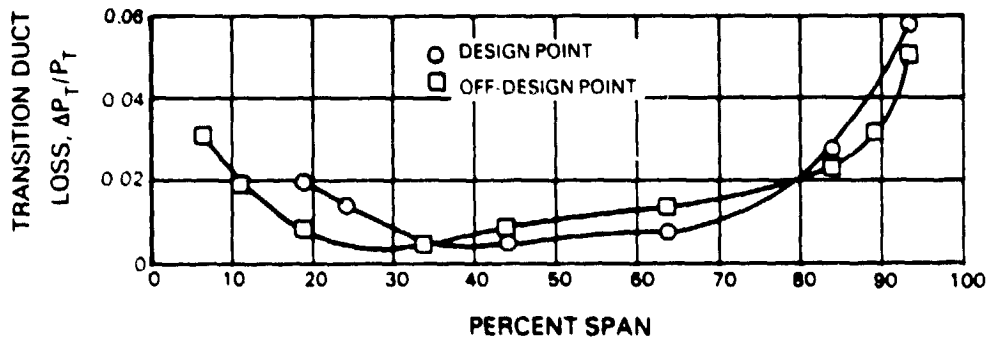


Figure 5-6 Build 2 Transition Duct Pressure Loss

Figure 5-7 presents a pressure loss contour of the strut fairing exit plane for build 2 at design conditions. This profile shows the influence of the strut fairing wake, as well as inner and outer endwall loss gradients. As indicated, the majority of loss is restricted to the endwall region. At off-design conditions, shown in Figure 5-8, endwall losses are somewhat lower, while the pressure loss is increased in the midspan region of the strut fairing wake.

Exit Air Angle Assessment

In Figure 5-9, measured spanwise strut fairing exit angle data at design and off-design conditions are compared to the design prediction for the build 1 configuration. The data show the exit angle to be approximately 3 degrees more tangential than design across the span. In general, the data are in good agreement with the spanwise slope of the predicted air angle and within the accuracy range for air angle measurement. Although off-design data are limited, the trend suggests that even with a 4.1 degree more axial inlet angle the strut returned the flow to the same level of exit angle as was obtained with design point inlet conditions.

Similar spanwise trends of measured and predicted strut fairing exit angle data are presented in Figure 5-10 for build 2. At design conditions, the exit angle is approximately 4 degrees more axial than the design intent and becomes more tangential from 75 percent span to the tip. This distribution, which indicates a decrease in air flow toward the tip, is caused by viscous effects generated by the turning strut fairing. These effects were not included in the inviscid prediction. The absolute level of the measured air angle measurement showed an average of 4 degrees more axial air angle than the design prediction. Results from a pressure distribution analysis of the strut fairing, as discussed in Section 5.3.2, showed a 3 degree difference as a result of a measurement error. When the data are adjusted for this anomaly, as indicated by the dashed line in Figure 5-10, the overall impact is only an average of 1 degree. Therefore, the build 2 design point air angle profiles are close to the design intent and compatible to the low pressure turbine inlet guide vane.

At off-design, the measured data show the effect of 6.8 degrees more axial inlet flow. For this case, the air becomes 2.8 degrees more axial than the design point data. The spanwise slope of the data is similar to that for the design point and shows the same viscous flow effect in the tip region. This result shows a reduction in deviation (metal angle minus air angle) from the design point because of the lower amount of strut fairing turning at off-design conditions.

ORIGINAL PAGE IS
OF POOR QUALITY

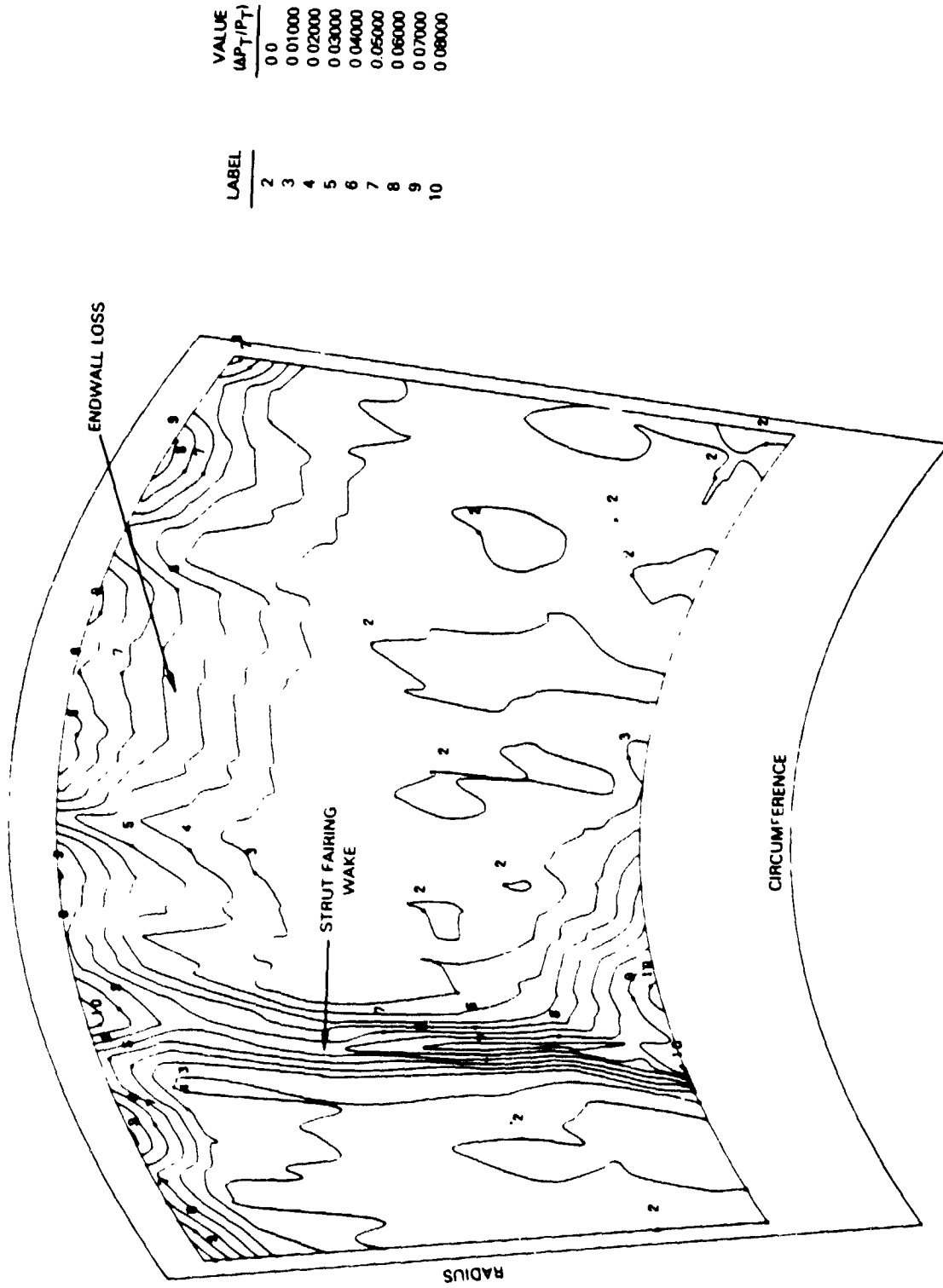


Figure 5-7 Strut Fairing Loss Contour Profile for Build 2 At Design Conditions

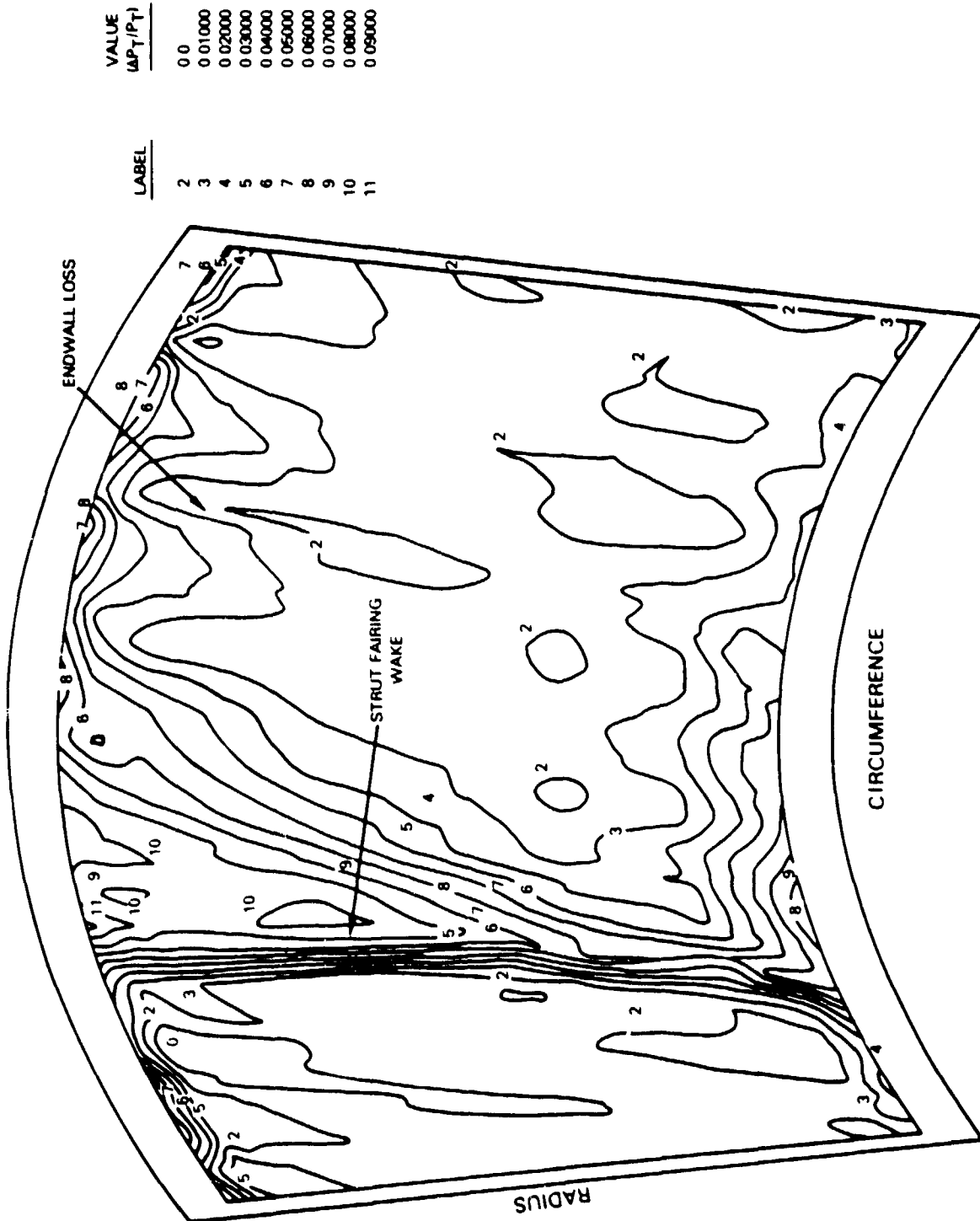


Figure 5-8 Strut Fairing Loss Contour Profile for Build 2 At Off-Design Conditions

ORIGINAL PAGE IS
OF POOR QUALITY

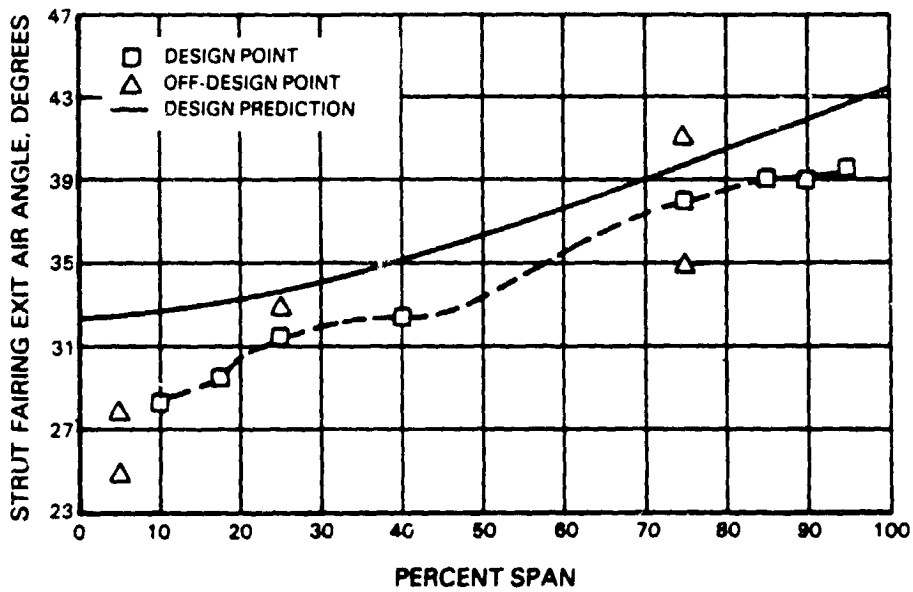


Figure 5-9 Strut Fairing Spanwise Exit Angle for Build 1 Configuration

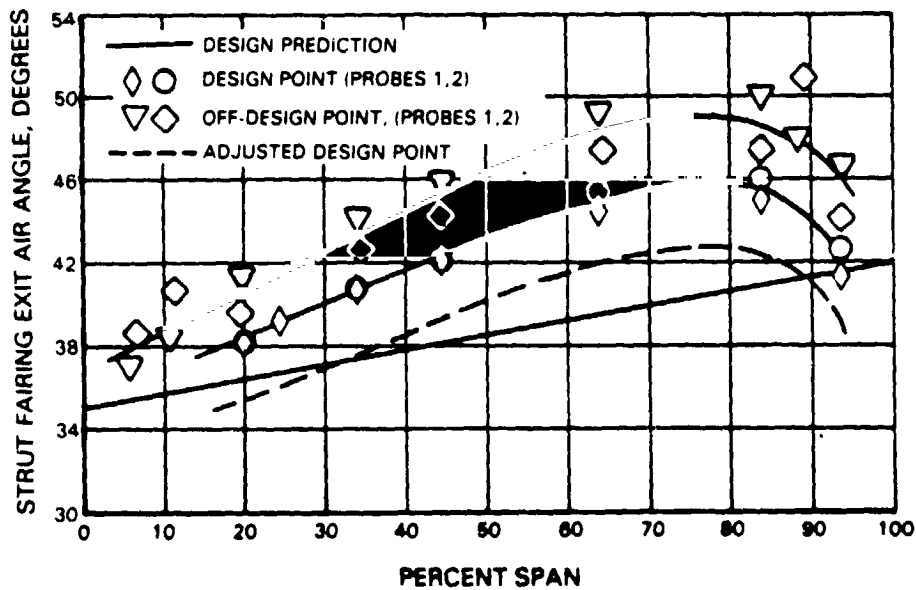


Figure 5-10 Strut Fairing Spanwise Exit Air Angle for Build 2 Configuration

Exit Mach Number Assessment

The strut fairing exit Mach number average spanwise profile was calculated using the spanwise total pressure data from the claw probes and a linear interpolation between the inner and outer wall static pressure taps. For the build 1 transition duct, the average spanwise profile at design and off-design conditions is shown in Figure 5-11. This profile shows Mach number increasing from the root to mid-span and then decreasing toward the tip. However, the slope is opposite to the prediction. This is because the prediction is based on a constant spanwise total pressure loss whereas the duct loss profile shown in Figure 5-5 is nonuniform with the expected higher losses at the root and tip. At design conditions the average absolute level agreed with the design prediction within 0.05. Off-design data show the same curve shape as the design data but at a higher level. The off-design average level agrees with the design prediction. These results confirm aerodynamic compatibility of the flow with the low-pressure turbine inlet requirements.

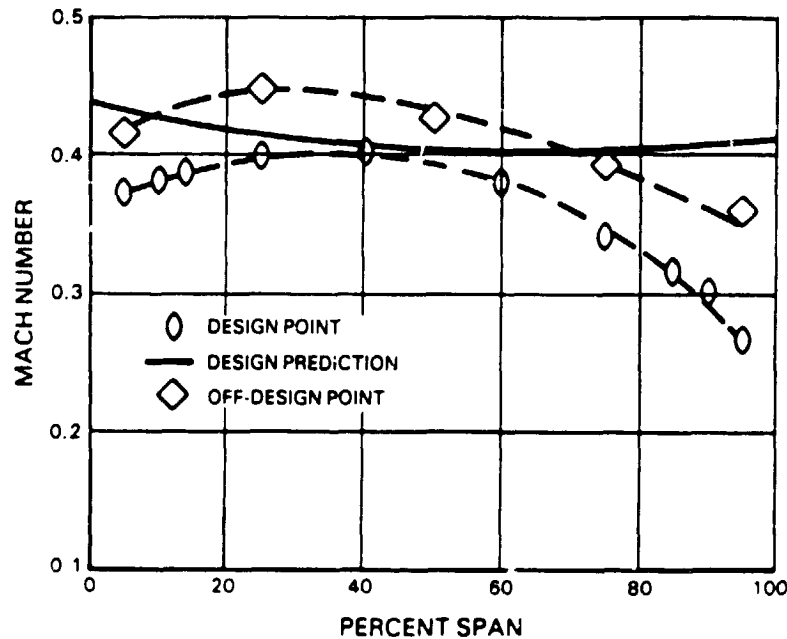


Figure 5-11 Build 1 Transition Duct Strut Fairing Average Spanwise Exit Mach Number Profile

The build 2 Mach number spanwise distribution is shown in Figure 5-12. This figure shows that the Mach number increases to approximately 30 percent span and then decreases. The shape of this distribution is similar to the design prediction, which was modified to incorporate the loss profile results from build 1. At design, the average level of the Mach number was above the design prediction level by 0.01. The off-design data show a similar curvature but a lower level, 0.03 below design prediction. The build 2 Mach number profiles are close to the design intent and compatible to the low pressure turbine inlet guide vane.

ORIGINAL PAGES
OF POOR QUALITY

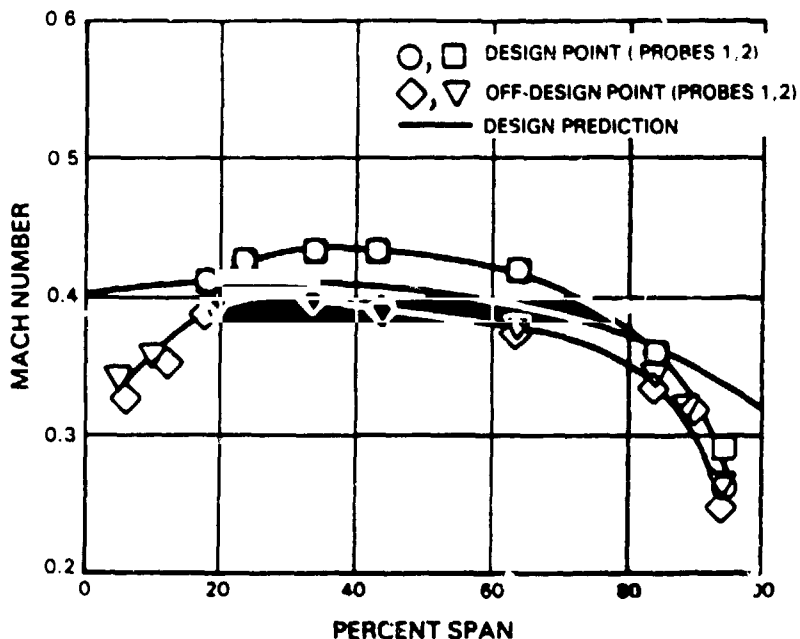


Figure 5-12 Build 2 Transition Duct Strut Fairing Average Spanwise Exit Mach Number Profile

5.2.3 Inlet Guide Vane Exit Aerodynamics

Pressure Loss Assessment

The total pressure loss, which is the loss across the transition duct and low-pressure turbine inlet guide vane, was measured by simultaneously traversing the strut fairing inlet and inlet guide vane exit planes. The loss for build 1 at design and off-design conditions is shown in Figure 5-13. The design point loss curve shows the higher loss regions to be within 20 percent of the inner and outer walls. The mass-averaged loss for the design point is 1.3 percent $\Delta P_T/P_T$. The mass-averaged loss level for the off-design testing increased to 2.1 percent $\Delta P_T/P_T$. Off-design results show an overall higher loss because of the previously discussed higher level of transition duct loss.

Figure 5-14 shows the total pressure loss for the build 2 configuration. The mass-averaged loss for the design point was 2.09 percent $\Delta P_T/P_T$. The data trend at off-design conditions shows a lower loss in the root region and higher loss in the mid-span region, which is consistent with the strut fairing exit plane loss at off-design. The mass-averaged loss for off-design of 2.04 percent $\Delta P_T/P_T$ is lower than the design point level because of the reduction in transition duct loss at off-design conditions more than compensated for increased low-pressure turbine inlet guide vane loss at off-design.

ORIGINAL PAGE IS
OF POOR QUALITY

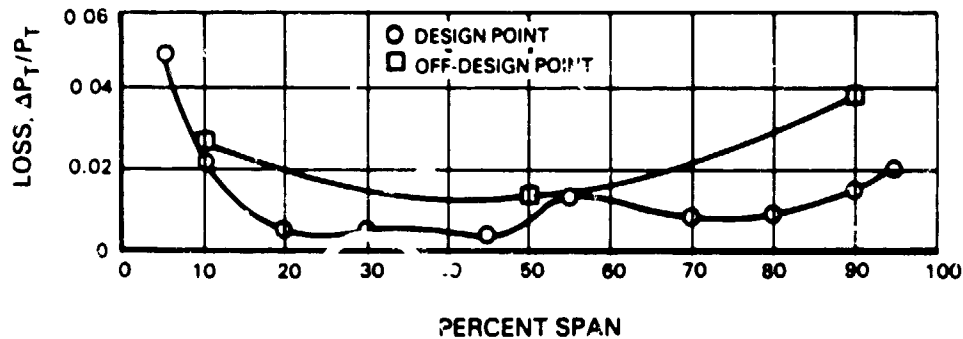


Figure 5-13 Build 1 Transition Duct and Inlet Guide Vane Pressure Loss

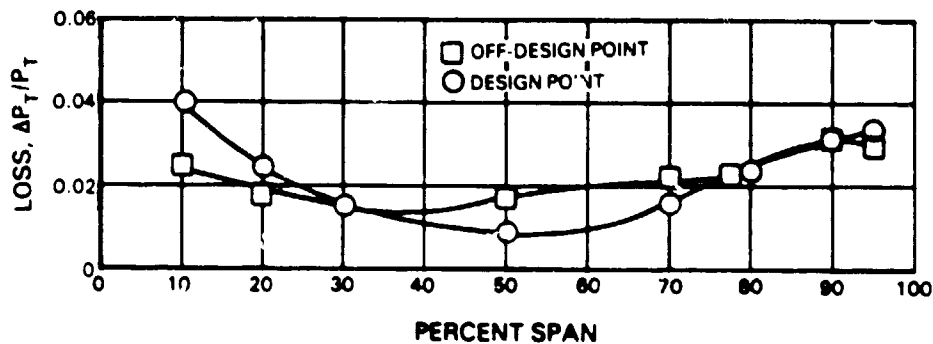


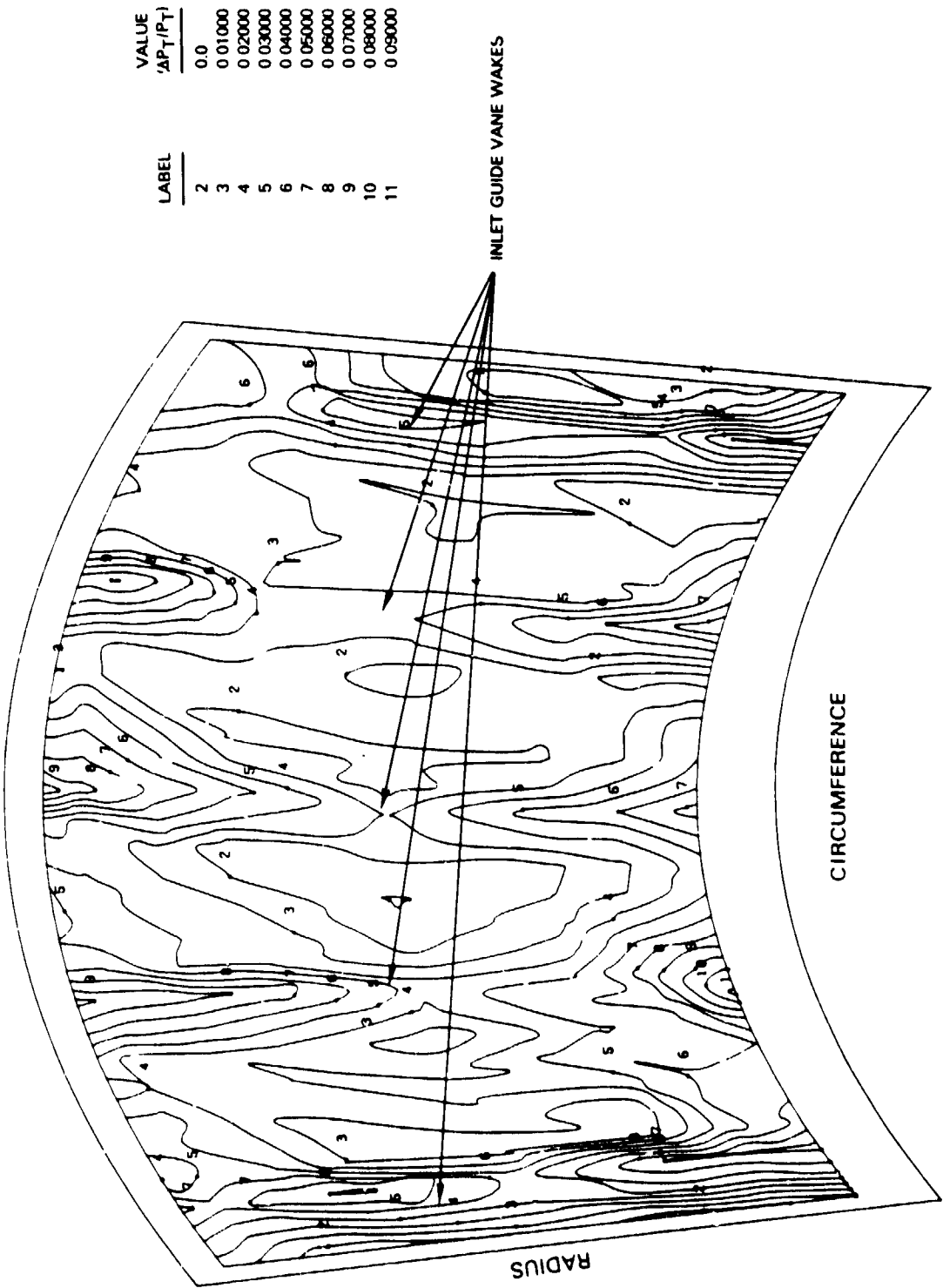
Figure 5-14 Build 2 Transition Duct and Inlet Guide Vane Pressure Loss

The inlet guide vane pressure loss was calculated from the difference between the measured transition duct loss and the measured transition duct and inlet guide vane loss. The calculated build 1 inlet guide vane loss is 0.6 percent $\Delta P_T/P_T$ for design and 0.8 percent $\Delta P_T/P_T$ for off-design. This higher level of loss at the off-design condition is a result of off-design strut fairing aerodynamics.

The calculated inlet guide vane loss for build 2 is 0.49 percent $\Delta P_T/P_T$ at design and 0.68 percent $\Delta P_T/P_T$ at off-design. The increase for the off-design test resulted from the 2.8 degree more positive incidence at the off-design point.

The exit pressure loss contour is shown in Figure 5-15 for build 2 at design conditions. This plot shows the wakes from the low-pressure turbine inlet guide vanes, the strut fairing and the endwall loss over one strut fairing pitch. Figure 5-16 presents a pressure loss contour at off-design conditions. As compared to Figure 5-15, the overall pressure loss distribution is similar.

ORIGINAL PAGE IS
OF POOR QUALITY



LABEL	VALUE ' $\Delta P_T / P_T$ '
2	0.0
3	0.01000
4	0.02000
5	0.03000
6	0.04000
7	0.05000
8	0.06000
9	0.07000
10	0.08000
11	0.09000

Figure 5-15 Build 2 Loss Contour Plot At Design Conditions Showing the Makes from Low-Pressure Turbine Inlet Guide Vanes

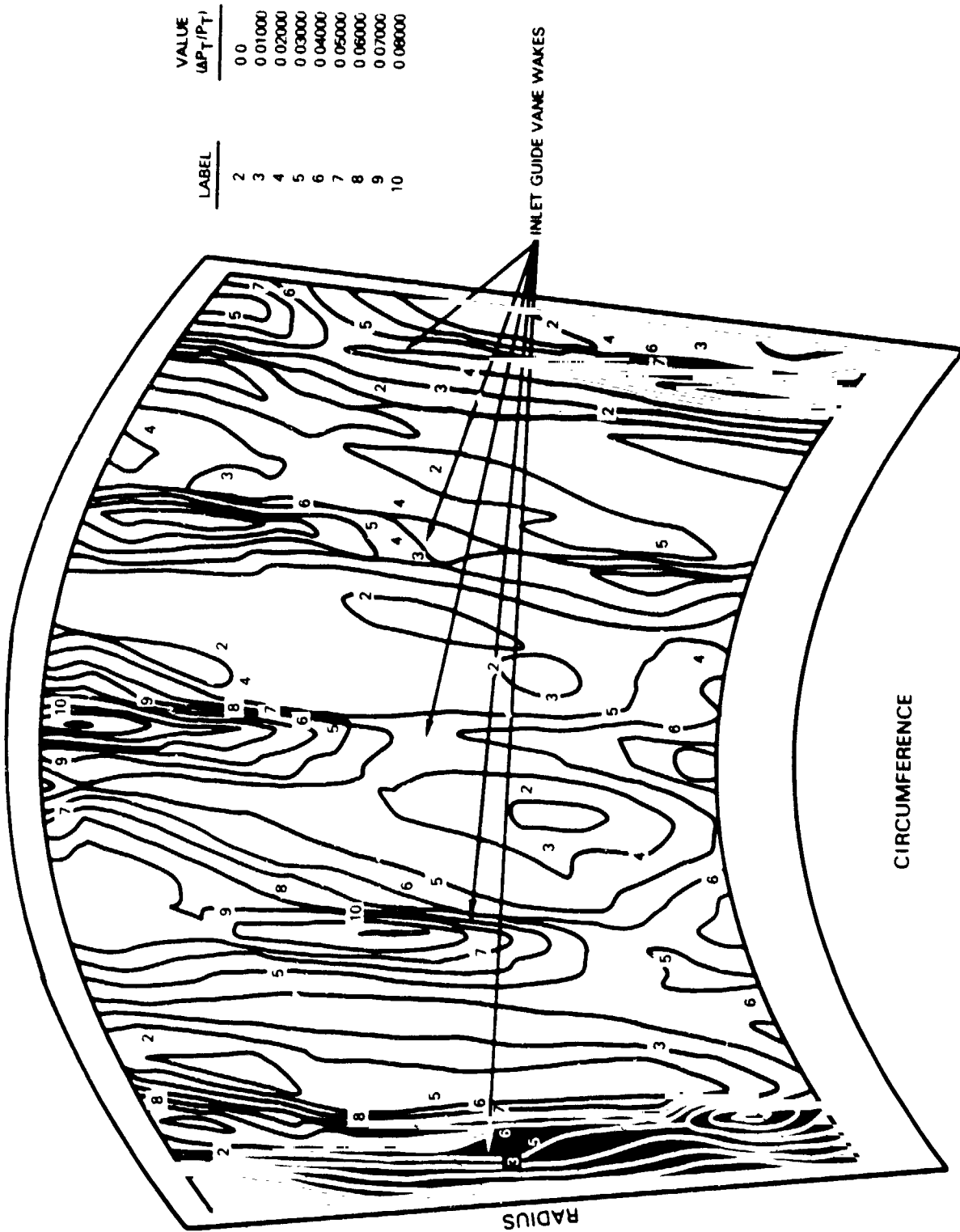


Figure 5-16 Build 2 Loss Contour Plot At Off-Design Conditions Showing the Wakes from Low-Pressure Turbine Inlet Guide Vanes

Exit Air Angle Assessment

The spanwise distribution of the inlet guide vane exit air angle for build 1 is shown in Figure 5-17. At design, the exit angle is generally consistent with the prediction. This result shows that the inlet guide vane is performing as designed and that the low-pressure turbine first rotor will have the desired spanwise inlet angle. Off-design data show the air angle to be 4 degrees more tangential than the design prediction. Since the measured loss for the inlet guide vane showed only a slight change from design to off design and inlet air angles indicated no change from design to off design, this result is inconsistent and suspected to be erroneous. The net result should be an angle closer to the design intent. This disparity in results is attributed to the air angle measurement instrumentation.

Inlet guide vane exit air angle data from build 2 are presented in Figure 5-18. Design data show the exit angle average to be within 1 degree of the prediction as well as conform to the same spanwise contour. This indicates that the inlet guide vane performed suitably and the first low-pressure turbine rotor will have an acceptable inlet angle contour. At off-design, the inlet guide vane accepted the additional 2.8 degree more positive incidence flow and returned it to within 0.7 degree of the design data. Also, the same spanwise distribution was nearly maintained. This shows that off-design high-pressure turbine exit conditions will have little or no effect on the desired air angle into the low-pressure turbine first rotor.

Exit Mach Number Assessment

Vane exit Mach number was calculated using the average spanwise total pressure measurements and a linear interpolation between the inner and outer wall static pressure measurements. As indicated in Figure 5-19, build 1 design data have a lower Mach number than predicted by 0.04. Also, the Mach number increases from the root to approximately 30 percent span and then decreases toward the tip. This contour is different than predicted since for build 1 the prediction assumed a constant spanwise loss, whereas measured losses, as expected, were higher at the root and tip. The off-design data show a similar trend but at a slightly lower level. This further supports the conclusion that off-design high-pressure turbine exit conditions will have little or no effect to the low-pressure turbine rotor inlet conditions.

The spanwise Mach number trends for build 2 are shown in Figure 5-20. At design, the data show the same contour as the prediction, but at a level of 0.04 lower. The off-design curve shows a similar contour at a level 0.01 lower than the design intent. These results further confirm that the inlet guide vane is performing adequately and the rotor will have an acceptable inlet Mach number profile.

Performance Summary

Table 5-II presents a synopsis of the transition duct performance characteristics for builds 1 and 2. These values are the actual measured values and do not reflect any adjustments from data interpretation.

ORIGINAL PAGE IS
OF POOR QUALITY

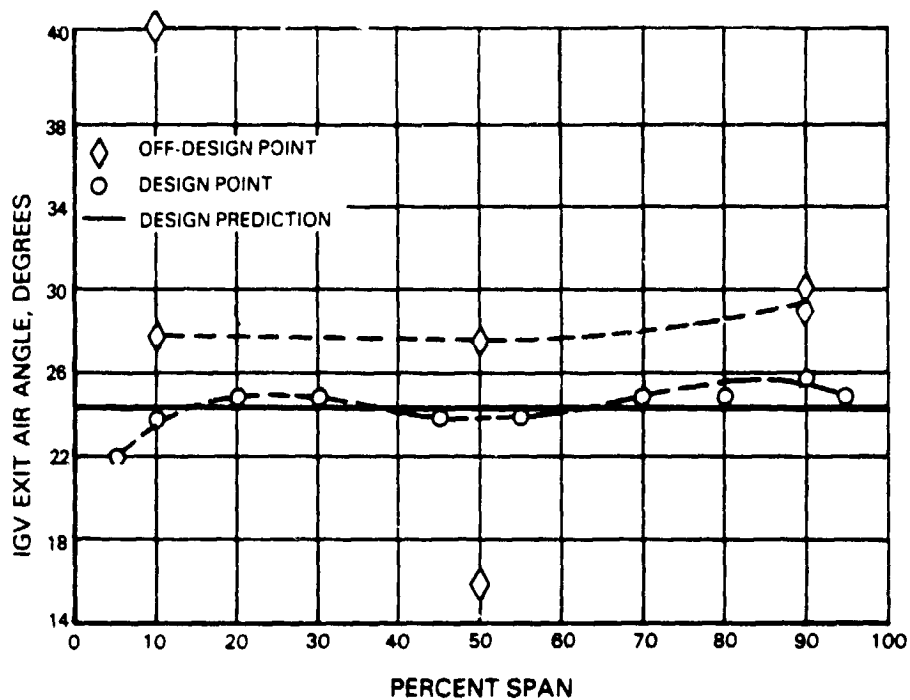


Figure 5-17 Build 1 Inlet Guide Vane Exit Air Angle Data

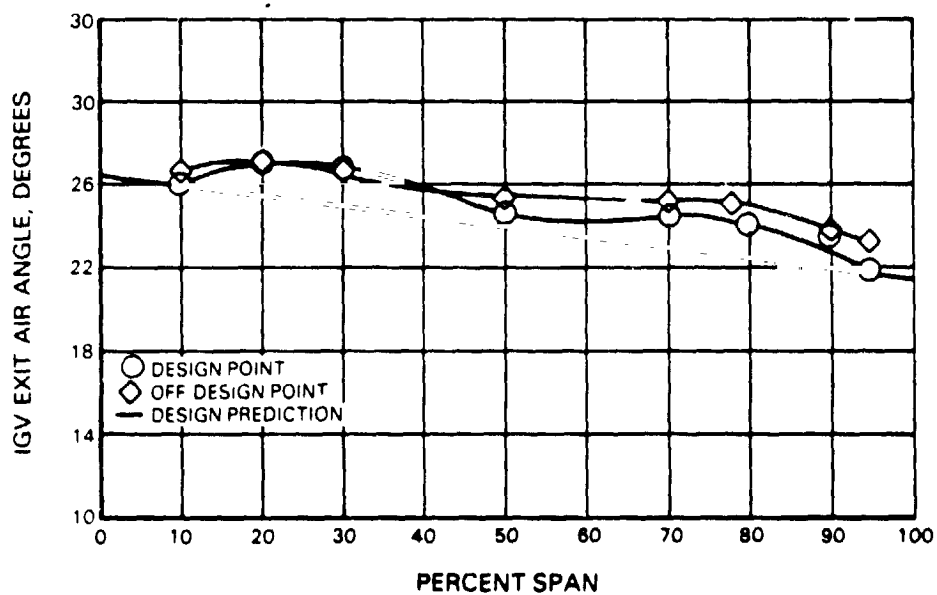


Figure 5-18 Build 2 Inlet Guide Vane Exit Air Angle Data

ORIGINAL PAGE IS
OF POOR QUALITY

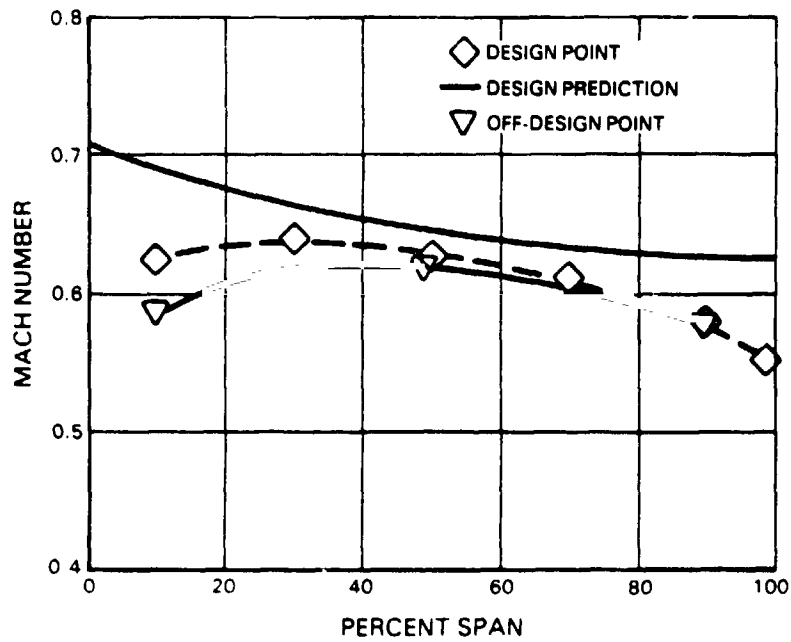


Figure 5-19 Inlet Guide Vane Exit Mach Number Trends for Build 1

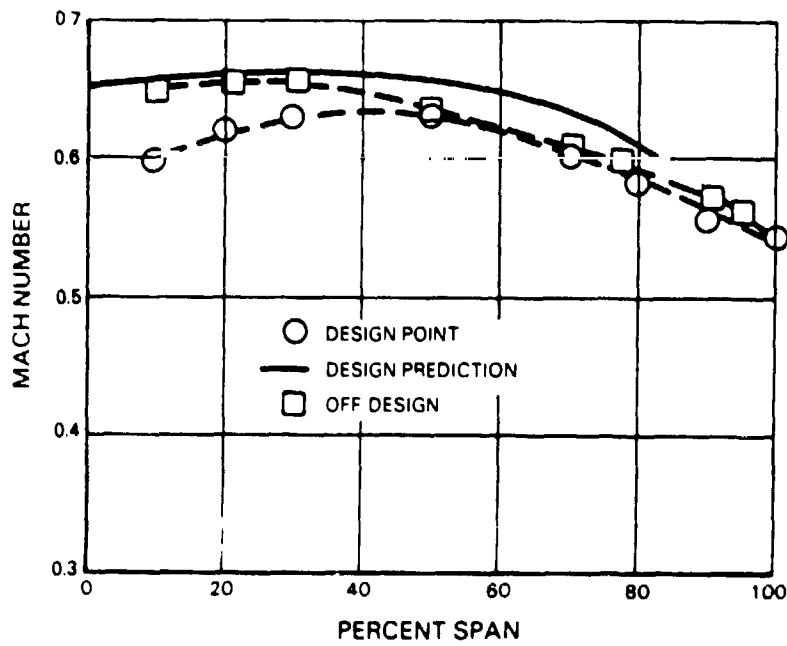


Figure 5-20 Inlet Guide Vane Exit Mach Number Trends for Build 2

TABLE 5-II
ENERGY EFFICIENT ENGINE TRANSITION DUCT PERFORMANCE

Measured Average Conditions	Build 1		Build 2	
	<u>Design</u>	<u>Off-Design</u>	<u>Design</u>	<u>Off-Design</u>
Strut Fairing Inlet				
Inlet Mach No.	0.48	0.44	0.60	0.51
Inlet Air Angle, deg	45.20	49.30	42.40	49.20
Strut Fairing Exit				
Exit Mach No.	0.36	0.41	0.40	0.36
Exit Air Angle, deg	34.10	34.00	42.30*	45.10*
$\Delta P_T/P_T$ Strut, %	0.70	1.30	1.59	1.37
Inlet Guide Vane Exit				
Exit Mach No.	0.61	0.60	0.60	0.63
Exit Air Angle, deg	24.20	--	25.20	25.90
$\Delta P_T/P_T$ IG, %	0.60	0.80	0.49	0.68
$\Delta P_T/P_T$ Duct, %	1.30	2.10	2.08	2.05

* See text for final results on build 2 strut exit air angle on page 42

5.3 AIRFOIL/DUCT PRESSURE DISTRIBUTION

5.3.1 Duct Wall Loadings (Duct Wall Diffusion)

The duct wall loading for build 1 is shown in Figures 5-21 and 5-22. These profiles show the variation of inner and outer wall loading as a function of axial distance for design and off-design testing. Figure 5-21 presents the measured static pressure data, while Figure 5-22 shows the data normalized to the average strut fairing inlet conditions and compared to the design streamline prediction.

The outer wall, because of its curvature, was predicted to have the highest wall loading, thereby operating the closest to a separated condition. As indicated in Figure 5-22, for the design point conditions the flow diffuses past the strut fairing in good agreement with the prediction, except for the strut fairing leading edge where the flow accelerates sooner than predicted. This difference is a result of the strut fairing bow wake turning the flow. The bow wake, which extends forward from the strut fairing, was not modeled in the design prediction. After leaving the strut fairing passages, the wall loading shows the flow accelerating through the inlet guide vane passage. The inner wall loading for the design point conditions (Figure 5-22) shows a lower loading than the outer wall through the strut passage, as predicted, and the same bow wake effect as the outer wall. After leaving the strut passage the wall loading shows the flow accelerating through the inlet guide vane passage.

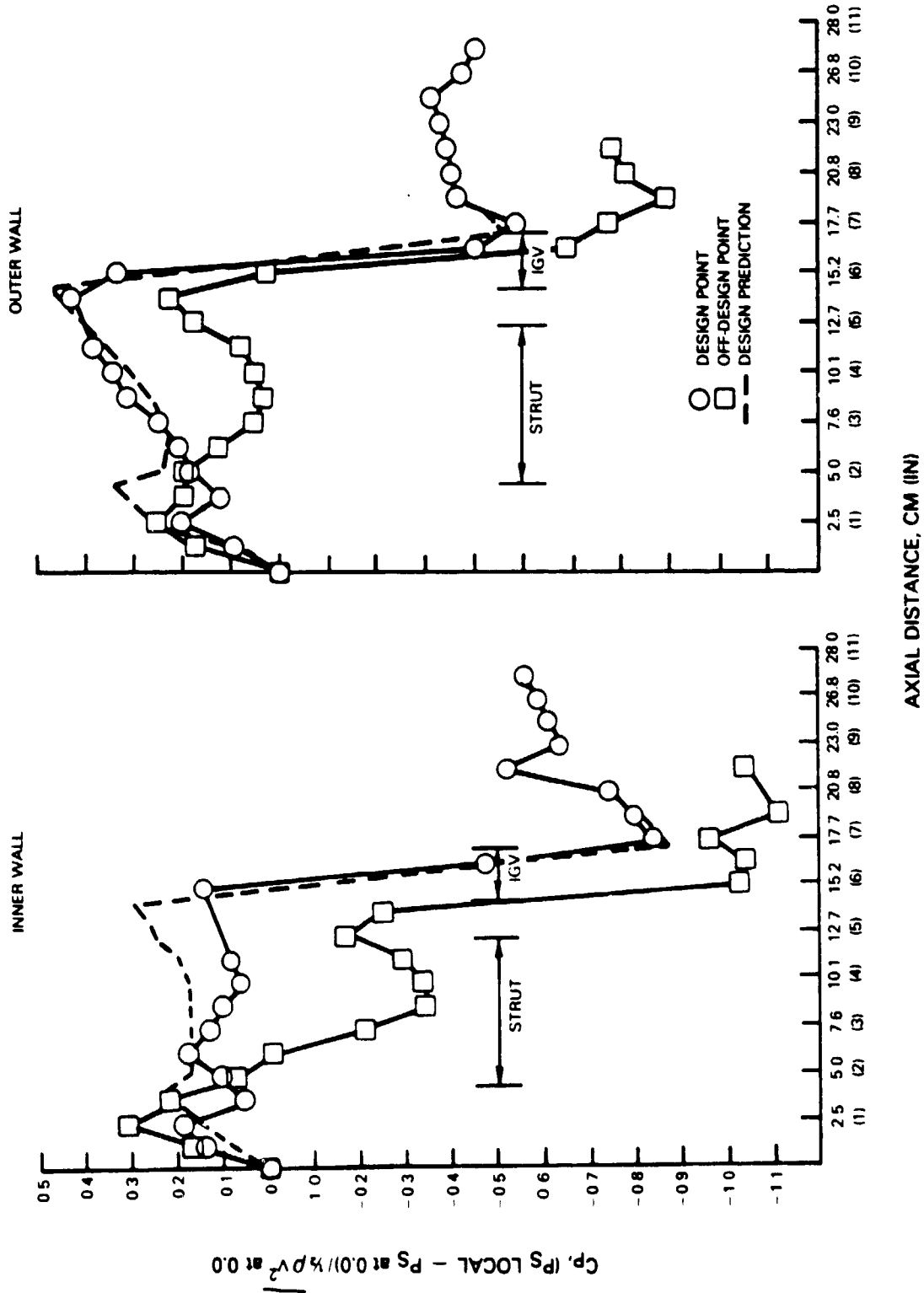


Figure 5-22 Build 1 Transition Duct Wall Loadings At Design and Off-Design Conditions

ORIGINAL PAGE IS
OF POOR QUALITY

The outer wall off-design data show the effect of the average inlet flow being 4 degrees more axial. In this case, the strut fairing, which for the build 1 configuration is a nonworking airfoil, turns the flow more tangentially. This turning causes an acceleration over 50 percent of the airfoil length at which point the flow begins to decelerate through the remaining strut passage. The inner wall profile shows essentially the same effect as the outer wall for off-design conditions. However, acceleration at the inner wall appears somewhat stronger. This is caused by: (1) design point data not showing as much diffusion as the outer wall, and (2) the inner inlet flow angle shift being greater than the outer angle shift, as shown in Figure 5-1.

On the basis of these data, the build 1 transition duct achieved the desired diffusion and the flow along the inner and outer walls was separation free at both design and off-design conditions.

Duct wall loadings for build 2 are presented in Figures 5-23 and 5-24. Again, the measured data are shown in Figure 5-23 and the data normalized to the average strut fairing inlet conditions and compared to the design streamline predictions are shown in Figure 5-24.

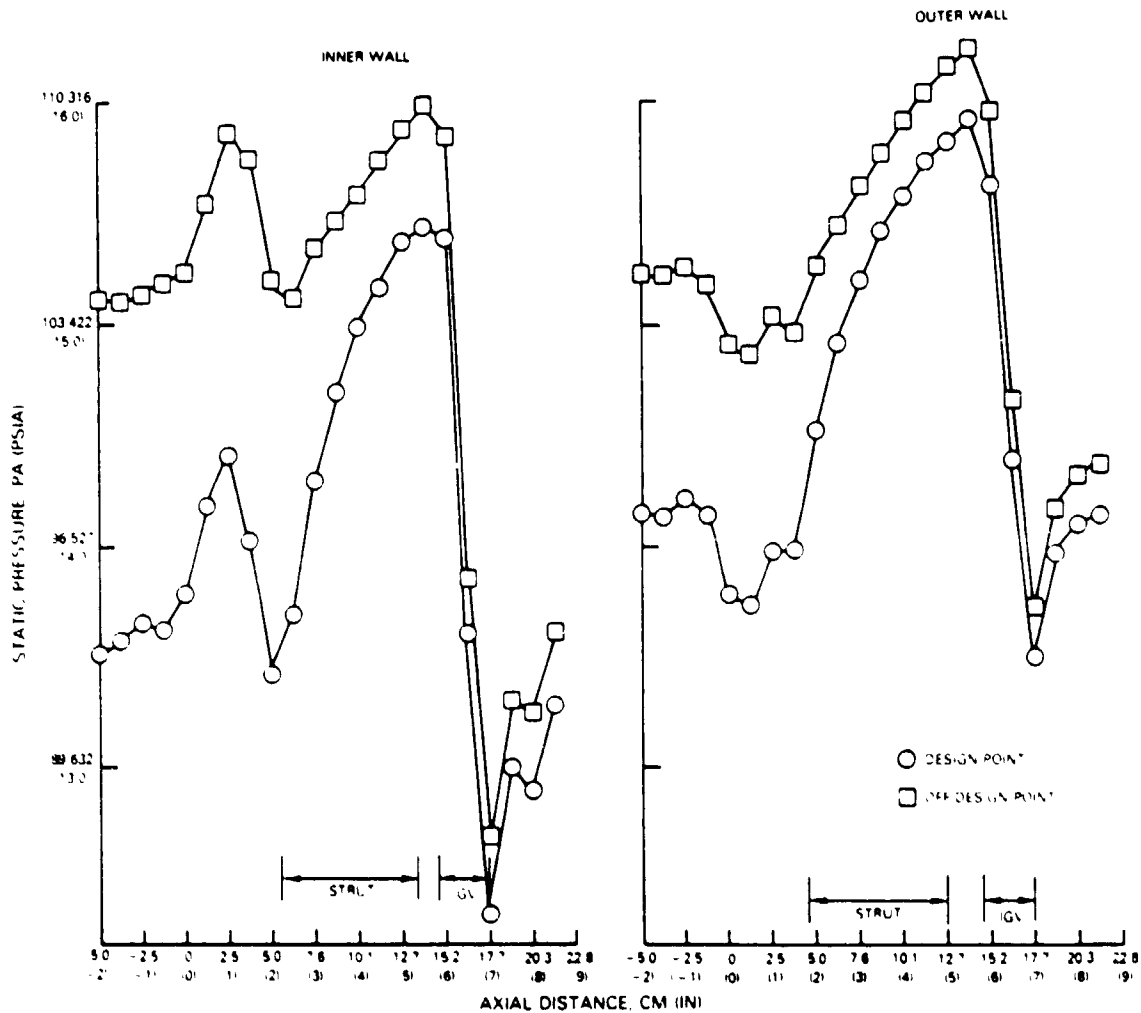


Figure 5-23 Build 2 Transition Duct Wall Loadings At Design and Off-Design Conditions

ORIGINAL PAGE IS
OF POOR QUALITY

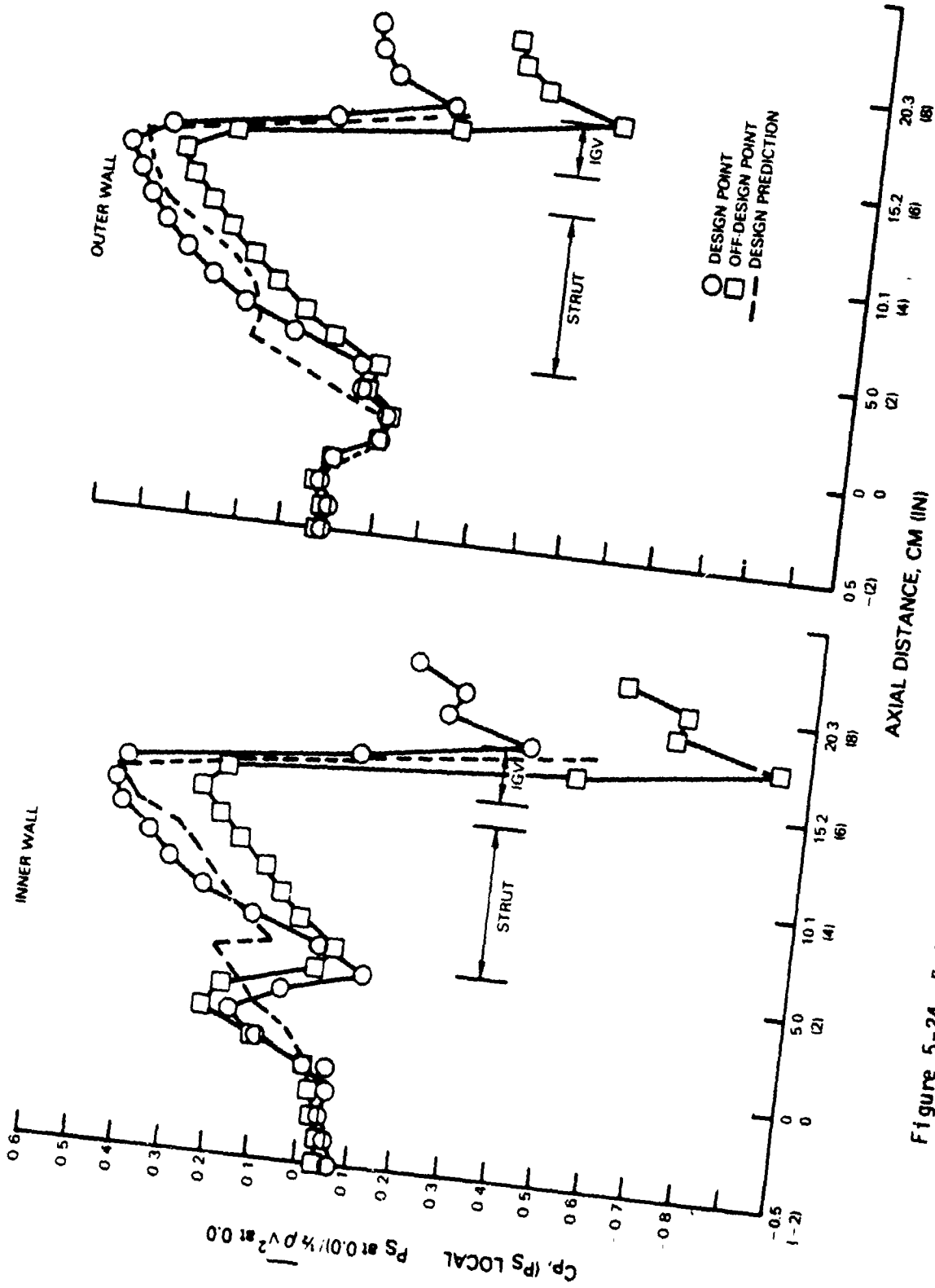


Figure 5-24 Build 2 Transition Duct Wall Loadings At Design and Off-Design Conditions

As indicated in Figure 5-24, the outer wall profile at design shows the flow diffusing from the inlet to the strut fairing exit. This result is in good agreement with the prediction, except that acceleration occurred around the strut fairing leading edge sooner than predicted, as in build 1. The inner wall profile also shows acceleration at the leading edge occurring sooner than predicted and over a longer distance because of the effect of the bow wake, as observed in the build 1 results. The flow then diffuses through the strut passage and accelerates through the inlet guide vane passage.

The outer wall off-design data show the effect of the average inlet flow being 6.8 degrees more axial. For this case the strut fairing turning is reduced from the design test level but still turns the air axially. This reduced turning, as shown by the wall loadings, causes the flow to diffuse through the strut fairing passage but to a lower level than the design condition test. This data also show the leading edge acceleration occurred sooner than predicted. The inner wall off-design data show a similar trend in front of the strut fairing leading edge as indicated by the design point data. The diffusion past the strut fairing shows a reduction similar to that shown by the outer wall off-design performance.

On the basis of these results, the build 2 transition duct also achieved the desired diffusion and the flow along the inner and outer walls was separation free at both design and off-design conditions.

5.3.2 Strut Fairing Aerodynamics

Two strut fairings were instrumented to acquire pressure distribution profiles at three radial locations on both surfaces of the airfoil. Pressure measurements verified the separation-free performance of the airfoil designs in both the build 1 and 2 transition duct configurations at design and off-design conditions.

Build 1 design point static pressure distributions are presented in Figures 5-25, 5-26 and 5-27 for the 10, 50 and 90 percent span locations, respectively. In essence, the similarities between the pressure surface and suction surface pressure distributions show that the strut fairing was unloaded. Therefore, it was not turning the air and it was performing according to the design intent for the build 1 configuration.

Results at off-design are shown in Figures 5-28, 5-29, and 5-30 for the 10, 50 and 90 percent span locations, respectively. These results show the effect of the 4 degrees more axial inlet flow. The differences between the pressure surface and the suction surface pressure distributions indicate that the strut fairing was loaded to turn the air to the design exit air angle, as shown in Figure 5-9. Data at both the 50 and 90 percent span location show that turning is completed by the time the flow has reached approximately 50 percent of the airfoil axial chord. This agrees with the wall loading distribution in Figure 5-22, which showed the off-design wall loading returning to the design slope at approximately 50 percent axial chord.

ORIGINAL PAGE IS
OF POOR QUALITY

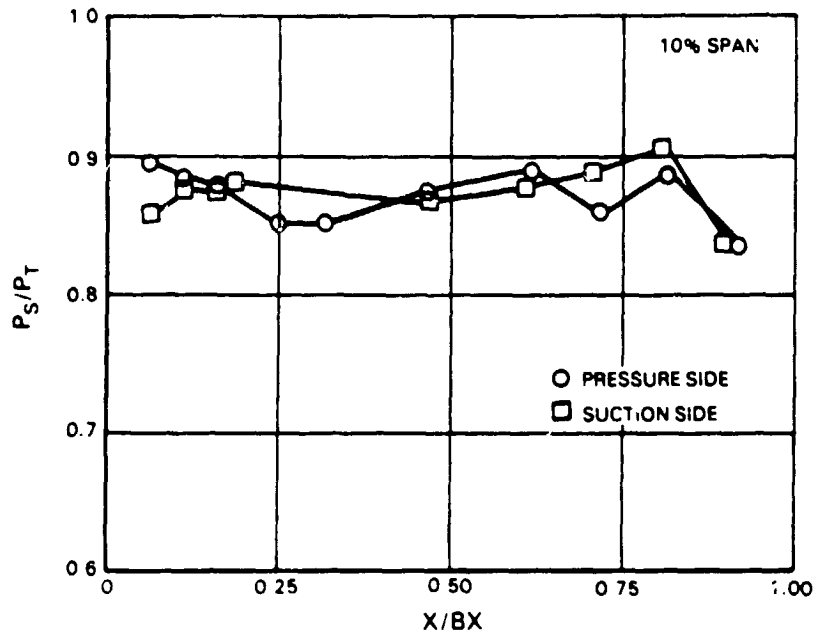


Figure 5-25 Build 1 Strut Fairing Design Point Static Pressure Distributions at 10 Percent Span

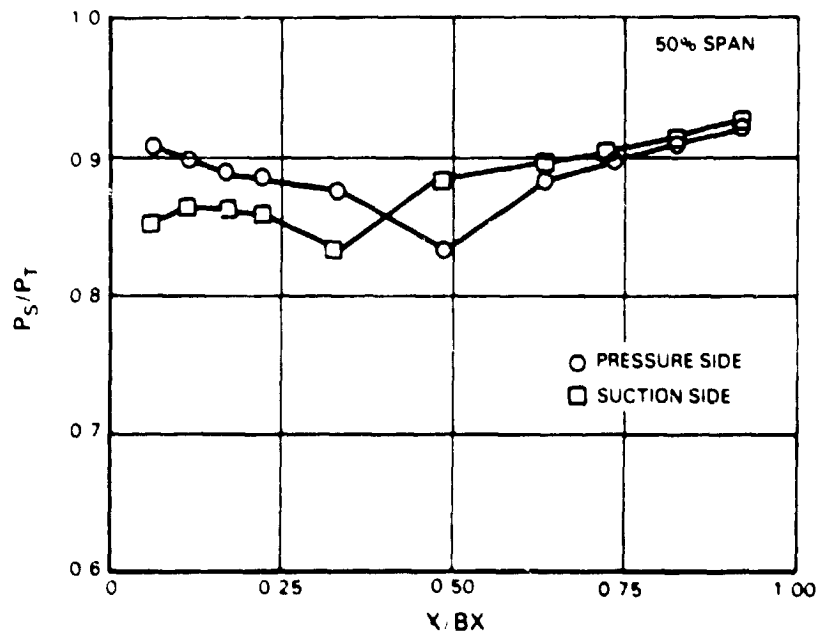


Figure 5-26 Build 1 Strut Fairing Design Point Static Pressure Distributions at 50 Percent Span

ORIGINAL DESIGN
OF POOR QUALITY

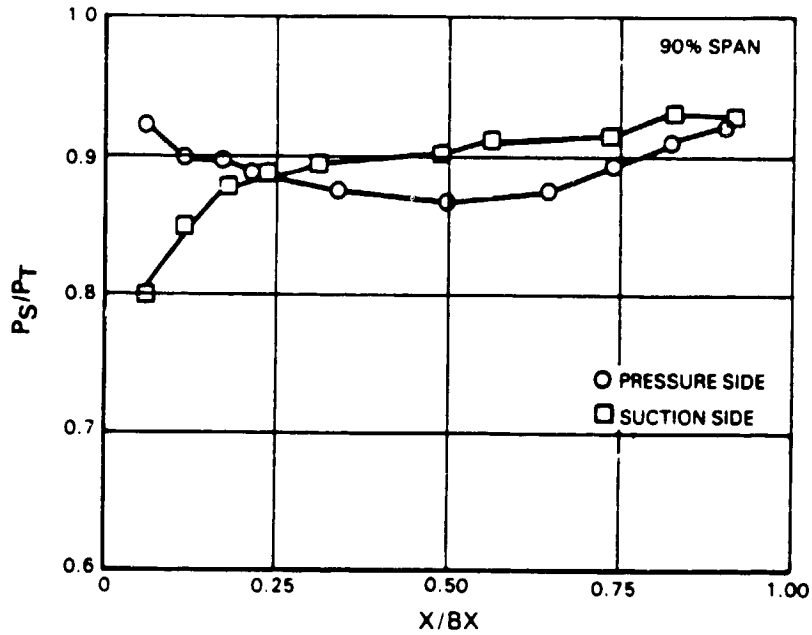


Figure 5-27 Build 1 Strut Fairing Design Point Static Pressure Distributions at 90 Percent Span

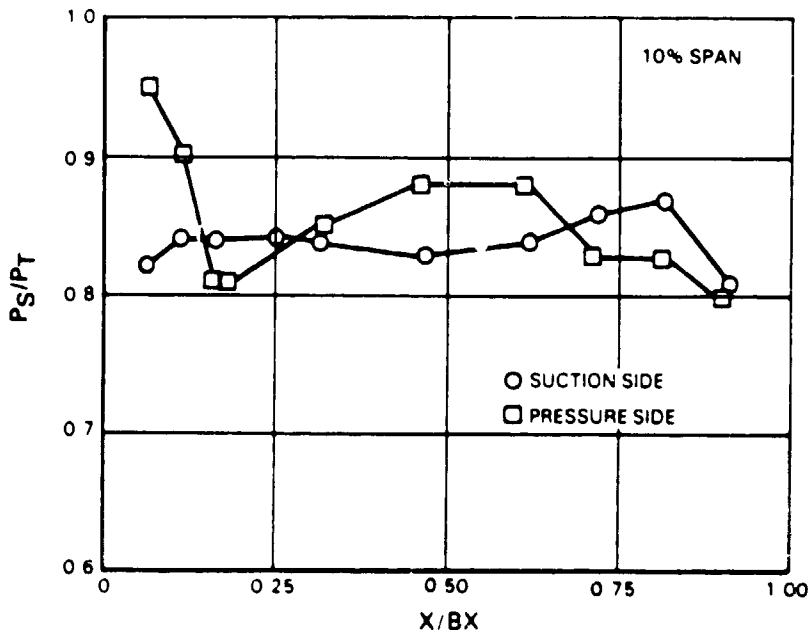


Figure 5-28 Build 1 Strut Fairing Off-Design Static Pressure Distributions at 10 Percent Span

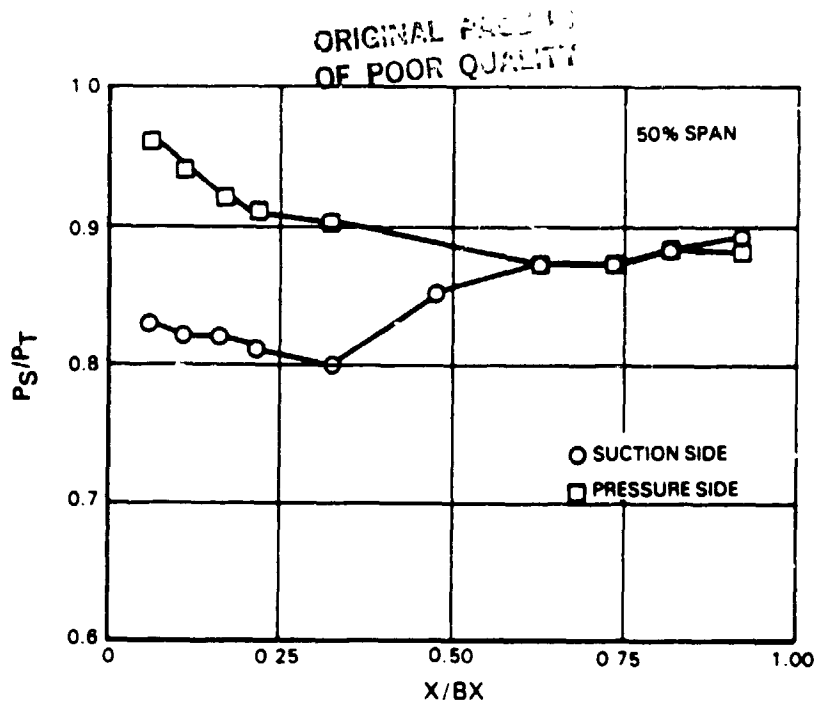


Figure 5-29 Build 1 Strut Fairing Off-Design Static Pressure Distributions at 50 Percent Span

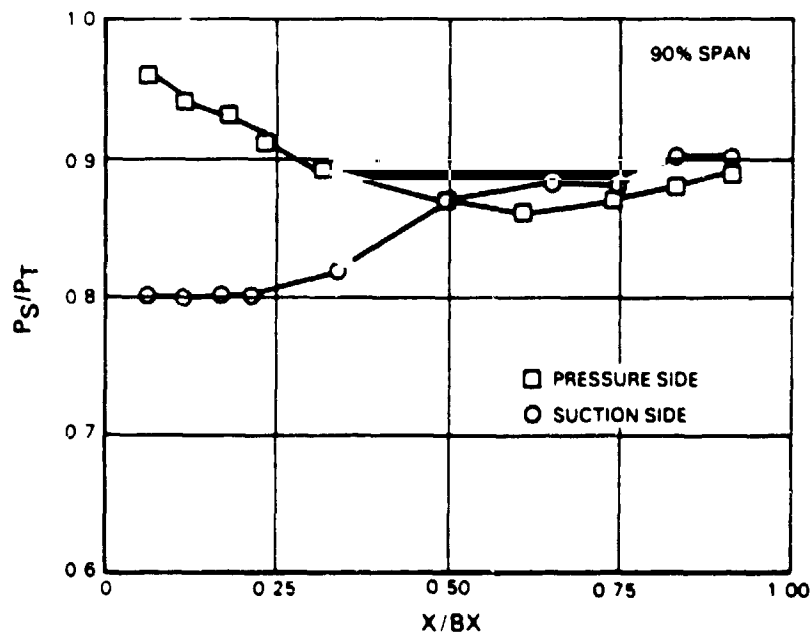


Figure 5-30 Build 1 Strut Fairing Off-Design Static Pressure Distributions at 90 Percent Span

Build 2 design point static pressure distributions are shown in Figures 5-31, 5-32 and 5-33 for the 15, 53 and 90 percent span locations. The data are compared to the predicted pressure distributions at 0, 50 and 100 percent span. These distributions show the positive loading level that is required to turn the air. The data show reasonable agreement with the predictions at 10 and 50 percent span. At 90 percent span, data are in good agreement at the exit but not at the leading edge. This is probably due to the fact that the data were acquired at 90 percent span and the prediction was made for the tip (100 percent span) location.

Results at off-design are presented in Figures 5-34, 5-35 and 5-36 for the same spanwise locations. These pressure distributions show the effect of the 5.8 degree more axial inlet flow, which is a reduction in loading (or turning). This result agrees with the measured air angle probe results, which showed that turning at off-design was reduced to 1 degree from the design level.

The build 2 mean section pressure distribution data were matched using a potential flow analysis to confirm the level of the measured air angles. Results of this analysis for the design point are presented in Figures 5-37 through 5-46. The first 5 figures (5-37 through 5-41) show the variation in the predicted pressure distribution with variations in inlet angle. The leading edge pressure surface appears sensitive to an inlet angle variation of approximately 1 degree. The best match with the data was generated with an inlet angle of 144 degrees. This angle was matched with a streamline analysis that used the test rig inlet conditions of Mach number and angle. The result confirms the level of measured inlet angle by approximately 1 degree. Using this strut fairing inlet angle, the exit angle was adjusted in 1 degree increments to match the trailing edge region pressure data.

The results in Figures 5-39, 5-42, and 5-43 are for exit angles of 44.4, 41.5 and 40.5 degrees, respectively. These pressure distributions show the exit angle of 40.5 degrees to be the closest data match. When this angle is compared to the measured exit angle, a discrepancy of approximately 3 degrees is found. The air angle from the pressure distribution analysis is closer to the design exit air angle.

This analysis was repeated for the build 2 off-design data, and the results are presented in Figures 5-44 through 5-46. For this analysis, strut fairing inlet conditions were matched with a streamline to calculate a strut fairing inlet angle of 137 degrees. Using this angle, the leading edge region of the pressure distribution matched the measured data, confirming the inlet angle probe data to within approximately 1 degree. The trailing edge region of the pressure distribution was matched by varying the exit angle from 47.5 degrees to 43.5 degrees. The best match with the data occurs at 43.5 degrees. When this angle is compared to the measured exit angle, however, a discrepancy of approximately 3 degrees is again found with the pressure distribution analysis being closer to the design exit angle. Since the same measured exit angle errors were calculated for both design and off-design cases, it is likely that the strut fairing exit air angle probe had a bias error of 3 degrees for build 2.

ORIGINAL PAGE IS
OF POOR QUALITY

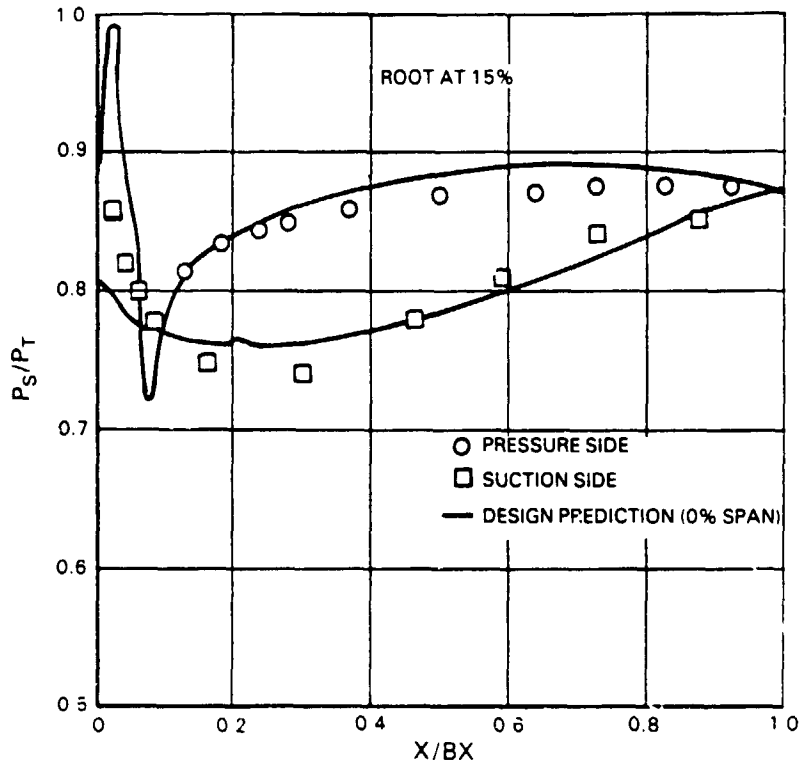


Figure 5-31 Build 2 Strut Fairing Design Point Static Pressure Distributions at 15 Percent Span

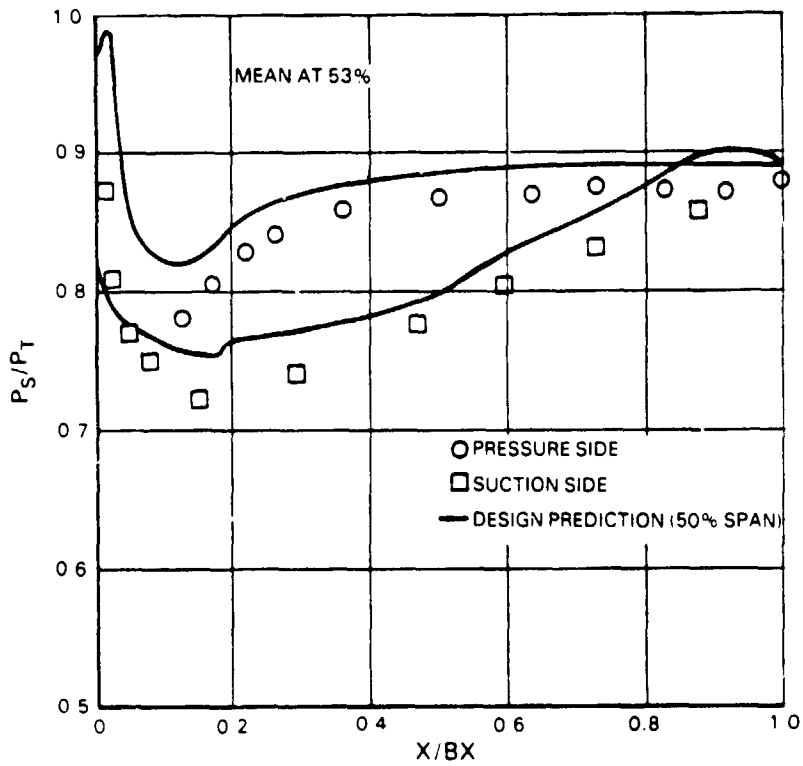


Figure 5-32 Build 2 Strut Fairing Design Point Static Pressure Distributions at 53 Percent Span

ORIGINAL PAGE IS
OF POOR QUALITY

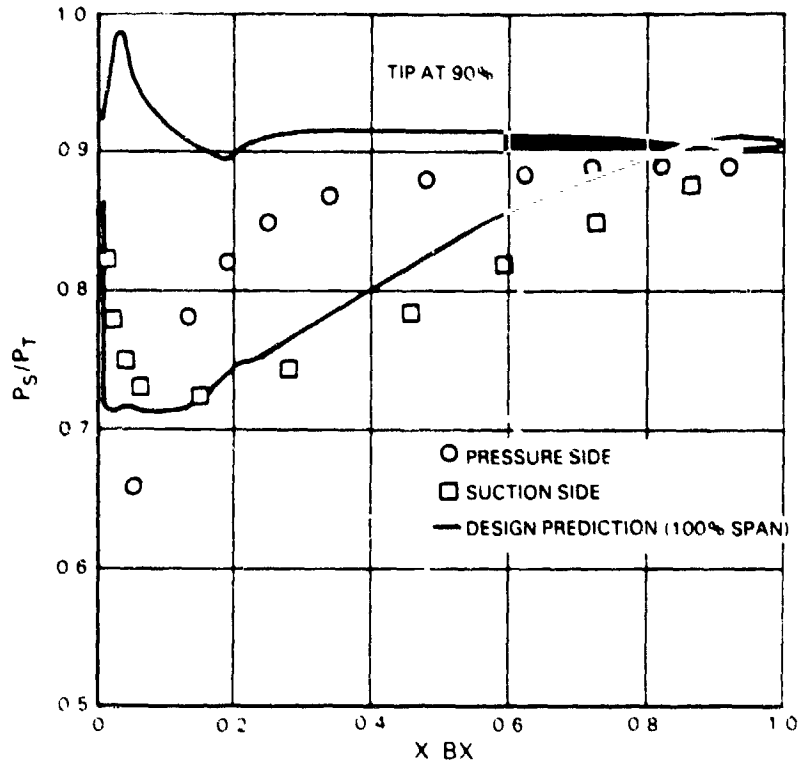


Figure 5-33 Build 2 Strut Fairing Design Point Static Pressure Distributions at 90 Percent Span

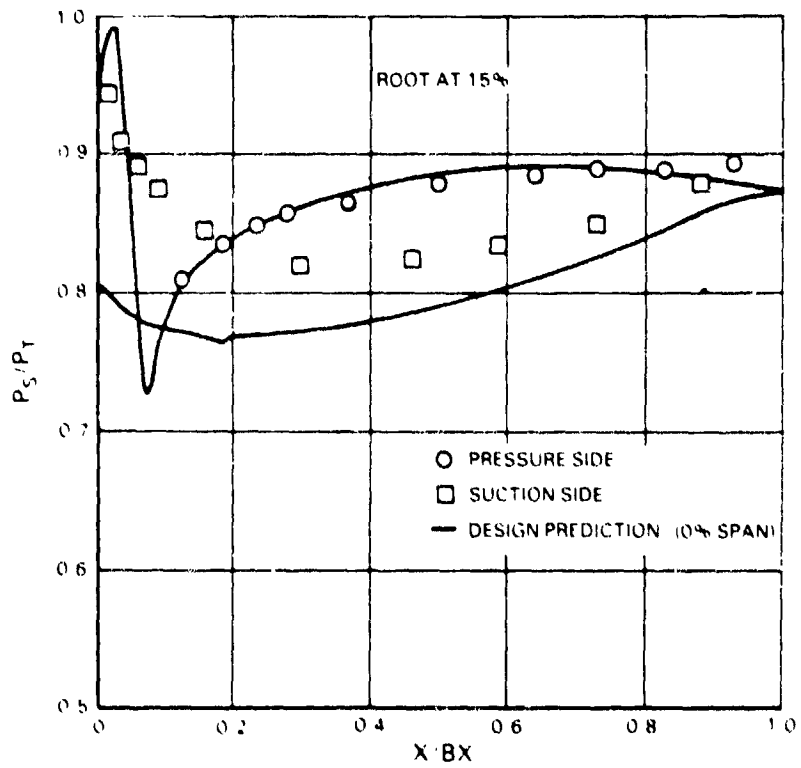


Figure 5-34 Build 2 Strut Fairing Off-Design Static Pressure Distributions at 15 Percent Span

ORIGINAL PAGE IS
OF POOR QUALITY

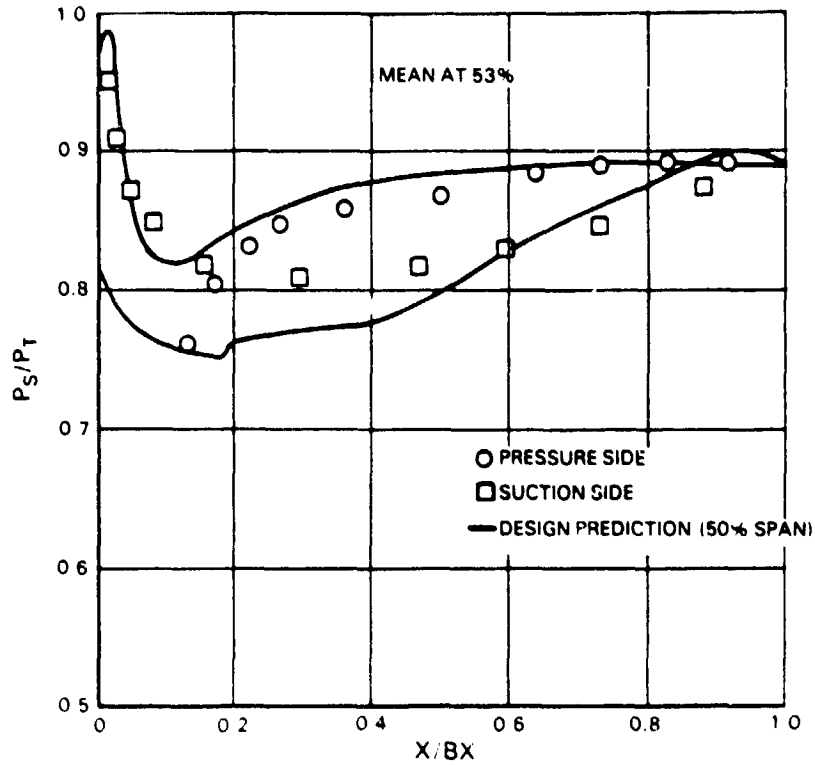


Figure 5-35 Build 2 Strut Fairing Off-Design Static Pressure Distributions at 53 Percent Span

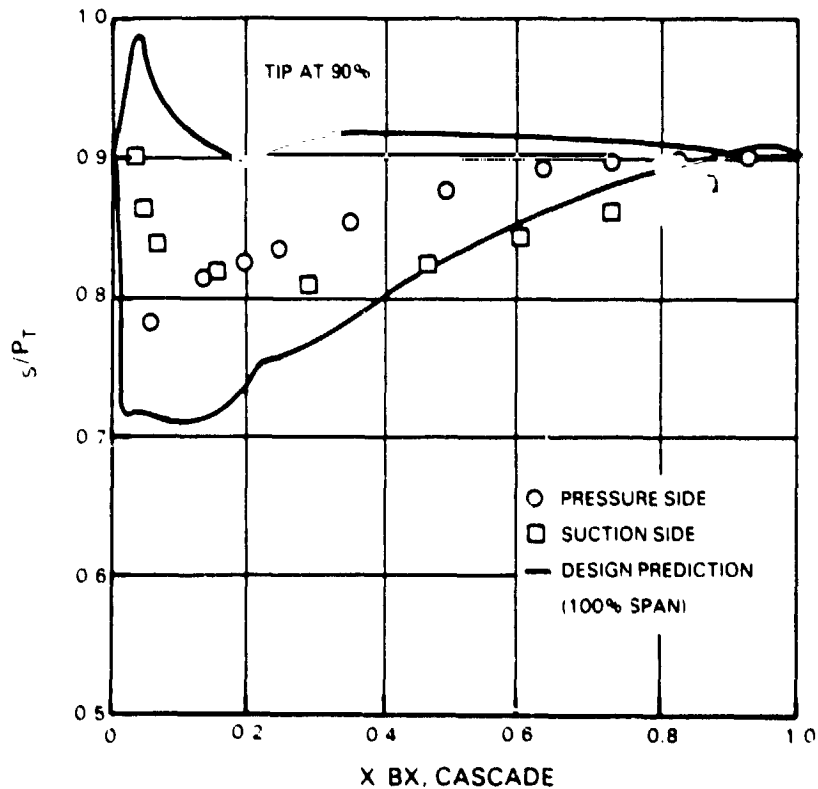


Figure 5-36 Build 2 Strut Fairing Off-Design Static Pressure Distributions at 90 Percent Span

ORIGINAL PAGE IS
OF POOR QUALITY

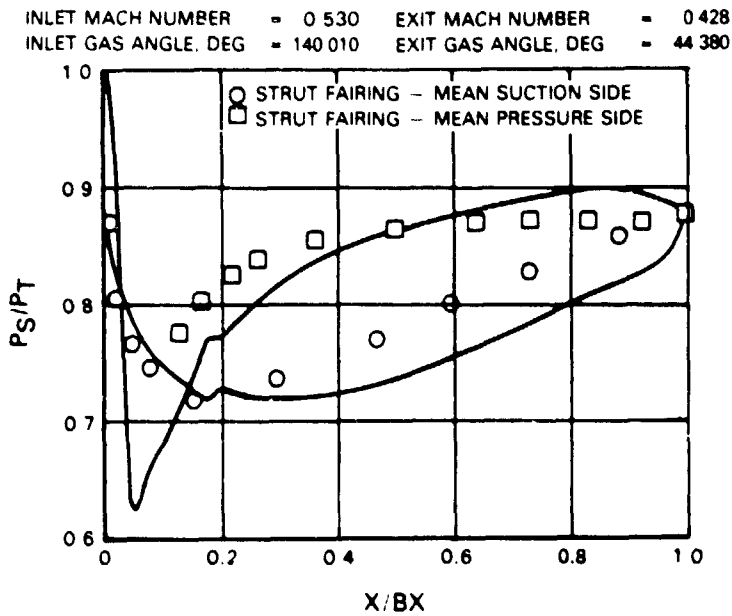


Figure 5-37 Build 2 Strut Fairing Mean Section Pressure Distribution Data

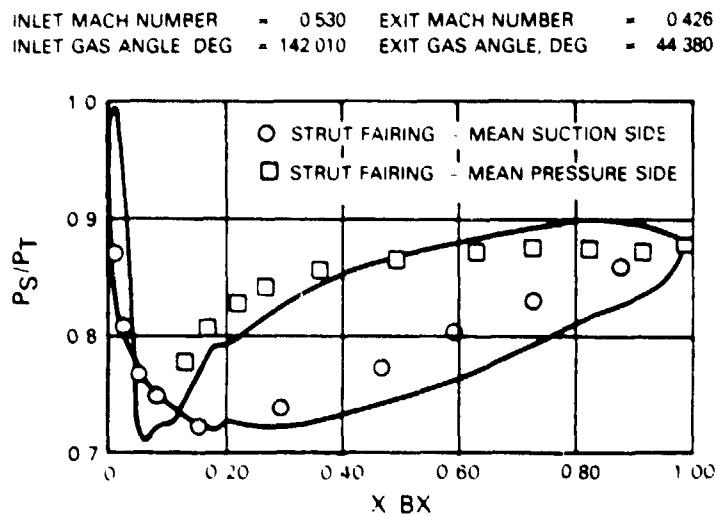


Figure 5-38 Build 2 Strut Fairing Mean Section Pressure Distribution Data

ORIGINAL PAGE IS
OF POOR QUALITY

INLET MACH NUMBER = 0.530 EXIT MACH NUMBER = 0.426
INLET GAS ANGLE, DEG. = 144.010 EXIT GAS ANGLE, DEG. = 44.380

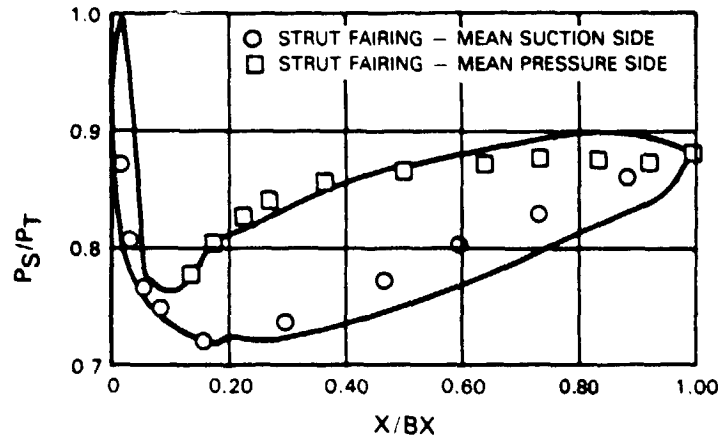


Figure 5-39 Build 2 Strut Fairing Mean Section Pressure Distribution Data

INLET MACH NUMBER = 0.530 EXIT MACH NUMBER = 0.426
INLET GAS ANGLE, DEG. = 146.010 EXIT GAS ANGLE, DEG. = 44.380

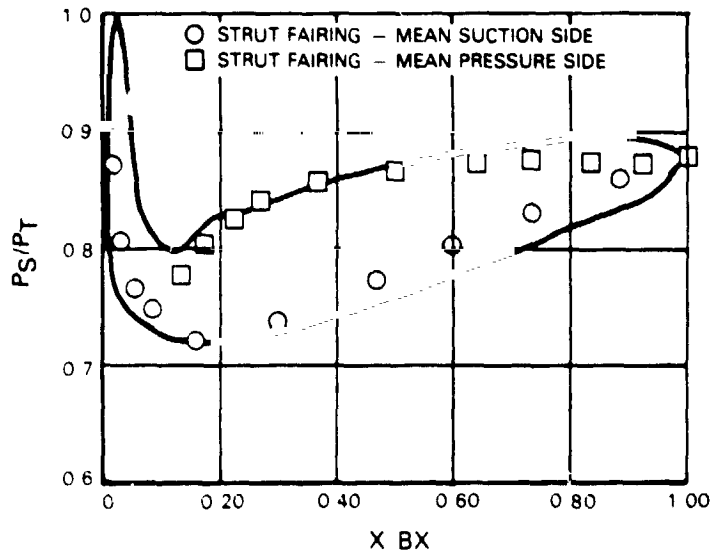


Figure 5-40 Build 2 Strut Fairing Mean Section Pressure Distribution Data

ORIGINAL PAGE IS
OF POOR QUALITY

INLET MACH NUMBER = 0.530 EXIT MACH NUMBER = 0.426
INLET GAS ANGLE, DEG = 148.010 EXIT GAS ANGLE, DEG = 44.380

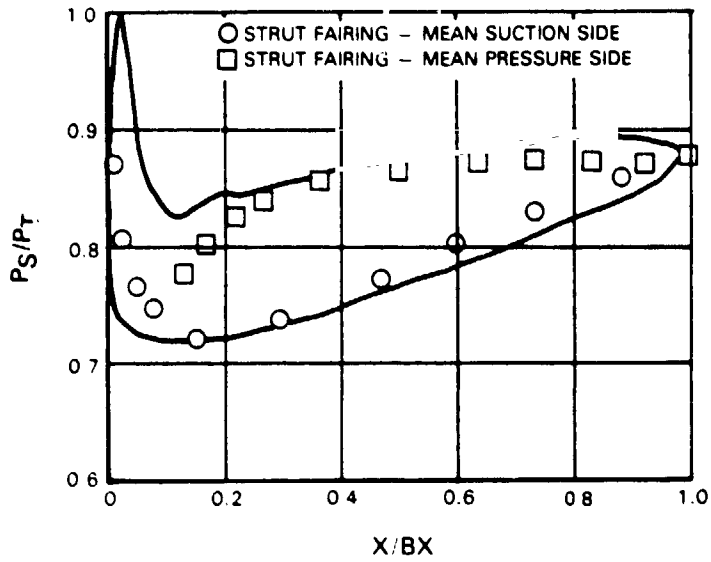


Figure 5-41 Build 2 Strut Fairing Mean Section Pressure Distribution Data

INLET MACH NUMBER = 0.530 EXIT MACH NUMBER = 0.426
INLET GAS ANGLE, DEG = 144.010 EXIT GAS ANGLE, DEG = 41.500

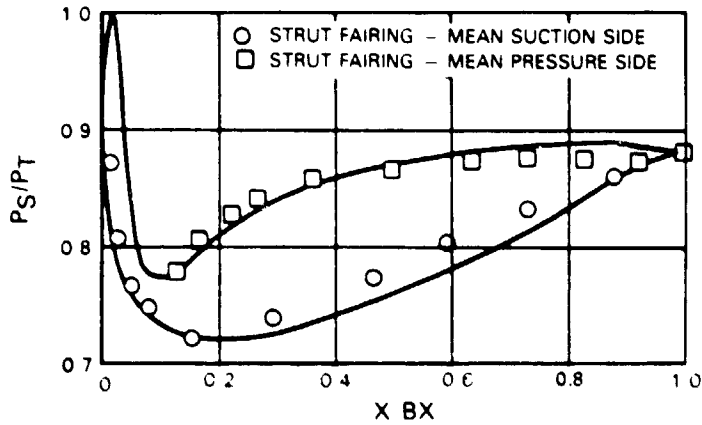


Figure 5-42 Build 2 Strut Fairing Mean Section Pressure Distribution Data

ORIGINAL PAGE IS
OF POOR QUALITY

INLET MACH NUMBER = 0.530 EXIT MACH NUMBER = 0.426
INLET GAS ANGLE, DEG = 144.010 EXIT GAS ANGLE, DEG. = 40.500

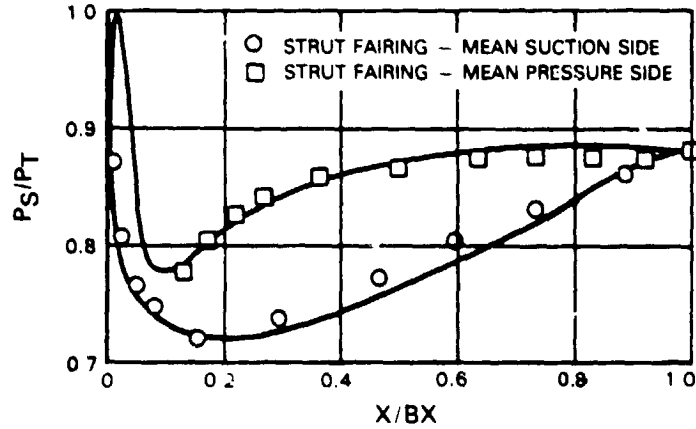


Figure 5-43 Build 2 Strut Fairing Mean Section Pressure Distribution Data

INLET MACH NUMBER = 0.430 EXIT MACH NUMBER = 0.374
INLET GAS ANGLE, DEG = 136.980 EXIT GAS ANGLE, DEG = 47.520

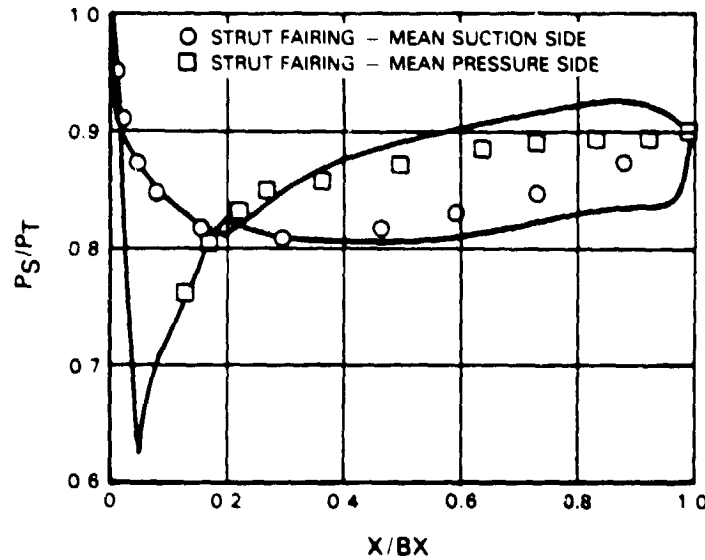


Figure 5-44 Build 2 Strut Fairing Mean Section Pressure Distribution Data, Off-Design

ORIGINAL PAGE IS
OF POOR QUALITY

INLET MACH NUMBER = 0.430 EXIT MACH NUMBER = 0.374
 INLET GAS ANGLE, DEG. = 138.980 EXIT GAS ANGLE, DEG. = 44.520

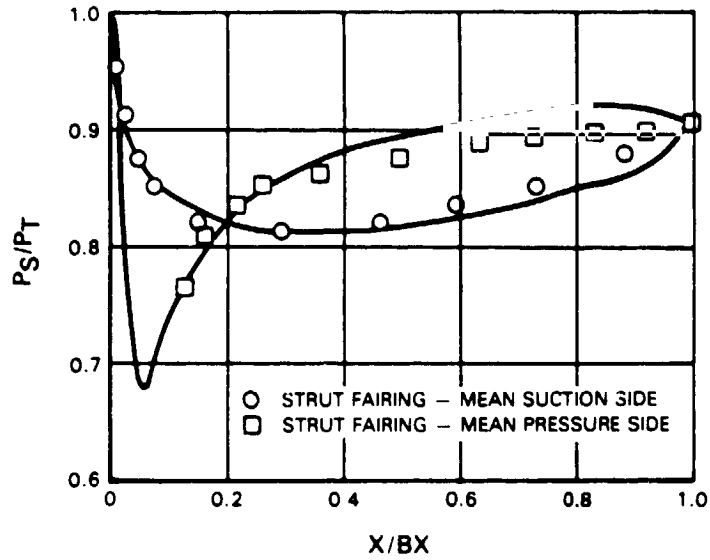


Figure 5-45 Build 2 Strut Fairing Mean Section Pressure Distribution Data, Off-Design

INLET MACH NUMBER = 0.430 EXIT MACH NUMBER = 0.374
 INLET GAS ANGLE, DEG. = 138.980 EXIT GAS ANGLE, DEG. = 43.520

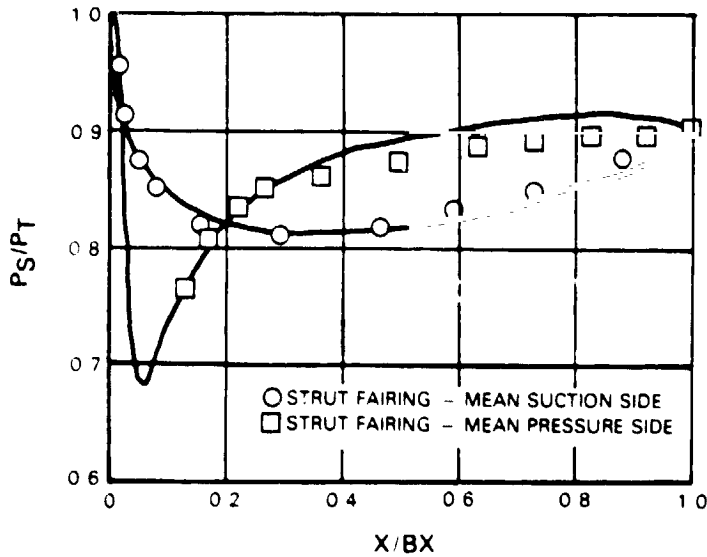


Figure 5-46 Build 2 Strut Fairing Mean Section Pressure Distribution Data, Off-Design

5.3.3 Low-Pressure Turbine Inlet Guide Vane Aerodynamics

The inlet guide vane was instrumented with static pressure taps at approximately 50 percent span on both the pressure and suction surfaces. Data acquired by this instrumentation are compared to the design prediction for build 1 design and off-design testing in Figures 5-47 and 5-48.

Since the inlet guide vane has essentially the same inlet angle and Mach number for both the design and off-design conditions, it should have similar pressure distributions. The data in Figures 5-47 and 5-48 show similar distributions except for the trailing edge region where the design point data appear to be in error. The off-design pressure distribution, presented in Figure 5-48, shows a well-behaved airfoil and indicates that the off-design build 1 inlet guide vane exit angle data, which disagrees with the design prediction previously shown in Figure 5-17, may be in error. As indicated in Section 5.3.1, this error was attributed to the air angle measurement instrumentation.

Two observations can be made from the comparison of these pressure distributions to the design predictions. First, the leading edge pressure surface, as shown in Figure 5-47, shows an overspeed that can be attributed to the inlet incidence angle being 3 degrees more negative compared to the design. Second, the trailing edge static pressure is above the predicted level. This is a result of the vane exit Mach number being slightly below the predicted level.

The build 2 design and off-design data are shown in Figures 5-49 and 5-50, respectively. The design point static pressure distribution shows good agreement with the prediction. Off-design data also show agreement with the design point data. This indicates that the build 2 vane is tolerant to the 2.8 degrees more positive incidence without showing a significant change in the leading edge loading. This tolerance results from the use of an elliptical airfoil leading edge.

5.4 SUMMARY OF RESULTS

Overall, the results from these tests indicate that the transition duct designs for both the flight propulsion system and integrated core/low spool are aerodynamically stable and provide the low-pressure turbine rotor inlet with a flowfield that is insensitive to the range of high-pressure turbine exit conditions evaluated. The total pressure loss goal of 0.7 percent $\Delta P_T/P_T$ was verified for transition duct design in the flight propulsion system. On the basis of these results, a duct design with an area ratio 1.5, length-to-height ratio of 3.0 and a nonworking strut fairing was confirmed for the flight propulsion system. Although this goal level was not achieved in the duct designed for the integrated core/low spool, the performance was better than predicted.

In general, data trends are consistent with the design predictions, when considering that the effects of viscous flow were not accounted for in the analytical prediction. Transition duct wall diffusion profiles showed no evidence of flow separation either at design or off-design conditions, as predicted. Similarly, the strut fairing in each duct configuration performed according to the design intent, either as a nonworking (build 1) or working (build 2) airfoil. Also, pressure distributions of the strut fairing and the inlet guide vane showed that these airfoils performed separation free, as predicted, at all test conditions.

ORIGINAL INTENT
OF POOR QUALITY

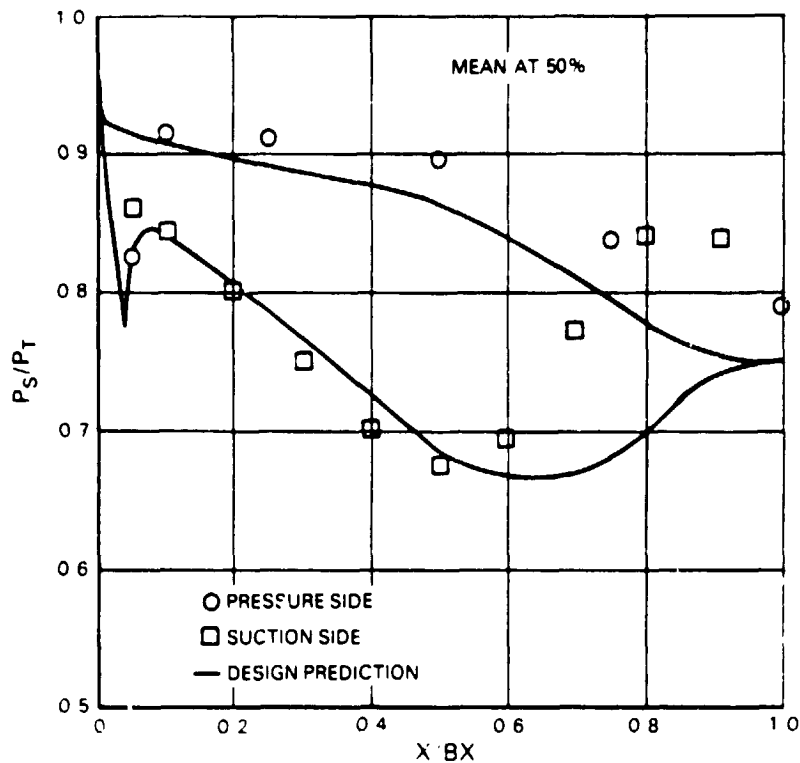


Figure 5-47 Build 1 Inlet Guide Vane Design Measured Pressure Distribution Data

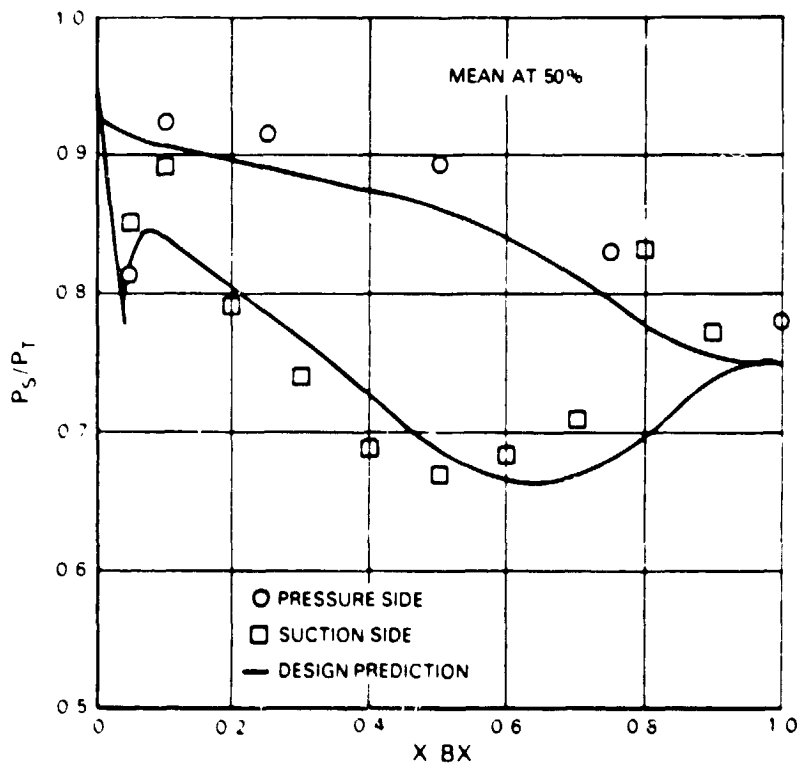


Figure 5-48 Build 1 Inlet Guide Vane Measured Off-Design Pressure Distribution Data

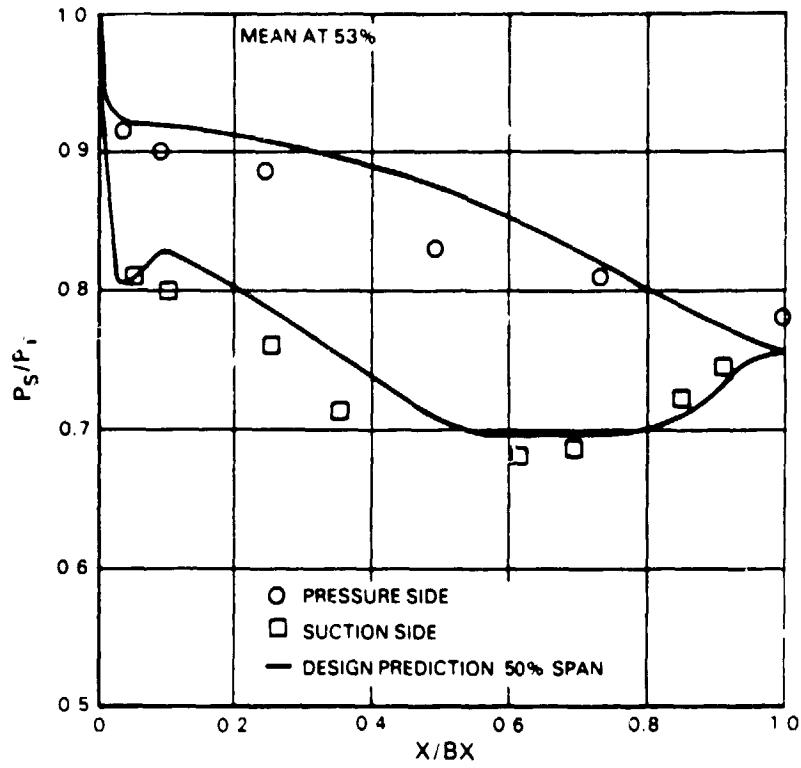


Figure 5-49 Build 2 Inlet Guide Vane Design Measured Pressure Distribution Data

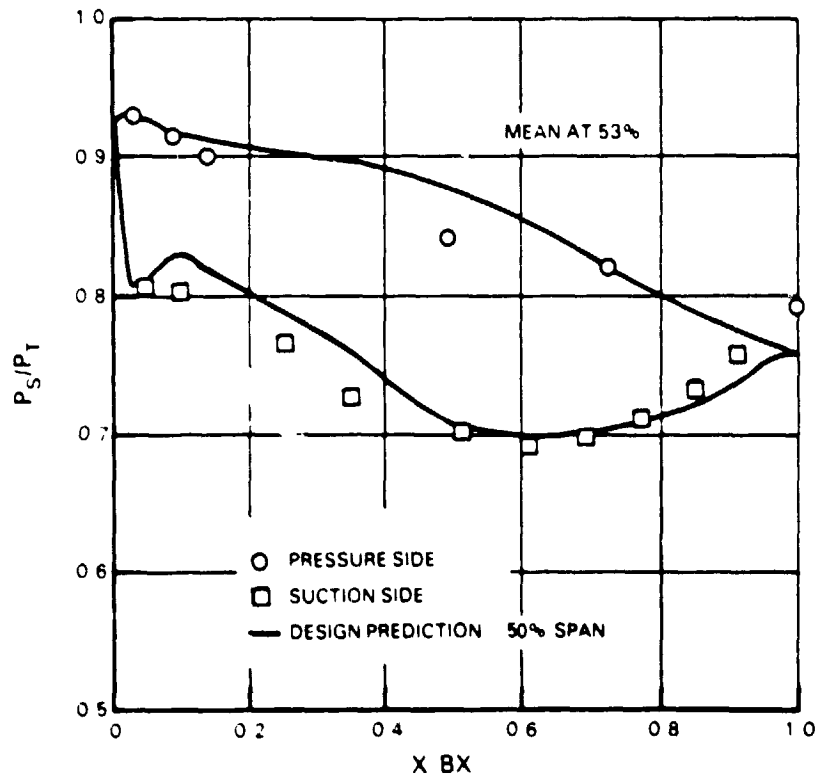


Figure 5-50 Build 2 Inlet Guide Vane Off-Design Measured Pressure Distribution Data

SECTION 6.0

CONCLUDING REMARKS

Subscale model testing has proved to be a useful design tool, as well as an expedient method for substantiating the aerodynamic definition of a turbine transition duct for both the integrated core/low spool and the flight propulsion system. Testing has verified that a low loss system, which is insensitive to the high-pressure turbine exit conditions, is achievable in a relatively compact duct design. Since model results are directly scaleable to the full size component, they provide a firm basis for the transition duct design in the integrated core/low spool. These results have also contributed substantially toward extending the data base for designing low loss transition ducts, if required, for the next generation of gas turbine engines.

APPENDIXES

APPENDIX A

Build 1 Airfoil Coordinates

STRUT FAIRING
 ROOT SECTION (HOT RADIUS = 15.40000)

PERCENT X	X	Y TOP	Y BOT
0.0	0.0	-0.17945	-0.17945
0.010	0.04500	-0.04609	-0.34276
0.020	0.09001	-0.00191	-0.45710
0.030	0.13501	0.02354	-0.56086
0.040	0.18001	0.03698	-0.65797
0.050	0.22502	0.04060	-0.75128
0.060	0.27002	0.03492	-0.84192
0.070	0.31503	0.01914	-0.93051
0.080	0.36003	-0.00949	-1.01724
0.090	0.40503	-0.04566	-1.10226
0.100	0.45004	-0.08306	-1.18581
0.125	0.56255	-0.18281	-1.38949
0.150	0.67506	-0.29147	-1.58748
0.175	0.78756	-0.40644	-1.78081
0.200	0.90007	-0.52599	-1.96986
0.225	1.01258	-0.64984	-2.15472
0.250	1.12509	-0.77777	-2.33627
0.275	1.23760	-0.90939	-2.51522
0.300	1.35011	-1.04439	-2.69086
0.325	1.46262	-1.18262	-2.86263
0.350	1.57513	-1.32403	-3.03080
0.375	1.68764	-1.46884	-3.19535
0.400	1.80015	-1.61722	-3.35546
0.425	1.91266	-1.76883	-3.51110
0.450	2.02517	-1.92339	-3.66353
0.475	2.13767	-2.08154	-3.81359
0.500	2.25018	-2.24413	-3.96136
0.525	2.36269	-2.41138	-4.10678
0.550	2.47520	-2.58351	-4.24982
0.575	2.58771	-2.76204	-4.39057
0.600	2.70022	-2.94825	-4.52945
0.625	2.81273	-3.14116	-4.66698
0.650	2.92524	-3.34001	-4.80365
0.675	3.03775	-3.54557	-4.93996
0.700	3.15026	-3.75875	-5.07619
0.725	3.26277	-3.98017	-5.21247
0.750	3.37528	-4.20885	-5.34808
0.775	3.48778	-4.44333	-5.48557
0.800	3.60029	-4.68221	-5.62272
0.825	3.71280	-4.92460	-5.76054
0.850	3.82531	-5.16983	-5.89931
0.875	3.93782	-5.41717	-6.03927
0.900	4.05033	-5.66553	-6.18063
0.910	4.09534	-5.76489	-6.23761
0.920	4.14034	-5.86411	-6.29480
0.930	4.18534	-5.96315	-6.35223
0.940	4.23035	-6.06194	-6.40991
0.950	4.27535	-6.16048	-6.46781
0.960	4.32035	-6.25880	-6.52596
0.970	4.36536	-6.35683	-6.58434
0.980	4.41036	-6.45466	-6.64295
0.990	4.45536	-6.55224	-6.69077
1.000	4.50037	-6.65726	-6.65726

STRUT FAIRING
MEAN SECTION (HOT RADIUS = 17.13600)

PERCENT X	X	Y TOP	Y BOT
0.0	-0.05922	-0.52207	-0.52207
0.010	-0.01422	-0.38870	-0.66783
0.020	0.03079	-0.34452	-0.75992
0.030	0.07579	-0.31906	-0.84513
0.040	0.12080	-0.30562	-0.92515
0.050	0.16580	-0.30199	-1.00199
0.060	0.21080	-0.30767	-1.07667
0.070	0.25581	-0.32344	-1.14981
0.080	0.30081	-0.34938	-1.22167
0.090	0.34581	-0.37739	-1.29233
0.100	0.39082	-0.40653	-1.36195
0.125	0.50333	-0.48505	-1.53211
0.150	0.61584	-0.57098	-1.69820
0.175	0.72835	-0.66221	-1.86113
0.200	0.84086	-0.75765	-2.02143
0.225	0.95336	-0.85708	-2.17915
0.250	1.06587	-0.96035	-2.33452
0.275	1.17838	-1.06713	-2.48827
0.300	1.29089	-1.17723	-2.64046
0.325	1.40340	-1.29059	-2.79030
0.350	1.51591	-1.40719	-2.93745
0.375	1.62842	-1.52718	-3.08211
0.400	1.74093	-1.65068	-3.22402
0.425	1.85344	-1.77757	-3.36252
0.450	1.96595	-1.90764	-3.49792
0.475	2.07846	-2.04126	-3.63124
0.500	2.19097	-2.17925	-3.76303
0.525	2.30348	-2.32208	-3.89332
0.550	2.41599	-2.46986	-4.02211
0.575	2.52850	-2.62351	-4.14941
0.600	2.64101	-2.78457	-4.27541
0.625	2.75351	-2.95307	-4.40064
0.650	2.86602	-3.12809	-4.52566
0.675	2.97853	-3.30998	-4.65101
0.700	3.09104	-3.49961	-4.77715
0.725	3.20355	-3.69787	-4.90427
0.750	3.31606	-3.90446	-5.03244
0.775	3.42857	-4.11796	-5.16178
0.800	3.54108	-4.33691	-5.29238
0.825	3.65359	-4.56028	-5.42410
0.850	3.76610	-4.78764	-5.55673
0.875	3.87861	-5.01962	-5.69007
0.900	3.99112	-5.25374	-5.82391
0.910	4.03612	-5.34927	-5.87756
0.920	4.08113	-5.44574	-5.93127
0.930	4.12613	-5.54331	-5.98506
0.940	4.17113	-5.64204	-6.03892
0.950	4.21614	-5.74134	-6.09282
0.960	4.26114	-5.84306	-6.14681
0.970	4.30614	-5.94534	-6.20086
0.980	4.35115	-6.04884	-6.25497
0.990	4.39615	-6.15353	-6.30902
1.000	4.44116	-6.26648	-6.26648

STRUT FAIRING
TIP SECTION (HOT RADIUS = 18.87000)

PERCENT X	X	Y TOP	Y BOT
0.0	-0.00086	-1.07478	-1.07478
0.010	0.04408	-0.94146	-1.21456
0.020	0.08903	-0.89728	-1.29509
0.030	0.13397	-0.87180	-1.36859
0.040	0.17892	-0.85832	-1.43685
0.050	0.22386	-0.85463	-1.50205
0.060	0.26881	-0.86021	-1.56519
0.070	0.31375	-0.87544	-1.62674
0.080	0.35870	-0.89426	-1.68695
0.090	0.40364	-0.91424	-1.74591
0.100	0.44858	-0.93550	-1.80379
0.125	0.56095	-0.99462	-1.94450
0.150	0.67331	-1.06002	-2.08085
0.175	0.78567	-1.12984	-2.21366
0.200	0.89803	-1.20347	-2.34337
0.225	1.01039	-1.28076	-2.47022
0.250	1.12275	-1.36135	-2.59458
0.275	1.23511	-1.44494	-2.71694
0.300	1.34747	-1.53145	-2.83715
0.325	1.45983	-1.62083	-2.95453
0.350	1.57220	-1.71309	-3.06890
0.375	1.68456	-1.80825	-3.18047
0.400	1.79692	-1.90623	-3.28899
0.425	1.90928	-2.00691	-3.39413
0.450	2.02164	-2.11049	-3.49638
0.475	2.13400	-2.21768	-3.59660
0.500	2.24636	-2.32892	-3.69514
0.525	2.35872	-2.44437	-3.79206
0.550	2.47109	-2.56458	-3.88743
0.575	2.58345	-2.69061	-3.98131
0.600	2.69581	-2.82253	-4.07395
0.625	2.80817	-2.95953	-4.16576
0.650	2.92053	-3.10155	-4.25713
0.675	3.03289	-3.24899	-4.34851
0.700	3.14525	-3.40226	-4.44018
0.725	3.25761	-3.56123	-4.53229
0.750	3.36997	-3.72488	-4.62491
0.775	3.48234	-3.89214	-4.71815
0.800	3.59470	-4.06209	-4.81208
0.825	3.70706	-4.23431	-4.90667
0.850	3.81942	-4.40844	-5.00184
0.875	3.93178	-4.58428	-5.09754
0.900	4.04414	-4.76199	-5.19370
0.910	4.08909	-4.83366	-5.23228
0.920	4.13403	-4.90571	-5.27094
0.930	4.17898	-4.97814	-5.30967
0.940	4.22392	-5.05096	-5.34846
0.950	4.26886	-5.12417	-5.38733
0.960	4.31381	-5.19779	-5.42626
0.970	4.35875	-5.27177	-5.46527
0.980	4.40370	-5.34618	-5.50435
0.990	4.44864	-5.42098	-5.54331
1.000	4.49359	-5.50579	-5.58227

INLET GUIDE VANE
ROOT SECTION (HOT RADIUS = 16.54999)

PERCENT X	X	Y TOP	Y BOT
0.0	-0.85548	1.07909	1.07909
0.010	-0.83898	1.11398	1.04137
0.020	-0.82248	1.12257	1.01797
0.030	-0.80598	1.12401	0.99448
0.040	-0.78948	1.11911	0.97100
0.050	-0.77298	1.10578	0.94747
0.060	-0.75648	1.08993	0.92392
0.070	-0.73998	1.07410	0.90036
0.080	-0.72348	1.05829	0.87675
0.090	-0.70698	1.04248	0.85311
0.100	-0.69048	1.02668	0.82946
0.125	-0.64923	0.98716	0.77018
0.150	-0.60798	0.94763	0.71073
0.175	-0.56673	0.90806	0.65108
0.200	-0.52547	0.86841	0.59123
0.225	-0.48422	0.82861	0.53113
0.250	-0.44297	0.78862	0.47083
0.275	-0.40172	0.74835	0.41030
0.300	-0.36047	0.70769	0.34955
0.325	-0.31922	0.66653	0.28859
0.350	-0.27797	0.62477	0.22740
0.375	-0.23672	0.58221	0.16601
0.400	-0.19547	0.53870	0.10440
0.425	-0.15422	0.49393	0.04257
0.450	-0.11297	0.44772	-0.01945
0.475	-0.07172	0.39973	-0.08165
0.500	-0.03047	0.34956	-0.14403
0.525	0.01078	0.29687	-0.20661
0.550	0.05203	0.24119	-0.26931
0.575	0.09328	0.18213	-0.33222
0.600	0.13453	0.11923	-0.39528
0.625	0.17578	0.05220	-0.45851
0.650	0.21703	-0.01929	-0.52183
0.675	0.25829	-0.09536	-0.58535
0.700	0.29954	-0.17591	-0.64904
0.725	0.34079	-0.26075	-0.71286
0.750	0.38204	-0.34951	-0.77679
0.775	0.42329	-0.44188	-0.84106
0.800	0.46454	-0.53748	-0.90551
0.825	0.50579	-0.63589	-0.97027
0.850	0.54704	-0.73686	-1.03535
0.875	0.58829	-0.84000	-1.10121
0.900	0.62954	-0.94503	-1.16807
0.910	0.64604	-0.98748	-1.19549
0.920	0.66254	-1.03022	-1.22297
0.930	0.67904	-1.07310	-1.25085
0.940	0.69554	-1.11630	-1.27951
0.950	0.71204	-1.15963	-1.30892
0.960	0.72854	-1.20318	-1.33904
0.970	0.74504	-1.24690	-1.36959
0.980	0.76154	-1.29078	-1.39786
0.990	0.77804	-1.33479	-1.40229
1.000	0.79454	-1.38256	-1.38256

INLET GUIDE VANE
MEAN SECTION (HOT RADIUS = 18.87785)

PERCENT X	X	Y TOP	Y BOT
0.0	-0.86297	1.12461	1.12461
0.010	-0.84647	1.15421	1.09977
0.020	-0.82997	1.15944	1.06305
0.030	-0.81347	1.15631	1.03733
0.040	-0.79599	1.14490	1.01160
0.050	-0.78048	1.13215	0.98587
0.060	-0.76398	1.11938	0.96012
0.070	-0.74748	1.10650	0.93437
0.080	-0.73098	1.09350	0.90861
0.090	-0.71449	1.08039	0.88284
0.100	-0.69799	1.06717	0.85707
0.125	-0.65674	1.03357	0.79261
0.150	-0.61550	0.99922	0.72812
0.175	-0.57425	0.96404	0.66359
0.200	-0.53301	0.92802	0.59904
0.225	-0.49176	0.89112	0.53447
0.250	-0.45052	0.85329	0.46988
0.275	-0.40927	0.81447	0.40528
0.300	-0.36803	0.77462	0.34086
0.325	-0.32678	0.73365	0.27604
0.350	-0.28554	0.69149	0.21141
0.375	-0.24429	0.64806	0.14677
0.400	-0.20305	0.60323	0.08213
0.425	-0.16180	0.55692	0.01749
0.450	-0.12056	0.50893	-0.04715
0.475	-0.07931	0.45912	-0.11180
0.500	-0.03907	0.40726	-0.17645
0.525	0.00317	0.35306	-0.24109
0.550	0.04442	0.29620	-0.30574
0.575	0.08566	0.23620	-0.37039
0.600	0.12691	0.17254	-0.43504
0.625	0.16815	0.10464	-0.49968
0.650	0.20940	0.03197	-0.56434
0.675	0.25064	-0.04583	-0.62902
0.700	0.29189	-0.12898	-0.69372
0.725	0.33313	-0.21732	-0.75840
0.750	0.37438	-0.31062	-0.82313
0.775	0.41562	-0.40838	-0.88784
0.800	0.45687	-0.51009	-0.95265
0.825	0.49811	-0.61511	-1.01748
0.850	0.53936	-0.72297	-1.08242
0.875	0.58060	-0.83319	-1.14749
0.900	0.62185	-0.94543	-1.21279
0.910	0.63834	-0.99076	-1.23897
0.920	0.65484	-1.03640	-1.26533
0.930	0.67134	-1.08222	-1.29180
0.940	0.69784	-1.12830	-1.31839
0.950	0.70434	-1.17454	-1.34531
0.960	0.72083	-1.22102	-1.37256
0.970	0.73733	-1.26763	-1.40054
0.980	0.75383	-1.31448	-1.42703
0.990	0.77033	-1.36142	-1.43160
1.000	0.78683	-1.41196	-1.41196

INLET GUIDE VANE
TIF SECTION (HOT RADIUS = 21.19000)

PERCENT X	X	Y TOP	Y BOT
0.0	-0.90497	1.01191	1.01191
0.010	-0.88848	1.04153	0.98001
0.020	-0.87198	1.04674	0.96107
0.030	-0.85548	1.04366	0.94199
0.040	-0.83899	1.03694	0.92278
0.050	-0.82249	1.03003	0.90346
0.060	-0.80600	1.02295	0.88398
0.070	-0.78950	1.01568	0.86439
0.080	-0.77300	1.00824	0.84465
0.090	-0.75651	1.00062	0.82477
0.100	-0.74001	0.99260	0.80478
0.125	-0.69877	0.97248	0.75412
0.150	-0.65753	0.95096	0.70258
0.175	-0.61629	0.92826	0.65016
0.200	-0.57504	0.90435	0.59681
0.225	-0.53380	0.87919	0.54255
0.250	-0.49256	0.85273	0.48738
0.275	-0.45132	0.82498	0.43131
0.300	-0.41008	0.79582	0.37437
0.325	-0.36884	0.76524	0.31656
0.350	-0.32760	0.73316	0.25794
0.375	-0.28635	0.69948	0.19849
0.400	-0.24511	0.66412	0.13825
0.425	-0.20387	0.62694	0.07727
0.450	-0.16263	0.58782	0.01556
0.475	-0.12139	0.54656	-0.04683
0.500	-0.08015	0.50298	-0.10985
0.525	-0.03891	0.45676	-0.17349
0.550	0.00234	0.40763	-0.23770
0.575	0.04358	0.35510	-0.30244
0.600	0.08482	0.29871	-0.36769
0.625	0.12606	0.23801	-0.43342
0.650	0.16730	0.17245	-0.49960
0.675	0.20854	0.10146	-0.56618
0.700	0.24978	0.02448	-0.63314
0.725	0.29102	-0.05893	-0.70047
0.750	0.33227	-0.14915	-0.76810
0.775	0.37351	-0.24635	-0.83611
0.800	0.41475	-0.35047	-0.90435
0.825	0.45599	-0.46111	-0.97283
0.850	0.49723	-0.57789	-1.04151
0.875	0.53847	-0.70026	-1.11036
0.900	0.57971	-0.82766	-1.17933
0.910	0.59621	-0.87984	-1.20694
0.920	0.61271	-0.93274	-1.23446
0.930	0.62920	-0.98620	-1.26188
0.940	0.64570	-1.04036	-1.28934
0.950	0.66220	-1.09502	-1.31651
0.960	0.67869	-1.15028	-1.34354
0.970	0.69519	-1.20599	-1.36996
0.980	0.71169	-1.26227	-1.39420
0.990	0.72818	-1.31894	-1.39865
1.000	0.74468	-1.37893	-1.37893

APPENDIX B

Build 2 Airfoil Coordinates

STRUT FAIRING
(Section 1)

X/BX	SUCTION SIDE Y/BX	PRESSURE SIDE Y/BX
1.00000	1.49436	1.49436
0.99000	1.50131	1.47229
0.98000	1.49121	1.45161
0.97000	1.47953	1.43120
0.96000	1.46802	1.41086
0.94000	1.44469	1.37039
0.92000	1.42121	1.33022
0.88000	1.37374	1.25066
0.84000	1.32558	1.17166
0.80000	1.27682	1.09275
0.76000	1.22760	1.01407
0.72000	1.17804	0.93597
0.68000	1.12812	0.85870
0.64000	1.07774	0.78248
0.60000	1.02677	0.70747
0.56000	0.97514	0.63384
0.52000	0.92274	0.56172
0.48000	0.86947	0.49125
0.44000	0.81524	0.42254
0.40000	0.75998	0.35574
0.36000	0.70350	0.29104
0.32000	0.64558	0.22870
0.28000	0.58590	0.16909
0.24000	0.52391	0.11288
0.20000	0.45907	0.06048
0.16000	0.39076	0.01330
0.12000	0.31792	-0.02335
0.08000	0.23837	-0.05686
0.06000	0.19460	-0.06494
0.04000	0.14702	-0.06583
0.03000	0.12077	-0.06286
0.02000	0.09091	-0.05704
0.01000	0.05806	-0.04654
0.0	0.0	0.0

PREVIOUS PAGE PLANK NOT FILMED

STRUT FAIRING
(Section 2)

X/BX	SUCTION SIDE Y/BX	PRESSURE SIDE Y/BX
1.00000	1.10108	1.10108
0.99000	1.10790	1.08457
0.98000	1.10073	1.07015
0.97000	1.09321	1.05592
0.96000	1.08568	1.04170
0.94000	1.07043	1.01338
0.92000	1.05502	0.98520
0.88000	1.02369	0.92923
0.84000	0.99167	0.87347
0.80000	0.95902	0.81753
0.76000	0.92588	0.76136
0.72000	0.89235	0.70524
0.68000	0.85842	0.64935
0.64000	0.82399	0.59389
0.60000	0.78897	0.53898
0.56000	0.75327	0.48474
0.52000	0.71682	0.43131
0.48000	0.67954	0.37898
0.44000	0.64136	0.32744
0.40000	0.60216	0.27693
0.36000	0.56184	0.22758
0.32000	0.52025	0.17971
0.28000	0.47699	0.13378
0.24000	0.43152	0.09022
0.20000	0.38331	0.04961
0.16000	0.33179	0.01316
0.12000	0.27586	-0.01819
0.08000	0.21359	-0.03993
0.06000	0.17900	-0.04759
0.04000	0.14022	-0.04955
0.03000	0.11861	-0.04713
0.02000	0.09506	-0.04199
0.01000	0.06674	-0.03271
0.0	0.0	-0.0

STRUT FAIRING
(Section 3)

X/BX	SUCTION SIDE Y/L	PRESSURE SIDE Y/BX
1.00000	0.88068	0.88068
0.99000	0.88727	0.86652
0.98000	0.88177	0.85490
0.97000	0.87625	0.84343
0.96000	0.87065	0.83196
0.94000	0.85932	0.80914
0.92000	0.84782	0.78643
0.88000	0.82435	0.74136
0.84000	0.80021	0.69649
0.80000	0.77547	0.65145
0.76000	0.75028	0.60619
0.72000	0.72473	0.56091
0.68000	0.69880	0.51578
0.64000	0.67238	0.47096
0.60000	0.64540	0.42656
0.56000	0.61777	0.38268
0.52000	0.58945	0.33942
0.48000	0.56034	0.29700
0.44000	0.53039	0.25537
0.40000	0.49950	0.21449
0.36000	0.46758	0.17453
0.32000	0.43445	0.13575
0.28000	0.39974	0.09852
0.24000	0.36926	0.06328
0.20000	0.32370	0.03044
0.16000	0.28144	0.00115
0.12000	0.23519	-0.02408
0.08000	0.18335	-0.04066
0.06000	0.15432	-0.04537
0.04000	0.12156	-0.04700
0.03000	0.10341	-0.04471
0.02000	0.08349	-0.03971
0.01000	0.05988	-0.03059
0.0	0.0	0.0

STRUT FAIRING
(Section 4)

X/BX	SUCTION SIDE Y/BX	PRESSURE SIDE Y/BX
1.00000	0.73531	0.73531
0.99000	0.74174	0.72222
0.96000	0.73716	0.71188
0.97000	0.73265	0.70170
0.96000	0.72805	0.69153
0.94000	0.71874	0.67132
0.92000	0.70929	0.65128
0.88000	0.68993	0.61164
0.84000	0.66999	0.57236
0.80000	0.64955	0.53310
0.76000	0.62876	0.49379
0.72000	0.60771	0.45462
0.68000	0.58635	0.41577
0.64000	0.56459	0.37734
0.60000	0.54234	0.33945
0.56000	0.51954	0.30217
0.52000	0.49614	0.26560
0.48000	0.47207	0.22988
0.44000	0.44726	0.19505
0.40000	0.42164	0.16115
0.36000	0.39511	0.12832
0.32000	0.36748	0.09677
0.28000	0.33843	0.06680
0.24000	0.30764	0.03878
0.20000	0.27477	0.01300
0.16000	0.23935	-0.00965
0.12000	0.20047	-0.02865
0.08000	0.15683	-0.04074
0.06000	0.13213	-0.04318
0.04000	0.10434	-0.04340
0.03000	0.08900	-0.04131
0.02000	0.07163	-0.03646
0.01000	0.04930	-0.02750
0.0	0.0	0.0

INLET GUIDE VANE
ROOT SECTION (HOT RADIUS 16.3900C)

PERCENT X	X	Y TOP	Y BOT
0.0	0.00209	2.29910	2.29910
0.010	0.01781	2.31407	2.25376
0.020	0.03354	2.30879	2.22621
0.030	0.04926	2.29923	2.20238
0.040	0.06498	2.28774	2.17851
0.050	0.08071	2.27433	2.15455
0.060	0.09643	2.26020	2.13065
0.070	0.11216	2.24533	2.10674
0.080	0.12788	2.23046	2.08285
0.090	0.14360	2.21553	2.05890
0.100	0.15933	2.20054	2.03505
0.125	0.19863	2.16276	1.97535
0.150	0.23794	2.12453	1.91567
0.175	0.27725	2.08583	1.85607
0.200	0.31656	2.04661	1.79639
0.225	0.35587	2.00683	1.73680
0.250	0.39518	1.96644	1.67723
0.275	0.43449	1.92538	1.61772
0.300	0.47380	1.88358	1.55824
0.325	0.51310	1.84097	1.49879
0.350	0.55241	1.79747	1.43937
0.375	0.59172	1.75300	1.38000
0.400	0.63103	1.70744	1.32066
0.425	0.67034	1.66068	1.26136
0.450	0.70965	1.61257	1.20210
0.475	0.74896	1.56296	1.14289
0.500	0.78827	1.51167	1.08370
0.525	0.82757	1.45850	1.02463
0.550	0.86688	1.40320	0.96556
0.575	0.90619	1.34548	0.90649
0.600	0.94550	1.28508	0.84756
0.625	0.98481	1.22178	0.78866
0.650	1.02412	1.15545	0.72977
0.675	1.06343	1.08607	0.67104
0.700	1.10274	1.01373	0.61235
0.725	1.14204	0.93862	0.55369
0.750	1.18135	0.86101	0.49515
0.775	1.22066	0.78117	0.43676
0.800	1.25997	0.69940	0.37852
0.825	1.29928	0.61597	0.32042
0.850	1.33859	0.53114	0.26245
0.875	1.37790	0.44513	0.20471
0.900	1.41721	0.35811	0.14734
0.910	1.43293	0.32307	0.12452
0.920	1.44865	0.28789	0.10178
0.930	1.46438	0.25259	0.07917
0.940	1.48010	0.21718	0.05669
0.950	1.49582	0.18167	0.03441
0.960	1.51155	0.14607	0.01247
0.970	1.52727	0.11037	-0.00911
0.980	1.54299	0.07460	-0.02337
0.990	1.55872	0.03873	-0.03382
1.000	1.57444	-0.00202	-0.00202

INLET GUIDE VANE
MEAN SECTION (HOT RADIUS = 18.11501)

PERCENT X	X	Y TOP	Y BOT
0.0	0.00652	2.36065	2.36065
0.010	0.02218	2.37622	2.31705
0.020	0.03783	2.37197	2.29072
0.030	0.05349	2.36463	2.26651
0.040	0.06915	2.35471	2.24219
0.050	0.08481	2.34311	2.21787
0.060	0.10047	2.33083	2.19355
0.070	0.11613	2.31861	2.16912
0.080	0.13178	2.30620	2.14472
0.090	0.14744	2.29371	2.12046
0.100	0.16310	2.28111	2.09612
0.125	0.20225	2.24912	2.03537
0.150	0.24139	2.21642	1.97443
0.175	0.28054	2.18293	1.91366
0.200	0.31968	2.14862	1.85280
0.225	0.35883	2.11341	1.79198
0.250	0.39797	2.07725	1.73125
0.275	0.43712	2.04005	1.67052
0.300	0.47626	2.00174	1.60982
0.325	0.51541	1.96225	1.54914
0.350	0.55455	1.92146	1.48848
0.375	0.59370	1.87928	1.42784
0.400	0.63284	1.83561	1.36723
0.425	0.67199	1.79031	1.30664
0.450	0.71113	1.74327	1.24607
0.475	0.75028	1.69434	1.18553
0.500	0.78942	1.64339	1.12502
0.525	0.82857	1.59024	1.06458
0.550	0.86772	1.53473	1.00418
0.575	0.90686	1.47670	0.94368
0.600	0.94601	1.41595	0.88329
0.625	0.98515	1.35232	0.82300
0.650	1.02430	1.28566	0.76258
0.675	1.06344	1.21580	0.70231
0.700	1.10259	1.14263	0.64216
0.725	1.14173	1.06605	0.58200
0.750	1.18088	0.98599	0.52185
0.775	1.22002	0.90241	0.46171
0.800	1.25917	0.81529	0.40164
0.825	1.29831	0.72468	0.34171
0.850	1.33746	0.63065	0.28200
0.875	1.37660	0.53329	0.22242
0.900	1.41575	0.43273	0.16290
0.910	1.43141	0.39164	0.13918
0.920	1.44707	0.35006	0.11550
0.930	1.46272	0.30802	0.09188
0.940	1.47838	0.26552	0.06838
0.950	1.49404	0.22256	0.04503
0.960	1.50970	0.17918	0.02179
0.970	1.52536	0.13538	0.00088
0.980	1.54101	0.09115	-0.02006
0.990	1.55667	0.04652	-0.02222
1.000	1.57233	-0.00202	-0.00202

INLET GUIDE VANE
TIP SECTION (HOT RADIUS = 19.84001)

PERCENT X	X	Y TOP	Y BOT
0.0	0.01019	2.56710	2.56710
0.010	0.02580	2.58257	2.52332
0.020	0.04141	2.57929	2.49703
0.030	0.05702	2.57211	2.47173
0.040	0.07264	2.56276	2.44679
0.050	0.08825	2.55330	2.42165
0.060	0.10386	2.54263	2.39654
0.070	0.11948	2.53186	2.37142
0.080	0.13509	2.52094	2.34628
0.090	0.15070	2.50988	2.32112
0.100	0.16631	2.49868	2.29595
0.125	0.20535	2.47006	2.23298
0.150	0.24438	2.44048	2.16990
0.175	0.28341	2.40988	2.10674
0.200	0.32244	2.37816	2.04348
0.225	0.36147	2.34525	1.98011
0.250	0.40051	2.31109	1.91663
0.275	0.43954	2.27553	1.85304
0.300	0.47857	2.23850	1.78934
0.325	0.51760	2.19988	1.72551
0.350	0.55664	2.15955	1.66155
0.375	0.59567	2.11739	1.59746
0.400	0.63470	2.07326	1.53323
0.425	0.67373	2.02704	1.46884
0.450	0.71276	1.97858	1.40431
0.475	0.75180	1.92774	1.33960
0.500	0.79083	1.87437	1.27474
0.525	0.82986	1.81833	1.20969
0.550	0.86889	1.75949	1.14444
0.575	0.90792	1.69768	1.07900
0.600	0.94696	1.63277	1.01334
0.625	0.98599	1.56460	0.94746
0.650	1.02502	1.49298	0.88134
0.675	1.06405	1.41775	0.81496
0.700	1.10308	1.33871	0.74832
0.725	1.14212	1.25564	0.68138
0.750	1.18115	1.16832	0.61415
0.775	1.22018	1.07653	0.54660
0.800	1.25921	0.98001	0.47869
0.825	1.29824	0.87849	0.41041
0.850	1.33728	0.77168	0.34172
0.875	1.37631	0.65925	0.27261
0.900	1.41534	0.54088	0.20302
0.910	1.43095	0.49180	0.17505
0.920	1.44657	0.44169	0.14700
0.930	1.46218	0.39050	0.11886
0.940	1.47779	0.33827	0.09064
0.950	1.49341	0.28491	0.06232
0.960	1.50902	0.23042	0.03391
0.970	1.52463	0.17478	0.00540
0.980	1.54024	0.11794	-0.01855
0.990	1.55586	0.05989	-0.02150
1.000	1.57147	-0.00198	-0.00198

LIST OF SYMBOLS

b	Wire mesh diameter
C _p	Pressure Coefficient (P _s LOCAL - P _s at 0.0) / 1/2 $\bar{\rho}$ V ² at 0.0
ID	Inner diameter
IGV	Inlet guide vane
LE	Leading edge
OD	Outer diameter
M ₁	Inlet Mach Number
M ₂	Exit Mach Number
Pa	Pascal
$\Delta P_T/P_T$	Pressure loss
$\Delta P/Q$	Screen drag coefficient
N	Newtons
P _A	Ambient pressure
P _S	Static pressure
P _T	Total pressure
P _S /P _T	Pressure ratio
T _T	Total temperature
TE	Trailing edge
V _{x'} /V	Turbulence
X/B _x	Axial Distance/Axial Chord
X/b	Axial distance/wire mesh diameter ratio

PRECEDING PAGE BLANK NOT FILMED

REFERENCES

1. Sharma, O.P.: 'Energy Efficient Engine Low-Pressure Turbine Subsonic Cascade Technology Report,' PWA-5594-167, January 1982, NASA CR-165592

PRECEDING PAGE BLANK NOT FILMED